OCS Study
BOEMRE 2010-050

Satellite Data Assimilation into Meteorological/Air Quality Models

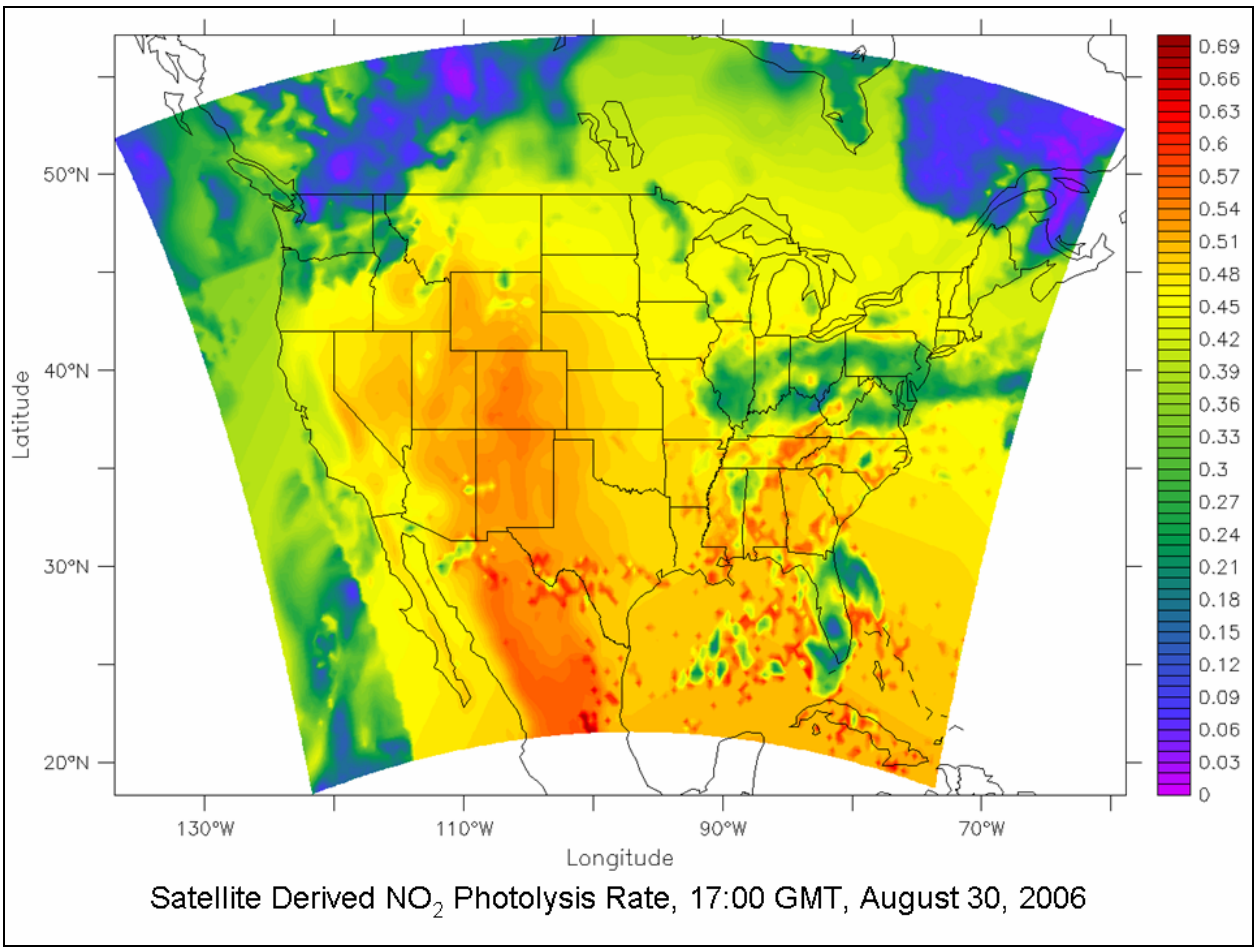

Satellite Derived NO_2 Photolysis Rate, 17:00 GMT, August 30, 2006

U.S. Department of the Interior
Bureau of Ocean Energy Management, Regulation and Enforcement
Gulf of Mexico OCS Region

OCS Study
BOEMRE 2010-050

Satellite Data Assimilation into Meteorological/Air Quality Models

Authors

A. Pour Biazar
R.T. McNider
S. Mackaro

Prepared under BOEMRE Cooperative Agreement
1435-01-04-CA-37002 (M054AC12302)
by
University of Alabama in Huntsville
National Space Science and Technology Center
Earth System Science Center
Huntsville, Alabama 35805

Published by

U.S. Department of the Interior
Bureau of Ocean Energy Management, Regulation and Enforcement
Gulf of Mexico OCS Region

New Orleans
December 2010

DISCLAIMER

This report was prepared under contract between the Bureau of Ocean Energy Management, Regulation and Enforcement (BOEMRE) and the University of Alabama in Huntsville (UAH). This report has been technically reviewed by the BOEMRE, and it has been approved for publication. Approval does not signify that the contents necessarily reflect the views and policies of the BOEMRE, nor does mention of trade names or commercial products constitute endorsement or recommendation for use. It is, however, exempt from review and compliance with the BOEMRE editorial standards.

REPORT AVAILABILITY

This report is available only in compact disc format from the Bureau of Ocean Energy Management, Regulation and Enforcement, Gulf of Mexico OCS Region, at a charge of $15.00, by referencing OCS Study BOEMRE 2010-050. The report may be downloaded from the BOEMRE website through the Environmental Studies Program Information System (ESPIS). You will be able to obtain this report also from the National Technical Information Service in the near future. Here are the addresses. You may also inspect copies at selected Federal Depository Libraries.

Bureau of Ocean Energy Management,
Regulation and Enforcement
Gulf of Mexico OCS Region
Public Information Office (MS 5034)
1201 Elmwood Park Boulevard
New Orleans, Louisiana 70123-2394
Telephone requests may be placed at
(504) 736-2519, 1-800-200-GULF, or
Rush Orders: 1-800-553-6847
Fax: (504) 736-2620

U.S. Department of Commerce
National Technical Information Service
5285 Port Royal Road
Springfield, Virginia 22161
Phone: (703) 605-6040
Fax: (703) 605-6900
Email: bookstore@ntis.gov

CITATION

Biazar, A.P., R.T. McNider, and S. Mackaro. 2010. Satellite data assimilation into meteorological/air quality models. U.S. Dept. of the Interior, Bureau of Ocean Energy Management, Regulation and Enforcement, Gulf of Mexico OCS Region, New Orleans, LA. OCS Study BOEMRE 2010-050. 70 pp.

ACKNOWLEDGMENTS

This work was accomplished under partial support from Cooperative Agreement Between the University of Alabama in Huntsville and the Bureau of Ocean Energy Management, Regulation and Enforcement on Gulf of Mexico Issues, Texas Commission on Environmental Quality (TCEQ), and the following grants: U.S. Environmental Protection Agency (USEPA) Star Grant R-826770-01-0, Southern Oxidant Study, USEPA Cooperative Agreement R-82897701-0 and Texas Air Research Center/Lamar University contracts TARC/LU-052UAL0030A and 123UAL2030A. Note the results in this study do not necessarily reflect policy or science positions by the funding agencies.

TABLE OF CONTENTS

LIST OF FIGURES

LIST OF TABLES

Page

1. INTRODUCTION

Improving understanding of the near shore environment is important in order to assess the impact of offshore oil and gas exploration on the environment including air quality impacts. Regulators at the federal level and coastal states have a responsibility to ensure that State Implementation Plans (SIP) and new source review adequately addresses air quality impacts both onshore and in the coastal environment of offshore facilities. Since Prevention of Significant Deterioration (PSD) regulations incorporate offshore facilities and onshore new sources, this responsibility includes developing and assessing tools for sources offshore and in the onshore coastal environment. The Bureau of Ocean Energy Management, Regulation and Enforcement has a long history of carrying out studies and developing tools to improve air quality characterization and prediction in the coastal and near shore environment.

Because of this responsibility, understanding of the coastal atmosphere including sea breezes, land breezes and nearshore atmospheric structure is important to properly assessing air quality impacts. The vertical shear in sea breeze regimes and timing of sea breeze events is important to plume spread and transport both for near shore facilities and on shore facilities. The behavior of sea breezes and coastal temperature and turbulence structure is tied to both sea surface temperatures and onshore land temperatures. Thus, the development of land surface parameterizations and parameter specifications (such as moisture availability, heat capacity, surface roughness) is important to proper specification of the atmospheric structure which is critical to air quality impacts assessment. Additionally, the coastal cloud structure is vitally important to surface heating rates, impacting boundary layer structure and temperature. Further, coastal cloud modification of photolysis fields in photochemical processes is important to ozone and aerosol formation and decay.

The work presented in this report is directed at improving the specification of surface parameters such as insolation, soil moisture and surface heat capacity that control the developing land boundary layer through use of satellite data. The tools and techniques using the satellite data are tested in the context of the type boundary layer models used in air quality models. In particular, the techniques using satellite data for determining soil moisture availability (McNider et al., 1994), surface heat capacity (McNider et al., 2005), insolation (McNider et al., 1995) and photolysis fields (Pour-Biazar et al., 2007) are examined in the context of recent national level air quality studies undertaken along the Texas Gulf Coast (TexAQS2000).

The University of Alabama in Hunstville (UAH) has had a long history of working with National Aeronautics and Space Administration (NASA), National Oceanic and Atmospheric Administration (NOAA) and applied agencies such as the National Weather Service, the U.S. Environmental Protection Agency (USEPA) and State air quality programs in developing and transferring satellite products and techniques to the user community. At the present UAH is supported by a NASA Applications Grant to transfer some of the techniques outlined in the present report into the USEPA Community Air Quality (CMAQ) modeling system. Through this process USEPA works with UAH and the user community in testing the techniques. The techniques then become part of the USEPA supported system that can be broadly disseminated

and used by states and air quality consultants. The UAH expects that this synergistic relationship between NASA, NOAA and the user community to extend satellite applications will continue.

2. IMPROVING PHOTOLYSIS RATES IN PHOTOCHEMICAL AIR QUALITY MODELS USING SATELLITE DATA

Note the following discussion was derived from Pour-Biazar et al. (2007).

A key component of air quality modeling is the correct estimation of photodissociation reaction rates (or photolysis rates) for chemical species. These rates (the rate at which photochemistry takes place) depend on the intensity of solar radiation reaching a given point in the atmosphere and the molecular properties of the molecule undergoing photodissociation. Therefore, attenuation or enhancement of radiant energy due to atmospheric absorption and scattering is an important factor in determining the photolysis rates. Since clouds can significantly alter the solar radiation in the wavelengths affecting the photolysis rates, they can have considerable impact on the photochemistry.

Reliable estimates of photolysis rates are essential in reducing the uncertainty in air quality modeling. Air quality models rely on radiative transfer models for the prediction of photolysis rates. There are a suite of radiative transfer models [see Barker et al., 2003] that take extraterrestrial solar flux, optical properties of the atmosphere, and surface albedo as inputs to describe the propagation of radiation in the atmosphere. These models are widely used for both research and in weather and climate models. Barker et al. (2003) compared the performance of 25 radiative transfer models with respect to the impact of unresolved clouds; most of the models used in their study underestimated atmospheric absorption of solar radiation. Other studies [Collins et al., 2000; Liao et al., 1999; Jacobson, 1998; Dickerson et al., 1997; Castro et al., 1997; Ruggaber et al., 1994; Madronich, 1987] have investigated the effects of changes in atmospheric conditions and surface albedo on the estimates of photolysis rates. Most of these studies conclude that aerosols and clouds play an important role in modifying the photolysis rate either by enhancing it due to light scattering, or by reducing it due to absorption and attenuation of light.

The Community Multiscale Air Quality modeling system (CMAQ) [USEPA, 1999] uses a two step approach for calculating the photolysis rates. This approach is similar to that of the Regional Acid Deposition Model (RADM) (Chang et al., 1987) and is a typical method used in most air quality models. First, in a preprocessor, a radiative transfer module (based on Madronich, 1987) is used to compute clear sky photolysis rates for a range of latitudes, altitudes, and zenith angles. Then, within the chemical transport model, the tabular photolysis rates are interpolated for each location and corrected for cloud cover. There are two major concerns with this approach as far as cloud correction is concerned. First, estimation of cloud transmissivity in models is highly parameterized and, therefore, introduces a large uncertainty. Second and most important, the cloud information is provided by a mesoscale model, which has difficulty with the spatial and temporal placement of clouds and their vertical extent. The mesoscale model used in the CMAQ modeling system is the Fifth-Generation Penn State/NCAR Mesoscale Model (MM5) (Grell et al., 1994; NCAR, 2003).

Prediction of clouds in mesoscale models used for air quality modeling applications has always been a difficult problem. Cloud processes on grid cell sizes of 4 km and greater are

highly parameterized and uncertain. One of the weakest areas of meteorological models is the correct prediction of clouds at the correct location at the correct time. In air quality case studies, observations could conceivably be used to improve the specification of clouds. Unfortunately, standard weather service observations are not sufficiently dense to be used for cloud specification. However, geostationary satellite data can provide the desirable coverage with sufficient spatial resolution. The Geostationary Operational Environmental Satellite (GOES) has the capability to measure cloud properties such as optical reflectance down to scales of 1 km and cloud top heights to 4 km, and for time scales down to an hour or less. Arola et al. (2002) evaluated satellite retrievals of ultraviolet radiation (UV) over Europe and did not find any significant systematic bias in many of the retrieval methods used.

In a previous study, McNider et al. (1998) used satellite-derived broadband cloud transmittance to correct NO_2 photolysis rates within the Regional Acid Deposition Model (RADM) [Chang et al., 1987]. The case study for August 3, 1988 episode focused on the eastern United States. They concluded that the overestimation of the clouds by the meteorological model significantly reduced the photolysis rates as compared to the satellite-derived rates.

This discussion presents the results from incorporating satellite-derived transmissivity and cloud top height to provide the cloud properties needed in photolysis rate calculations, and then use these revised photolysis fields in the CMAQ model. This is a first-order incorporation of the cloud effects. The GOES visible and infrared (IR) data collected and processed during the Texas Air Quality Study, 2000 (TexAQS2000) period are utilized. The impact of the satellite-based photolysis fields versus MM5-derived photolysis fields on ozone production is examined.

2.1. Methodology

The cloud correction method is based on the current CMAQ formulation. The CMAQ uses a two step approach for photolysis rate calculations, clear sky photolysis rates are calculated, and then they are corrected for the cloud cover. While the implementation within CMAQ is described, the method can be applied to any air quality model that uses a similar two step approach for the calculation of photolysis rates. First a brief description of the current method used in CMAQ is presented, followed by a brief description of our approach. The main issue explored here is the use of satellite-derived clouds as opposed to model-generated clouds for cloud correction. Therefore, the technique presented here can be beneficial to any other model that uses model-generated clouds for cloud correction.

Current Method for Cloud Correction in CMAQ

The method used for photolysis rate calculation and the subsequent cloud correction to those rates are described in USEPA's Models3 Science document [USEPA, 1999]. The Photolysis rate (s^{-1}) is represented by:

$$J = \int_{\lambda_1}^{\lambda_2} \sigma(\lambda)\varphi(\lambda)F(\lambda)d\lambda \quad (1)$$

Where $\sigma(\lambda)$ ($m^2/molecule$) is the absorption cross-section for the molecule undergoing photodissociation as a function of wavelength λ (μm); $\varphi(\lambda)$, the quantum yield (*molecules/photon*), is the probability that the molecule photodissociates in the direction of the pertinent reaction upon absorbing the radiation of wavelength λ; and $F(\lambda)$ is the actinic flux ($photons/m^2/s/\mu m$).

By providing the actinic flux for clear sky, photolysis rates (J_{clear}) can be calculated by equation (1). In CMAQ, clear sky rates are then corrected for cloud cover. The cloud correction is based on Chang et al. (1987) and Madronich (1987) with some alterations as described in CMAQ Science Document [USEPA, 1999]. Below the cloud, the rate is corrected by:

$$J_{below} = J_{clear}\left[1 + f_c(1.6tr_c\cos(\theta) - 1)\right] \quad (2)$$

Where f_c is the cloud fraction for a grid cell, tr_c is cloud transmissivity, and θ is the zenith angle. The above formulation leads to a lower value for the photolysis rates below the cloud, where the cloud transmissivity is reduced. Above the cloud, the photolysis rate is modified as:

$$J_{above} = J_{clear}\left[1 + f_c\alpha\cos(\theta)(1 - tr_c)\right] \quad (3)$$

Here α is a reaction dependent coefficient that further modifies the rates above the cloud [Chang et al., 1987]. This is to allow for the photolysis rate enhancement resulting from the reflected radiation from the cloud top. Within the cloud, the photolysis rates are obtained by interpolating between cloud base and cloud top values (which is a deviation from Chang et al. 1987). Therefore, based on the formulation above, the cloud transmittance and cloud fraction are required for calculating cloud correction for photolysis rates. Since in-cloud photolysis rates are interpolated, cloud-base and cloud-top heights must also be known.

In CMAQ, the calculation of cloud transmissivity is highly parameterized [USEPA, 1999] and is formulated based on a parameterization suggested by Stephens (1978). By obtaining cloud thickness (H_c) and liquid water content (w) the liquid water path (g/m^2) is calculated by:

$$LWP = wH_c \quad (4)$$

Then the broadband cloud optical depth (τ_c) as a function of liquid water path, assuming that the drop-size distribution within the cloud column is uniform, is calculated as [Stephens, 1978]:

$$\tau_c = 10^{.2633 + 1.7095\ln[\log_{10}(LWP)]} \quad (5)$$

Finally, cloud transmissivity is determined by:

$$tr_c = \frac{5 - e^{-\tau_c}}{4 + 3\tau_c(1 - \beta)} \quad (6)$$

Where β is the scattering phase-function asymmetry factor [USEPA, 1999]. In Equation (6) it is further assumed that β is constant and has a value of 0.86. For optically thin clouds where $\tau_c<5$ cloud correction is not performed. As evident from this formulation, even if the MM5-derived cloud fields were correct, there is some uncertainty in the calculation of cloud transmittance by equation (6) due to the assumptions used in different steps (as stated above).

From GOES satellite observations, we are able to recover broadband cloud transmissivity and the cloud top height. Also, since the GOES cloud mask algorithm can detect clouds (and the impact of sub-scale clouds) at 4 km resolution, an observed cloud fraction can be calculated for coarser grid cells as the fraction of cloudy pixels within a grid cell. Cloud base height is estimated as the local condensation level (LCL) from the temperature and mixing ratio profiles simulated by the mesoscale model. In this study, we replaced tr_c and f_c in equations (2) and (3) with the satellite-inferred quantities to perform the cloud correction.

2.2. Retrieval of Goes Broadband Visible Transmission and Cloud Top Heights

The Infrared Measurement and Processing Group (hereafter IR Group) at the National Space Science and Technology Center performed the satellite retrievals for this study. Currently, the IR group uses GOES Product Generation System (GPGS) to provide routine real-time retrievals of skin temperature, total precipitable water, cloud top pressure, cloud albedo, surface albedo and surface insolation for the use of meteorological and air quality models [Haines et al., 2004]. As input, GPGS needs a first guess field for its retrievals and the model grid information if the product is to be used in a grid model. For this study, the MM5 simulation that was utilized for the CMAQ runs provided the required information to GPGS and the retrievals reflected the MM5 grid cell values.

The algorithm used for the retrieval of albedo and surface insolation is the implementation of Gautier et al. (1980) method complemented by the improvements from Diak and Gautier (1983). The method uses information from the GOES Imager visible channel (0.52-0.72 μm) at 1 km resolution and employs a clear and a cloudy atmosphere to explain the observed upwelling radiant energy. The model (what model?) applies the effects of Rayleigh scattering, ozone absorption, water vapor absorption, cloud absorption, and cloud reflection. The effects of Rayleigh scattering are modeled after Coulson (1959) and Allen (1963) for the GOES visible band (radiant flux as viewed by the satellite) and for the bulk solar flux incident at the surface. Ozone absorption is modeled after Lacis and Hansen (1974). Water vapor absorption is assumed to be negligible in both the surface and cloud albedo calculations (explaining the observed radiance in the GOES visible band), but accounted for when applying the total solar flux in the surface insolation calculation. Water vapor absorption coefficients are obtained from Paltridge (1973), and total column water vapor is assumed to be 25 mm and adjusted for solar zenith angle. Cloud absorption (for thick clouds) is assumed to be a constant 7% of the incident flux at the top of the cloud (Diak and Gautier, 1983).

The surface albedo for the entire domain is calculated by using the clear-sky composite image. For the current study, a 20-day composite centered on the period of the case study was used to generate the clear-sky composite image. The single composite image records the minimum albedo value for each pixel for a given hour. Assuming that for any given hour during the day (for the entire month) each pixel experiences clear-sky at least once, the minimum value would represent the clear-sky value for that pixel. This formulation assumes that the visible channel surface albedo does not vary significantly within the time period of composite.

The insolation is calculated as the sum of solar radiation incident at the surface from both direct and diffuse sources and also includes the effect of attenuation by clouds. For the clear-sky case, the incident short-wave radiation at the surface is 1) the incident solar flux that is attenuated by Raleigh scattering, ozone and water vapor absorption, and 2) the surface reflected flux scattered back to the surface by Raleigh scattering. With the surface albedo known, and the absorption and scattering processes estimated, the surface insolation is calculated directly.

For the cloudy-sky, the satellite-derived radiant energy is the sum of atmospheric backscatter, reflection of the incident solar flux from the cloud surface, backscatter within the cloud by Rayleigh scattering, and the amount of surface reflection that reaches satellite after attenuation. Since the radiance at the satellite, the surface albedo, and estimates of the scattering and absorption are known, the radiation formulation can then be solved for the cloud albedo. In practice, the algorithm calculates a surface insolation using both the clear-sky and cloudy-sky formulations for a given scene. If the cloudy-sky calculation is greater than or equal to the clear-sky value, then the clear-sky value is used and the scene is assumed clear. This is consistent with the cloud albedo being near zero for clear-sky conditions. Since the effect of cloud albedo dominates in the insolation calculation, uncertainties in cloud thickness have been shown to produce only small effects on the surface insolation calculation [Haines et al., 2004].

Since the sum of cloud albedo (A_c), cloud absorption (a_c), and cloud transmittance is equal to one, then the broadband cloud transmittance is calculated as:

$$tr_c = 1. - (A_c + a_c) \qquad (7)$$

The other needed vital information for our cloud correction is the cloud top height. A cloud top pressure is assigned to each cloudy pixel. The GOES 11-μm window channel (of either the Imager or the Sounder) brightness temperature is used for this purpose. The clouds are assumed to be uniform in coverage and height over the GOES pixel. The brightness temperature for each cloudy pixel is referenced to the corresponding thermodynamic profile for the closest model grid. No attempt is made to correct the brightness temperature for the effect of water vapor above the cloud. The pressure assignment is similar to that used by Fritz and Winston (1962) and applied by Jedlovec et al. (2000). Log-linear interpolation is used between model vertical pressure levels to assign a corresponding pressure for the cloud top temperature.

The approach works well for opaque clouds where the cloud emissivity is close to unity and emission (measured by the satellite) comes primarily from the cloud top. Typical pressure assignment errors are on the order of 25-50 mb (0.5-2.0 K). For non-opaque clouds such as thin cirrus, emission from below the clouds is detected by the satellite and cannot be separated from

cloud emission without knowledge of the cloud emissivity. This is true for all relatively transparent clouds (non-opaque) including low clouds. Therefore, the bias would be greatest for non-opaque clouds.

For air quality applications, however, since the focus is on the boundary layer, the error in the cloud top pressure for the opaque clouds does not pose a significant problem. Furthermore, in our technique the cloud top height is only used for determination of the atmospheric layer in which photolysis rates are being interpolated, and does not impact the correction made to the photolysis rates within the boundary layer (as the transmittance is estimated directly from the satellite observations). In addition, the determination of cloud-top in CMAQ is limited by the vertical resolution of the model, which usually is too coarse in the free-troposphere. For the non-opaque clouds, the cloud transmissivity is large and therefore the modifications to photolysis rates are small and thus the impact of the error in the cloud top height is further reduced. Figures 1a and 2a illustrate a situation on August 24, 2000, where the satellite observation indicates most of the domain is cloudy, yet in fact only the cloud mass over the Galveston Bay area is opaque. For most of the domain, the clouds are almost transparent and the retrieved cloud transmittance is close to 1. For low transparent clouds the estimate of cloud top pressure is not reliable. Thus, in such a situation we still make the necessary corrections and allow for a thin cloud above the cloud base by assuming that the cloud is only one model-layer thick.

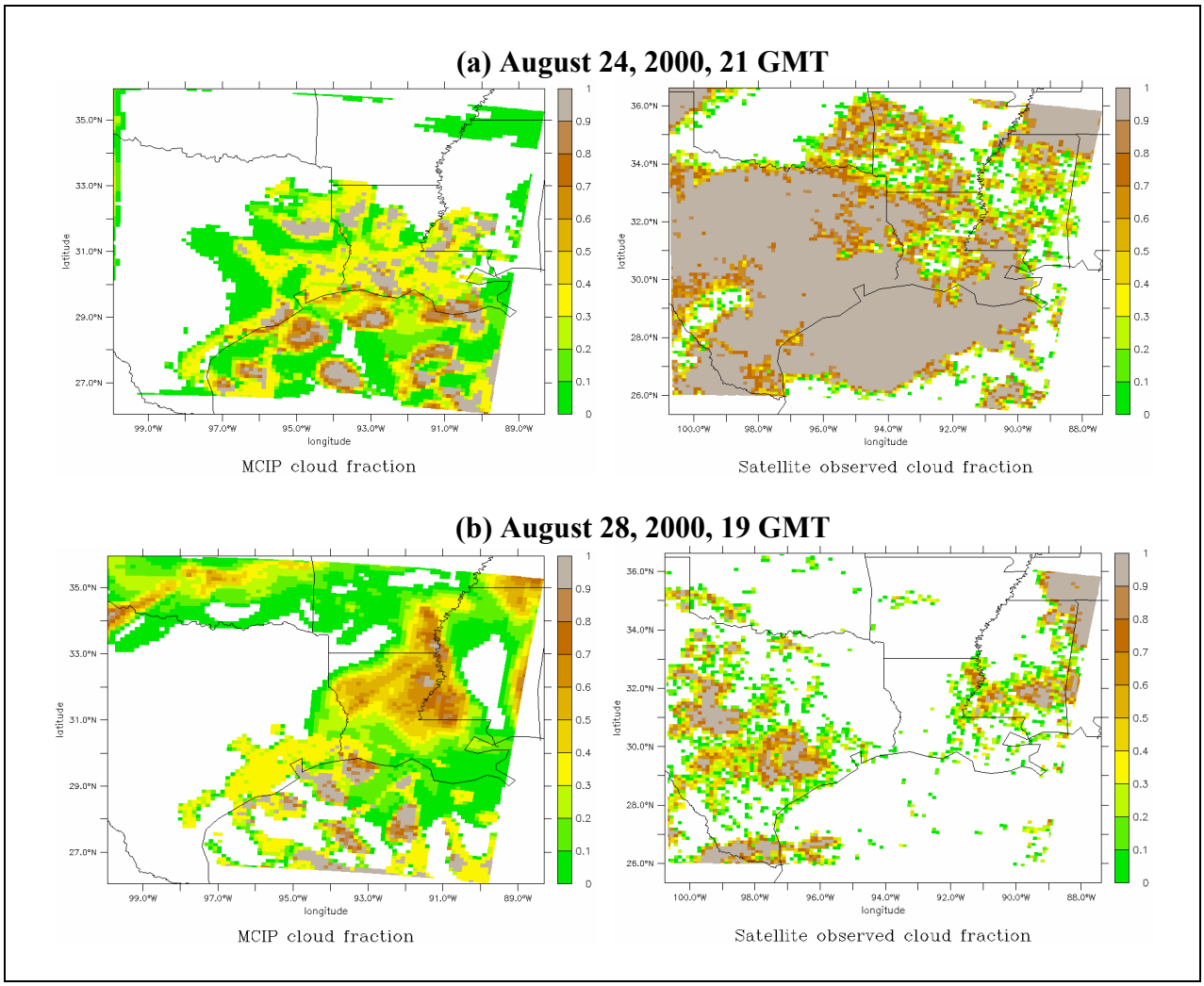

Figure 1. CMAQ/MM5 predicted and GOES satellite observed cloud fields for (a) August 24, 2000, 21 GMT, and (b) August 28, 19 GMT.

2.3. Implementation Within CMAQ

The current setup for CMAQ calculates the clear sky photolysis rates in a preprocessor and provides a tabular input to the Chemical Transport Model (CTM) [USEPA, 1999]. The meteorological data, including cloud information derived from MM5 predictions, is prepared in a Meteorology-Chemistry Interface Processor (MCIP) for the use in CTM. Within the CTM the attenuation to clear sky photolysis rates due to the presence of clouds is performed based on the input information from the meteorological model. We have made modifications to the MCIP to replace the MM5-derived (hereafter referred to as MCIP clouds) cloud information with the satellite observations.

Using satellite observations the cloud fraction in MCIP is replaced with the observed cloud fraction. From cloud top temperature (or pressure as discussed above), the corresponding

CTM layer is identified as the cloud top layer. Model surface temperature and mixing ratio are used to calculate the lifting condensation level, and is used as the cloud base height. Within the CTM, when satellite-retrieved transmissivity is present, the standard parameterization is bypassed and the satellite observations are used directly in equations 2 and 3.

2.4. Model Simulations

We implemented the technique, described above, in the CMAQ modeling system to perform a set of simulations for 12-km and 4-km resolution domains over Texas for the period of August 24 to August 31, 2000. The 12-km domain covers the eastern half of Texas, Louisiana, Mississippi, southern part of Oklahoma and Arkansas, and the southwestern corner of Tennessee. The first set of simulations utilizes CMAQ in its standard configuration, and is used as the control case (hereafter referred to as CMAQ_base or control simulation) for comparison. The second set of simulations (hereafter referred to as CMAQ_sat) uses the satellite-derived cloud information. Both sets of simulations use the same meteorological information from a single MM5 run.

The control MM5 simulation was configured to use FDDA gridded nudging, Dudhia moisture scheme, Grell convective parameterization, Medium Range Forecast (MRF) PBL scheme, RRTM radiation scheme, shallow convection scheme, and 5-layer soil model. Grell cumulus parameterization has proven to be useful for smaller grid sizes (10-30 km) as it tends to allow a balance between resolved scale rainfall and convective rainfall (Grell et al., 1991; Grell, 1993).

The CMAQ (version 4.3) was configured to use piecewise parabolic method for advection, multiscale horizontal diffusion and eddy vertical diffusion, 3rd generation aerosol model and 2nd generation aerosol deposition model, RADM cloud model, and SMVGEAR chemical solver. Carbon bond IV (CB4) chemical mechanism [Gery et al., 1989], including aerosol and aqueous chemistry is utilized to describe atmospheric reactions. The model uses 21 layers, with about 10 layers within the daytime boundary layer. The emissions for this study are based on USEPA's 1999 National Emissions Inventory (NEI99, version 2).

2.5. Results and Discussion

As described in the previous section, the meteorological information to drive CMAQ was obtained from a single MM5 run. This means that there is no change in the dynamic fields for the CMAQ simulations and the differences between CMAQ_base and CMAQ_sat simulations are only due to the impact of observed clouds on the photochemistry. This inconsistency also impacts the heterogeneous processes in the model. In the areas where the model is under-predicting clouds, use of observed clouds reduces the errors in the gas-phase chemistry but the accompanying heterogeneous chemistry in the cloud layer is non-existence in the model. On the

other hand, when the model over-predicts clouds, our technique will increase photolysis rates throughout the atmospheric column while the heterogeneous processes in the model are still active. Such errors in the current study are unavoidable (as they are inherent from the control MM5 simulation) and can only be corrected if the model is dynamically consistent with the observations. The current study is only focusing on the radiation impact of clouds on the photochemistry. The impact of cloud dynamics will be pursued in the subsequent papers.

It should be noted, however, that the uncertainty due to the impact of cloud dynamics on the vertical transport of the pollutants is also important and needs to be investigated. For example, on the afternoon of August 24, 2000, convective clouds developed over the Galveston Bay and expanded toward north/northwest. This feature was absent in the MCIP cloud fields, meaning that the vertical transport of pollutants over the Bay area into these convective cells is missing in our simulations. While our method corrects for the impact of the observed convective clouds on the photochemistry, there are still errors arising from the lack of accurate vertical distribution of pollutants due to errors in the dynamics. Therefore, here we only emphasize on model-to-model comparisons to illustrate the first-order photochemical impact of including the observed clouds. In the second part, however, we present comparisons with selected observations to illustrate that the large differences seen in the model-to-model comparison are indeed real and our technique is greatly improving the model performance.

2.5.1. Model-to-Model Comparisons

Texas and surrounding areas were extremely dry for the period of this study. With few clouds observed, this case study perhaps was not the best case to show the benefits of utilizing GOES information. Nevertheless, there was sufficient cloudiness to illustrate the impact of observed clouds on the photochemical model predictions. Figure 1 display two different cases in which the disagreement between CMAQ MCIP cloud fields and GOES satellite observations are depicted. In the case of August 24, 2000, MCIP indicated clouds in the south/southeastern part of the domain with most of it being subgrid scale (with cloud fractions less than 1) with only a few small areas of grid scale clouds over land. In contrast, satellite observations indicated a large area of cloudiness extending from south/southeast to the northwest part of the domain. Satellite observation also indicated clouds in the northeast and northern parts of the domain that were absent in the MCIP fields. However, as indicated in Figure 2, the broadband transmissivity for most of the observed clouds for this day is high, meaning that most of the clouds are not opaque and should not affect the photolysis rates significantly. But the area around Galveston Bay, including Houston, is covered with thick clouds that are missing in the MCIP fields. This is significant since this area is the major source of emissions for ozone precursors.

An error in the prediction of opaque clouds over the emission sources has major consequences. Opaque clouds (as seen in Figure 2) can significantly alter the cloud transmissivity and, thus, the photolysis rates. Over the source regions, an alteration (reduction in this case) in the photolysis rate has both a direct and an indirect impact on ozone chemistry. First, by slowing down the photochemistry, lower photolysis rates inhibit ozone production in the immediate vicinity of emission sources (direct impact). Second, due to the suppression of photochemistry, lifetime of ozone precursors is increased and the precursors can be transported

to the regions where the air mass has a different chemical composition (indirect impact). The indirect impact can take many forms depending on the type of the cloud and the time of occurrence. These include the impact on the boundary layer air further downwind (for the clouds with weak vertical motion during the day), the accumulation of the precursors in the residual layer (clouds late in the day), or alteration in the chemical composition of free troposphere (convective cells with strong vertical motion).

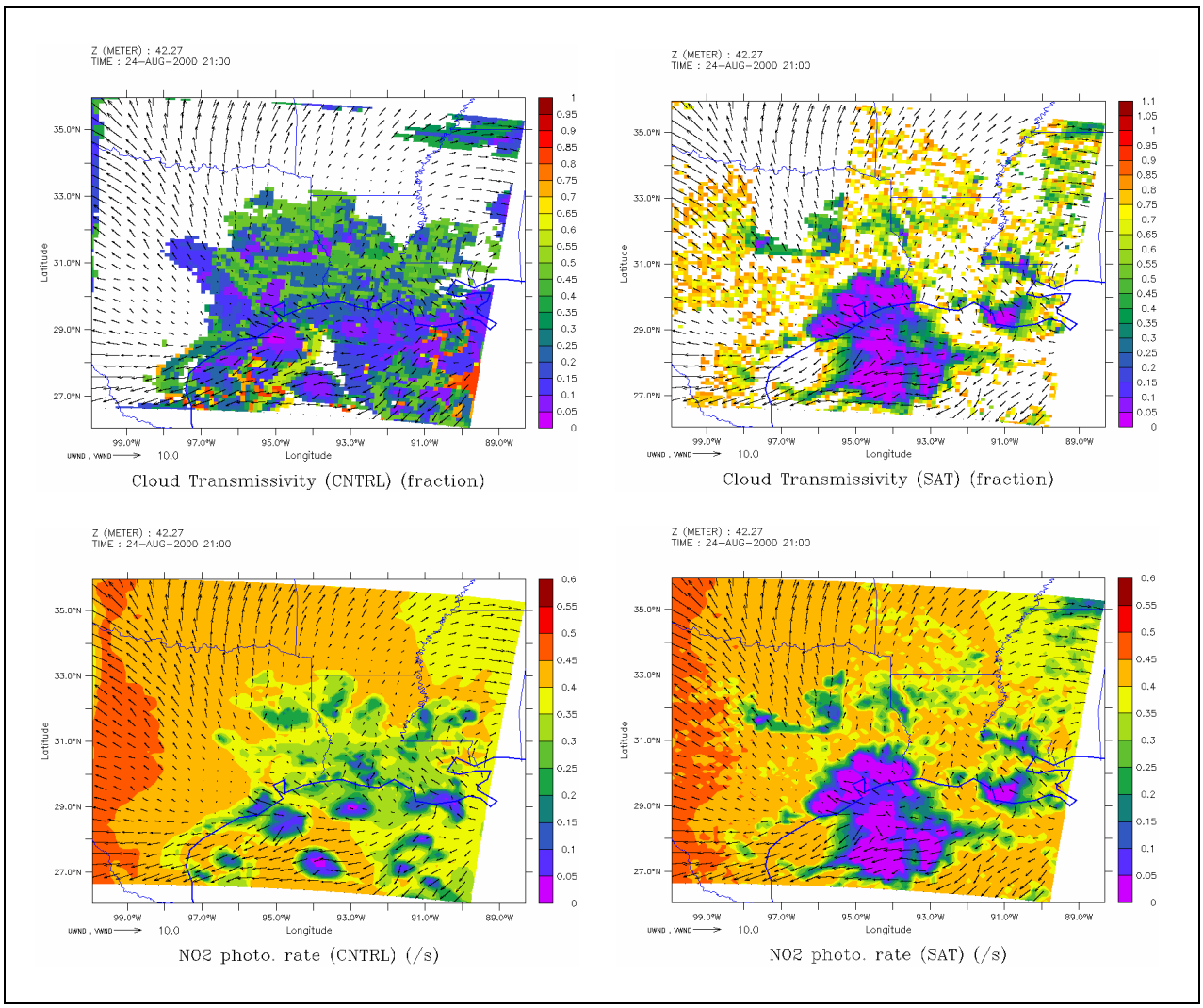

Figure 2. Cloud transmissivity and corresponding NO_2 photolysis rates for August 24, 2000, at 2100 GMT from CMAQ_base and CMAQ_sat simulations at the surface (first model layer). CNTRL simulation shows clouds in the general area as the satellite observations as indicated in the transmissivity plots (upper panel); however, they are spread out and are not as opaque as the observed clouds as indicated in both transmissivity plots and the resulting NO_2 photolysis rates (lower panel).

In the case of Galveston Bay region, nitrogen oxides (NO_x=NO+NO_2) and volatile organic compounds (VOC) are co-emitted (on the regional scale). Therefore, in this region under clear skies, ozone is rapidly produced while NO_x is transformed to products such as nitric acid (HNO_3) and peroxyacetyl nitrate (PAN). The inhibition of the photochemistry in the

presence of clouds on the other hand directly impacts the rapid formation of ozone in this area and by doing so both NO_x and VOCs remain active for a longer period of time. In short, such an event alters the chemical aging of the air mass, and the air mass continues to have the potential of producing ozone for a longer period of time during transport.

Another indirect impact of the clouds in this area is the alteration in partitioning of nitrogen oxides and the impact on nitrogen budget due to surface removal. This is caused by the disparity between the deposition velocity of NO_x and the nitrates that are produced from oxidation of NO_x. Under clear skies, as indicated before, NO_x in this region undergoes a chemical transformation and produces nitrates such as HNO_3 and PAN. In the presence of thick clouds, due to the reduction in the photochemical activities, nitrogen monoxide (NO) rapidly consumes ozone (O_3) and produces nitrogen dioxide (NO_2) while the production of HNO_3 and loss of NO_x due to chemical transformation is reduced. In this case while the partitioning of NO_x between NO and NO_2 has been altered, there is a net increase in NO_x due to its direct emissions.

Therefore in one case, under clear conditions over the Galveston Bay area in the control case, more O_3, HNO_3, PAN and other nitrates are produced in the expense of NO_x. But under cloudy conditions (satellite assimilation case), due to the slowing down of the photochemistry, most of the NO_x will remain intact and will not be lost in the ozone production to produce nitrates. The rate of surface removal for NO_x is an order of magnitude less than that of nitric acid [Biazar, 1995]. Therefore, in control simulation there is a much larger loss of total reactive nitrogen ($NO_y = NO_x + HNO_3 + PAN +$ other compounds produced from the oxidation of NO_x) than the assimilation simulation.

To show such an indirect impact, a grid point close to the bay (southeast of Houston at 29.7N, 95.3W (marked **A** on the map in Figure 3) was examined. On August 24, the control simulation indicates a small overprediction followed by a substantial underprediction of clouds for this location. Comparing the accumulated hourly surface deposition from the two simulations (CMAQ_base vs. CMAQ_sat) for NO_x and HNO_3 reveals that the absence of clouds (in the control case) increased the surface removal of HNO_3 for several hours for up to 9 g/hectare/hr (Figure 4). The loss of nitric acid positively correlates with the increased ozone production and increased NO_2 photolysis rate at this location (as shown in Figure 5a) and is a result of the increased HNO_3 production due to active photochemistry. The inclusion of clouds resulted in less than 1 g/hectare loss of NO_x in this case, as in the CMAQ_sat case NO_2 photolysis rate decreases, and consequently O_3 decreases and NO_2 increases.

In contrast to the August 24th case, on August 28, MCIP indicates a large area of cloudiness over western Mississippi, southern Arkansas, and Louisiana extending to the south Texas (Figure 1b). This is absent in the GOES observations. GOES observations indicate subgrid cloudiness in the western part of Texas. From Figure 2b it can be seen that these clouds are highly transparent and do not alter the photolysis rates significantly. Therefore, in this case we have a significant ozone formation in the vicinity of the emission sources that would be absent in the control simulation.

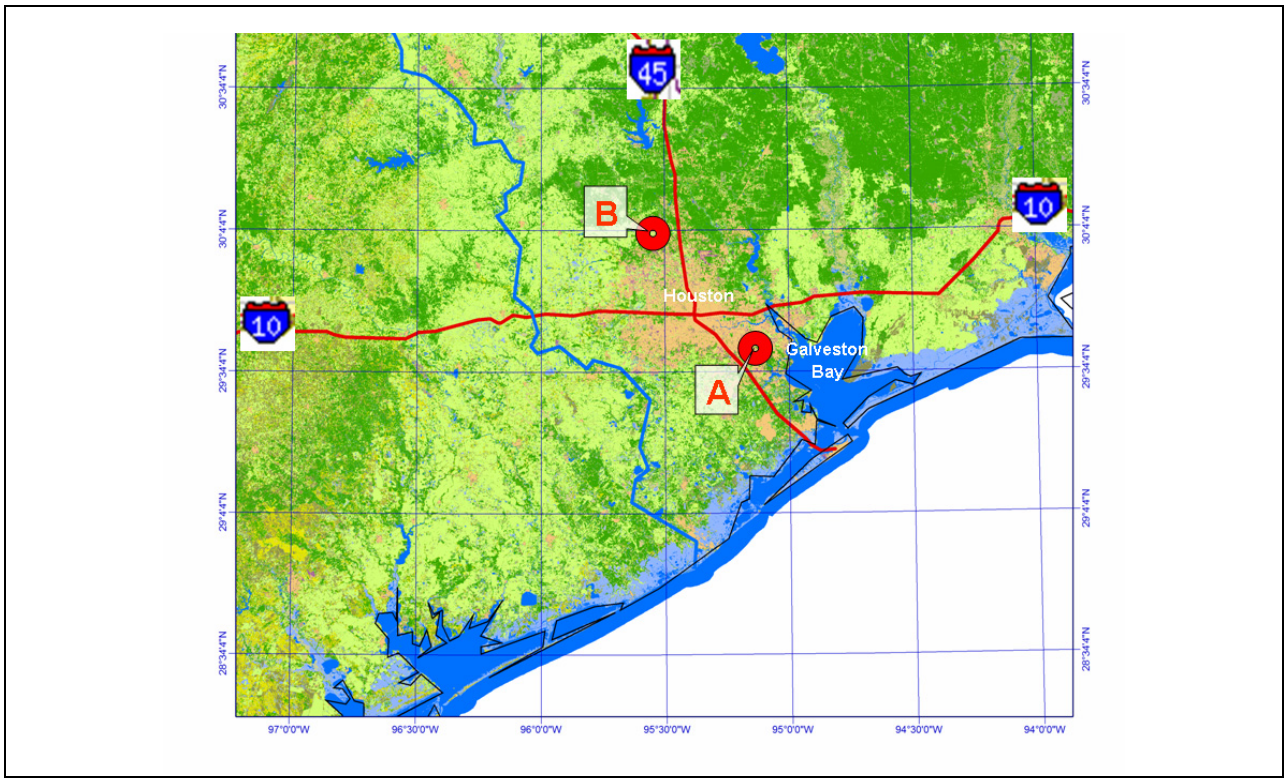

Figure 3. Image of Houston-Galveston Bay area. Locations at (A) 29.7°N, 95.3°W and (B) 30°N, 95.6°W are marked with red circles.

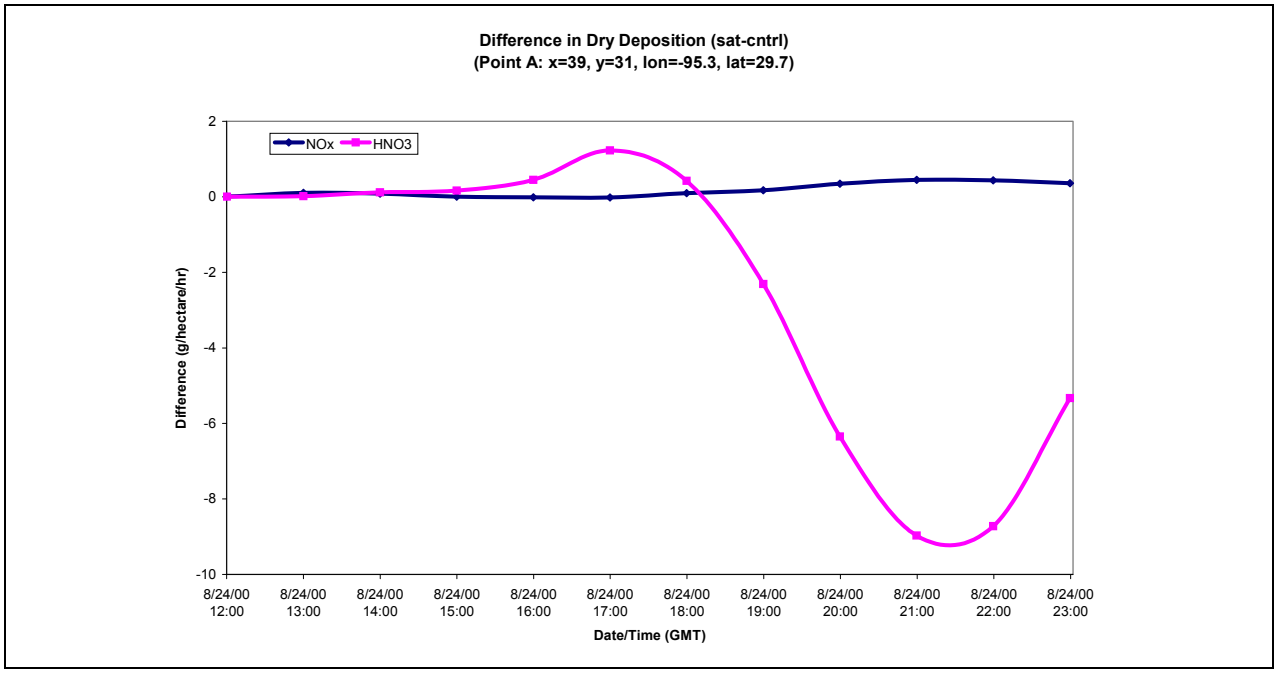

Figure 4. Hourly differences in NO_x and HNO_3 surface removal from the two simulations (control vs. satellite assimilation) for point A over Houston-Galveston Bay area for August 24, 2000. Control and base are used interchangeably throughout this document.

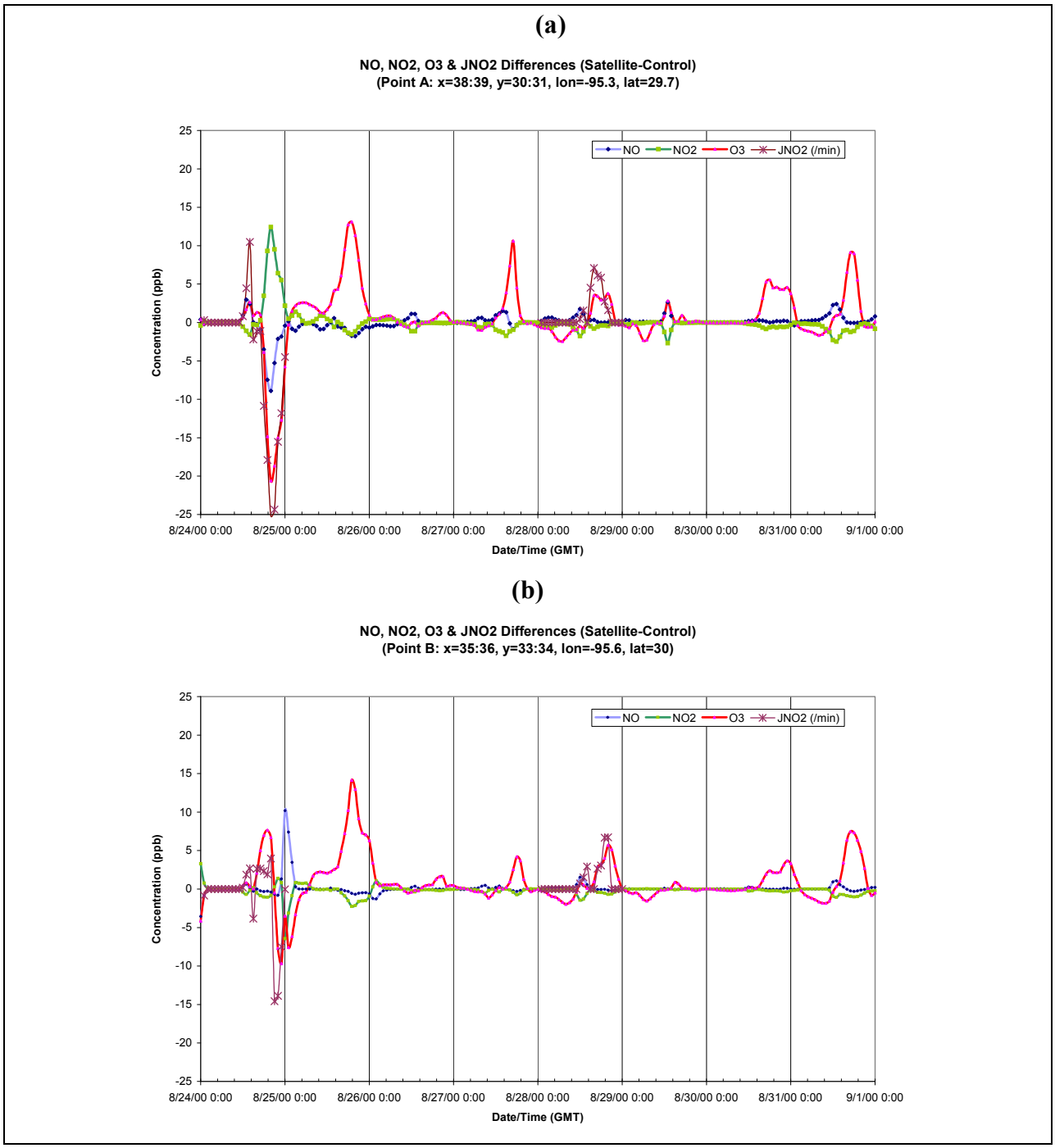

Figure 5. Differences between NO, NO_2, and O_3 (ppb) for August 24 through August 31 between satellite cloud assimilation and control simulations for grid cells A and B as marked in Figure 3 (A upper panel and B lower panel). JNO_2 (/min) is only presented for August 24 and August 28. In the text the emphasis is on the O3 decrease on August 24 for point A.

The impact of such alterations in the photolysis rates on the local atmospheric chemical composition can be substantial, especially on the chemical species with the shorter photochemical lifetime. Figures 6 and 7 exhibit the largest differences in NO, NO_2, NO_x, and ozone between the assimilation and control simulations over the entire period of study for the 12-km domain. The figures represent the extreme cases of discrepancy between control and assimilation simulations, and these extremes need not occur at the same time. However, examining the time series of larger values indicated that they occur about the same time and represent a shift in NO_x partitioning. This is evident in spatial patterns in Figure 6 as the negative/positive values for NO are co-located with the positive/negative values of NO_2. The areas marked with a large negative NO difference between the assimilation and control correspond to the situation where MCIP indicates over-prediction of clouds and therefore most of NO is converted to NO_2 (and vise versa). These areas are confined to the large source regions, as evident for example over the Houston-Galveston Bay area, indicating a much faster photochemical activity and rapid ozone formation.

For the NO_2 case (Figure 6b) there are broader areas of large discrepancy. Over the Texas region, this indicates the transport of NO_x outside the source region where the lifetime of NO_2 is increased. This is perhaps due to the transport and dilution of the air mass outside the source region and mixing with an air mass of lower VOC where the rapid ozone formation is inhibited. The evidence for the above statement can be seen in Figure 7b in which largest ozone differences are depicted. Also, the large discrepancy in NO_x (Figure 7a) to the north of Houston is indicative of NO_x transport out of the source area due to inhibition of photochemistry in the presence of clouds.

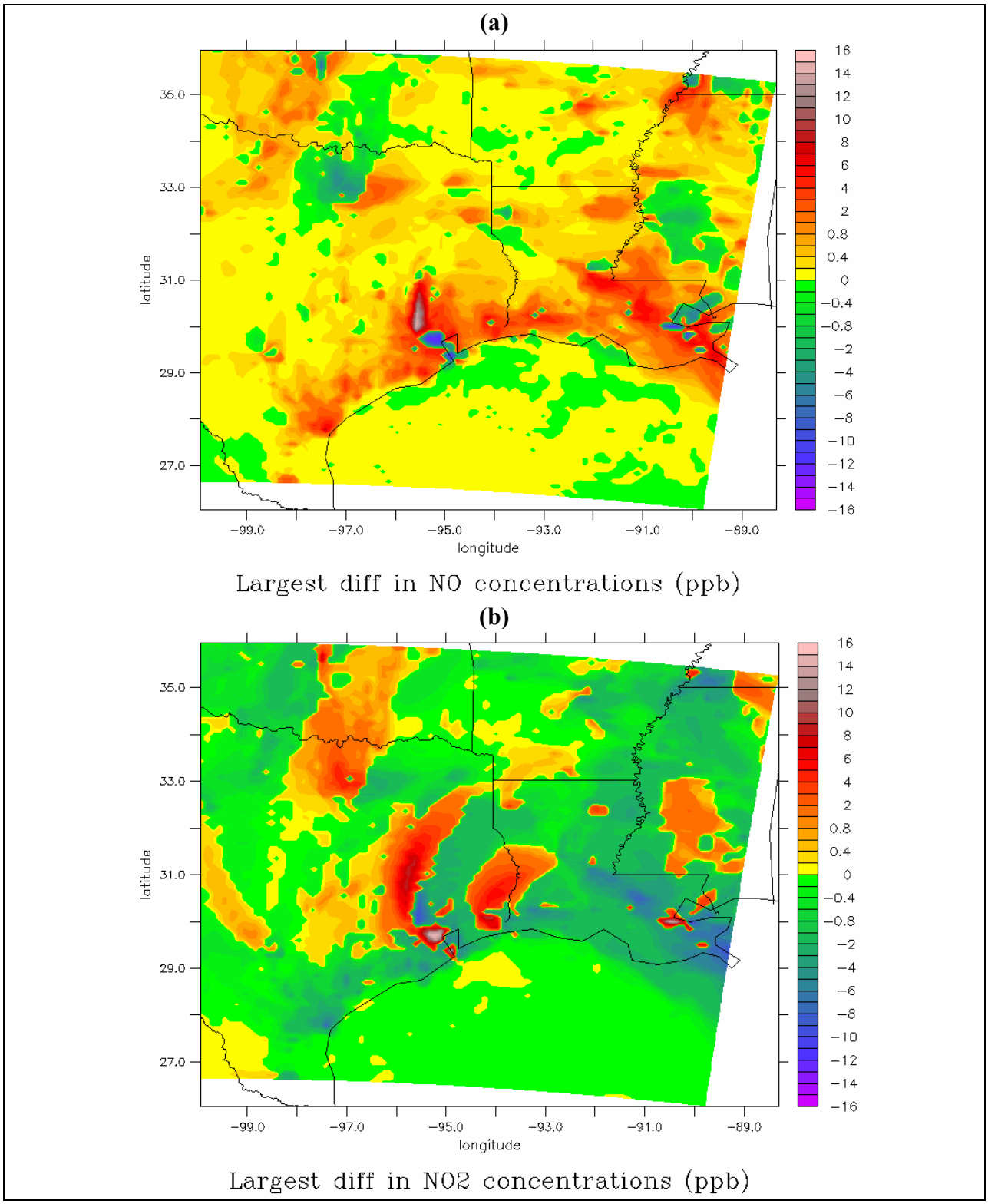

Figure 6. Extreme differences in (a) NO and (b) NO_2 between assimilation and control simulations (assim-control) for the entire period of study covering from 0 GMT, August 24, 2000, to 0 GMT, September 1, 2000.

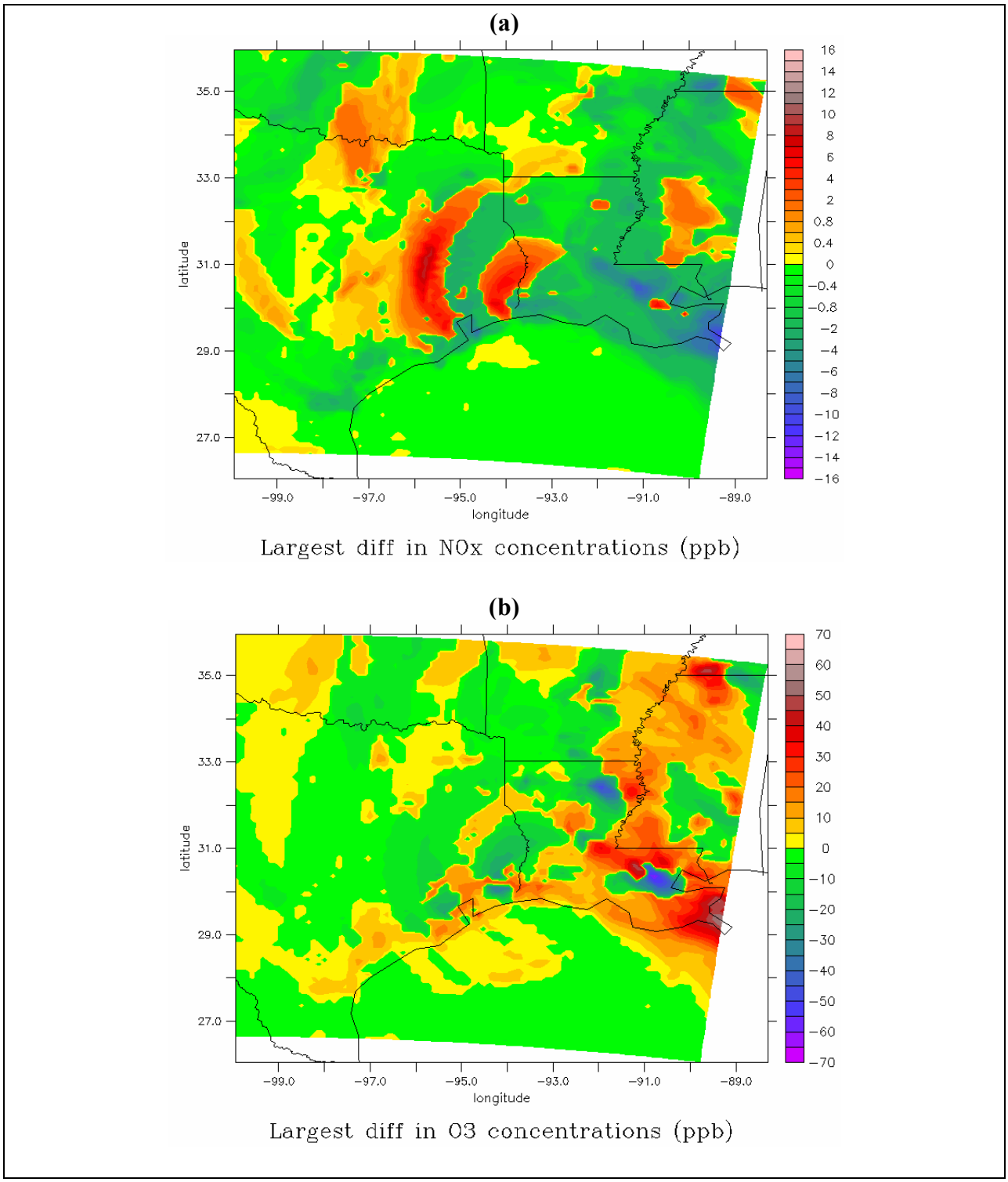

Figure 7. Largest differences in (a) NO_x and (b) O_3 between assimilation and control simulations (assim-control) for the entire period of study covering from 0 GMT, August 24, 2000, to 0 GMT, September 1, 2000.

Figure 7b also indicates that there are times that the impact of our method on ozone concentration can be quite high (as much as 60 ppb). While these extreme cases are mostly localized in space and time, sustained differences of several ppb over broader areas are more common. Comparing the extreme values of NO_x and ozone, there is a good correlation between higher ozone concentrations in the assimilation run and lower NO_x concentrations (and lower NO_2 concentrations). This indicates the presence of observed clear sky in contrast to MCIP indicating over-predictions of clouds. Therefore, the assimilation run produces more ozone and nitrates at the expense of NO_x. On the other hand, under-predictions of clouds in MCIP cloud fields resulted in higher ozone values in the control run for the east/southeast and northern part of Louisiana and a large part of central Texas.

As indicated in Figures 6 and 7, the impact of alterations in the photolysis rates on the local atmospheric chemical composition can be substantial, especially on the chemical species with the shorter photochemical lifetime. It should be noted, however, that the domain-averaged differences only show a maximum of 2 ppb for August 26 and are mostly between +/- 1 ppb for other days. Domain-averaged differences also exhibit a diurnal variation with higher predicted ozone for the assimilation run. This indicates that in this case study the overall impact of clouds in the two simulations over the 12 km domain is not drastically different, meaning that we have had as much under-predictions as we had over-predictions. This is an indirect way of comparing the impact of total cloud cover in the two simulations and concluding that they are not very different. But the large differences in ozone concentration in Figure 7, for example, indicate that the two simulations are very different in the temporal and spatial distribution of the clouds. Perhaps further analysis of these results with respect to daytime ozone on particular days would be needed to examine the impact of cloud correction on peak ozone.

Houston-Galveston Bay Area and the Case of August 24

As evident from Figure 6, there are large differences between the two simulations over Houston-Galveston Bay area. In particular, there seems to be a sharp contrast between the air to the southeast of Houston and that of north/northwest of Houston. We picked two representative grid cells for these areas to be examined in more detail. The cells are marked with red circles in Figure 3. The coordinate for the cell to the southeast of Houston is 29.7N, 95.3W (marked **A**), and the cell to the northwest has a coordinate of 30N, 95.6W (marked **B**).

Figure 5 illustrates the differences in NO, NO_2, and O_3 between the two simulations for these two grid cells (CMAQ_base-CMAQ-sat or control-sat). The figure also shows the differences in NO_2 photolysis rates between the two simulations for August 24 and August 28. Since the photolysis rates are not one of the standard outputs from the model, they were not saved for the entire period of simulation. However, the available data for both days clearly emphasizes the direct impact of the clouds as a positive difference in photolysis rate corresponds to a positive difference in O_3 concentration and a negative difference in NO_2 concentration.

Interestingly, the extreme differences noted in Figure 6 for cell A appear to be from August 24. This also coincides with a large difference in O_3 (Figure 7b) for this cell. While the differences on August 24 are extreme for cell A, large differences are observed on many days for

both grid cells. In almost all cases a good negative correlation exists between O_3 differences and that of NO_2, indicating that most of these daytime differences are due to a discrepancy between modeled and observed clouds, and are the result of alterations in photochemical activity. The difference in O_3 is more pronounced than that of NO and NO_2, since in the control run not only O_3 production has been abated, but also at the same time O_3 is being consumed by NO to produce NO_2. In some cases, as in the case of August 24, most of the difference seen is due to O_3 consumption by NO and the additional photochemical production is negligible. It should be noted, however, that our emissions over Houston-Galveston area could be low with respect to anthropogenic hydrocarbon emissions [Allen et al., 2002]. If this proves to be the case, an increase in the hydrocarbon emissions would result in fast photochemical reaction and even higher near source ozone production and will lead to a higher discrepancy between control and assimilation simulations. The increase in the hydrocarbon emissions would expedite the photochemical activity near NO_x sources with respect to ozone formation in the cloud-free areas. Therefore, abating the photochemistry in such a case would enhance the ozone decrease.

On August 24, in mid-morning to early-afternoon period, model dynamics indicate a nicely formed see breeze that extends deep (over 200 km) inland. The flow generally has a curvature, starting as an easterly/southeasterly flow offshore and turning to a southerly flow over land. Later in the afternoon, the inland flow becomes westerly and a convergence zone forms along the coast. In particular, over west/southwest of Houston-Galveston (HG) area the winds are calm after 20:00 GMT. About this time, satellite observations indicate the formation of the convective cells from south/southeast of HG area which later advances inland toward north/northwest. This created a situation in which the emissions to the southeast of HG were accumulating in the model as the cloud correction (according to the satellite observations) took place. The extreme values for point A occur at 21:00 GMT.

In the control simulation, only about 5 ppb of ozone is produced (net change due to all the processes) from 18:00 to 21:00 GMT (going from 18 ppb to 23 ppb). In the presence of clouds in the assimilation simulation, most of the ozone is consumed by NO producing NO_2 and creating large differences seen in Figure 5. As mentioned earlier, since the surface removal of NO_x is slower than that of HNO_3, most of the NO_2 in this air mass (50 ppb for the grid cell A) remains intact and will be converted instantly back to O_3 as soon as it is exposed to sunlight.

2.5.2. Verification of Model Results

Up to this point we have compared the results from the satellite assimilation simulation against the control simulation, in which CMAQ in its standard configuration was applied. Now, the question is that while the differences in concentrations of ozone and nitrogen oxides between the two simulations are large, are these differences real and have we been able to correct model errors of the same magnitude? In other words, can we verify these results against observations and show that model predictions have improved?

We acknowledge that the emissions used in this study need improvement and the uncertainties arising from the problems with the emissions are high. Nevertheless, for an area impacted by the cloud cover (or lack of it), we expect to see a variation in the concentrations that

is more in line with the observations. Our hypothesis was that, for the areas impacted, the errors due to incorrect cloud cover in the model far exceed the errors caused by inaccurate emissions. To test this hypothesis, we compared ozone concentrations from the two simulations (CMAQ_base vs. CMAQ_sat) with USEPA's AQS (Air Quality System, http://www.epa.gov/ttn/airs/airsaqs) observations for the entire period of simulations.

The overall large-scale spatial distribution of the predicted ozone for both the control and satellite assimilation simulations generally agreed with observations. Figure 8 depicts a snapshot of CMAQ_sat predictions at 21:00 GMT (15:00 CST) on August 24, 2000. The model is able to predict the low ozone concentrations next to Galveston Bay as well as the high ozone concentrations in the Dallas area. However, model predictions of high ozone concentrations in many rural areas and smaller towns cannot be substantiated due to the large gaps in the observational network.

By using satellite clouds, the bias (mean error) for surface ozone predictions was reduced by 26%, from -4.05 to -2.99, while the RMSE was reduced by 3%. The predictions of peak ozone were improved by 1%. The domain-average predictions of peak ozone exhibit an insignificant improvement, but examination of the individual sites impacted by cloud misalignment indicate a much greater improvement. While these statistics indicate an improvement in ozone predictions, they are unable to show the full impact of satellite assimilation. Several factors affect large-scale statistical evaluation for this study. First, there are large data voids in the observational network, and since there are large spatial variations in surface ozone, performing objective analysis to fill-in the gaps carries significant uncertainties. Second, most of the monitors are located in the vicinity of urban centers where they are largely impacted by local emissions and local weather. Therefore, several monitors that may reside within one model grid can exhibit large variations (up to 50 ppb for ozone). In such cases doing a simple averaging for the cluster of observations will not suffice, especially since the model also indicates a large spatial gradient from one cell to another (urban to rural). Additionally, the problems with emissions, lateral boundary conditions for a relatively small domain, and lack of clouds for a significant part of this study also contributed to errors over the entire domain. Such errors will lead to modest statistics that conceal the improvements at individual sites impacted by observed clouds. Therefore, to test our hypothesis we evaluated model predictions over selected locations where the cloud impact was significant.

For the selection of locations we referred to Figure 7b and identified the areas where the differences between the two simulations were the largest. In those areas, we picked the grid boxes that contained an observation site. Some of the largest differences occurred in the eastern part of the domain and over southern Mississippi and southeastern Louisiana. We could identify three grid boxes in that region fulfilling our requirements, namely two locations over New Orleans area and one over South Mississippi. As evident from Figure 7b, some of the extreme under- and over-predictions of ozone by the base simulation occurs over this region. While these extremes do not occur at the same time, having the largest under- and over-predictions of ozone in the same area indicates the importance of cloud effects in the source regions.

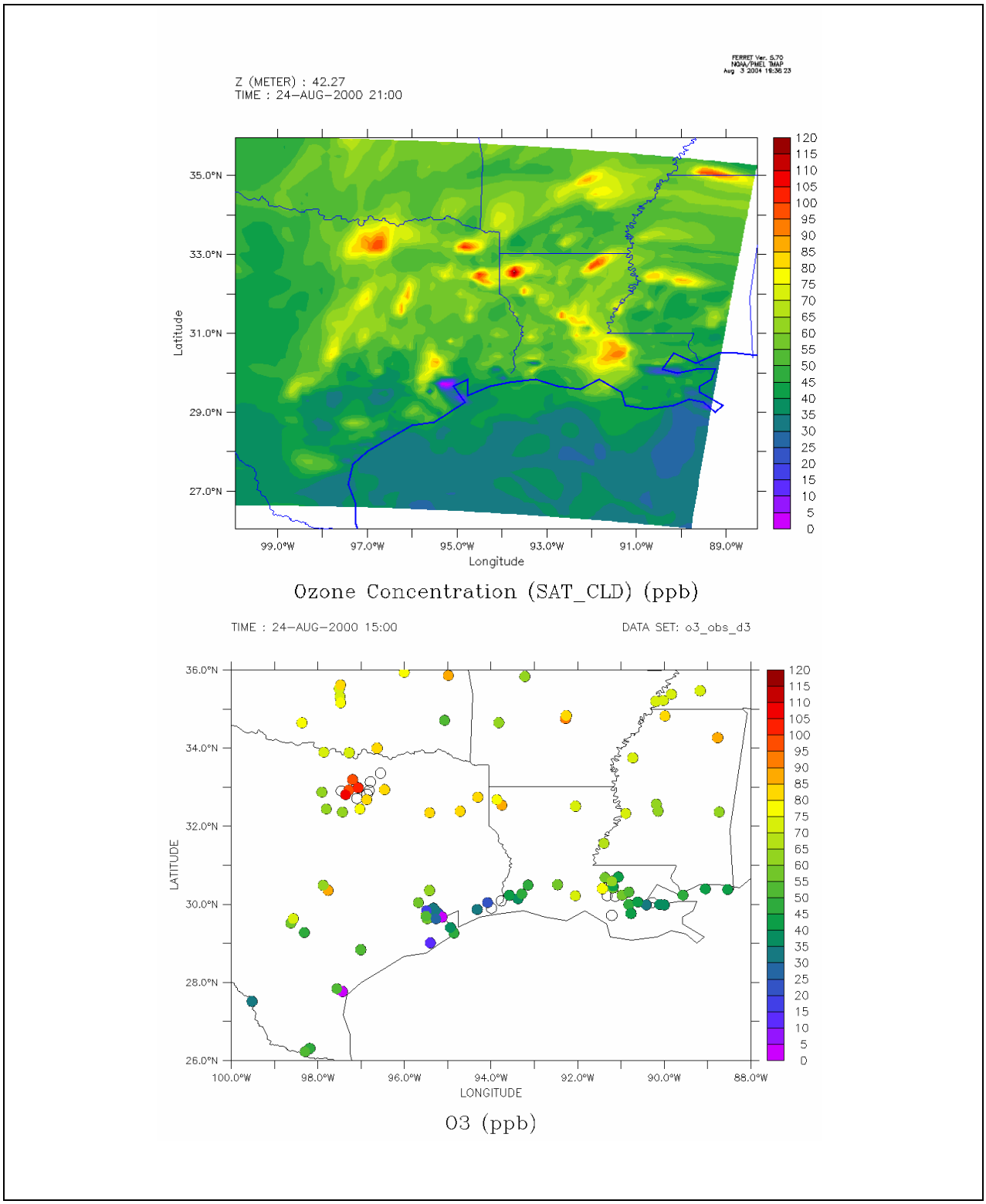

Figure 8. CMAQ Model predictions of ozone versus USEPA's AIRS observations for the 12-km domain on August 24, 2000, 21:00 GMT.

Figure 9 shows the time series of ozone concentrations from the two CMAQ simulations plotted alongside observations on August 26, 2000, for a location over the New Orleans area. Just before the sunrise, both model simulations drop to values close to the observation. But after the sunrise, ozone concentration in the control run does not increase at the same rate as the observation. The slow rate of the increase and the subsequent decrease in the ozone concentration is due to the over-prediction of clouds in MM5-derived fields for this location (based on examining the cloud cover for the simulations, not shown here). Since this location is impacted by high NO_x concentration, a reduction in the photochemical activity due to the overcast sky causes ozone consumption and therefore a reduction in ozone concentration. On the other hand, the satellite assimilation simulation (CMAQ_sat) for this location on August 26 indicates a better agreement with the observations. Clearly in this case the under-prediction of up to 35 ppb in ozone concentration is due to the MCIP indicating over-prediction of clouds and the use of satellite observed clouds has been able to correct this error.

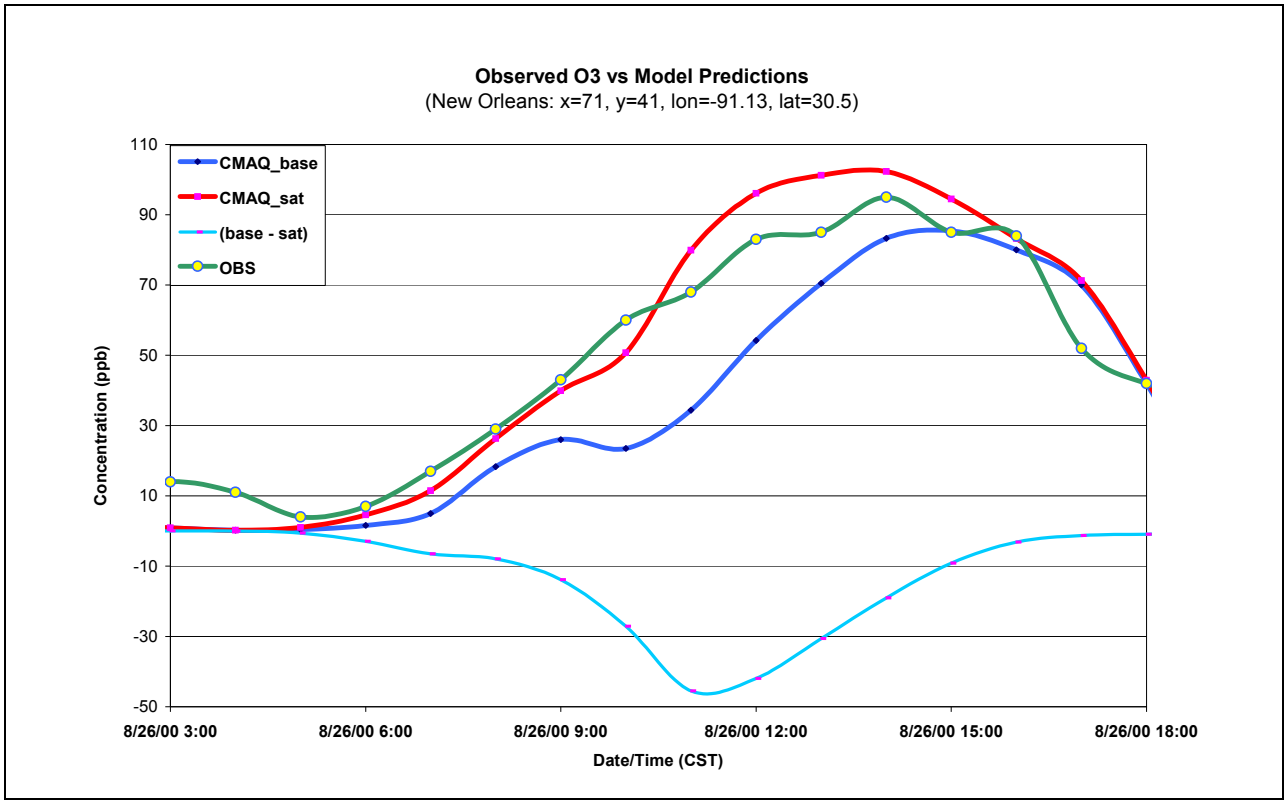

Figure 9. Time series of ozone predictions versus observations (OBS) for a location near New Orleans on August 26, 2000. CMAQ_base is the control simulation and CMAQ_sat is the satellite assimilation simulation. The light blue line shows the difference between the two model simulations. The control simulation under-predicted ozone by about 35 ppb.

The second example, as depicted in Figure 10, shows a scenario in which CMAQ_base is over-predicting ozone concentrations due to the lack of clouds in MCIP fields while in fact the sky is cloudy. In this case both the control and assimilation simulations over-predict ozone concentrations for most of the day over a location near New Orleans on August 31. This is perhaps due to the errors in the emissions for this location. However, in the afternoon, as the clouds move over this location, CMAQ_sat exhibits a sharp decrease in ozone concentration similar to that of the observation while the concentrations in the control run remain high. At 17:00, ozone concentration from the assimilation run agrees with the observation while the control simulation over-predicts ozone by 58 ppb. This also speaks to the impact of cloud correction and indicates that a reduction in photochemical activities in this location is enough to correct the large model over-prediction of ozone.

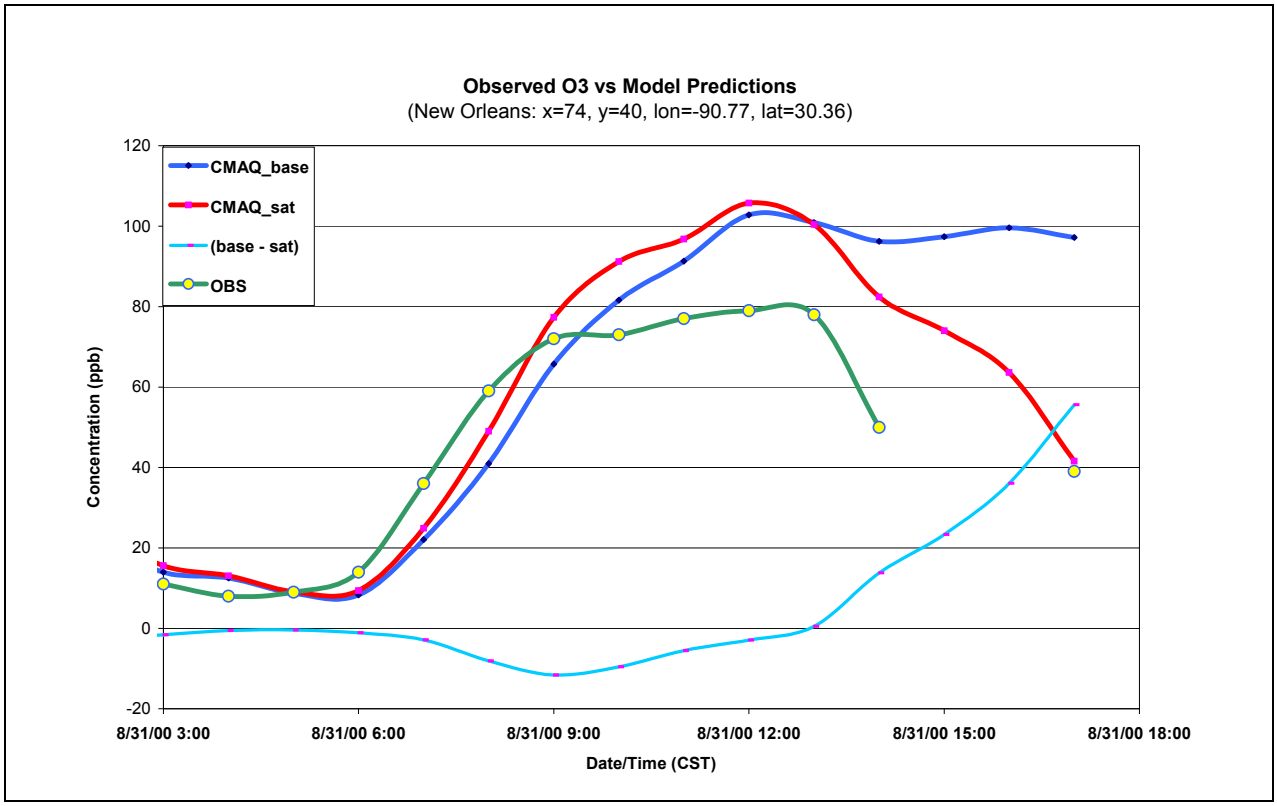

Figure 10. Time series of ozone predictions versus observations (OBS) for a location near New Orleans on August 31, 2000. CMAQ_base is the control simulation and CMAQ_sat is the satellite assimilation simulation. The light blue line shows the difference between the two model simulations. Control simulation over-predicted ozone by about 58 ppb.

The third case is from a location in southern Mississippi on August 31. As depicted in Figure 11, this case indicates under-predictions of ozone by the CMAQ_base run while the CMAQ_sat run again shows a better agreement with the observations. For this location the observations exhibit some variations which could be due to passing plumes that are not captured well in the simulations. But the largest discrepancy, which is an under-prediction of about 35 ppb at 16:00 in the control run, is due to the over-prediction of clouds in MM5-derived fields. Again in this case we observe a reasonable agreement between CMAQ_sat and observations at that time.

For all these locations during the nights CMAQ_base and CMAQ_sat are generally in agreement and their deviation from measured concentrations (that are due to other errors in the model) is smaller than the errors introduced due to incorrect cloud cover specification. Indeed in most of the domain, when there was a discrepancy between MCIP cloud fields and that of the observations, the largest errors could be attributed to the impact of clouds.

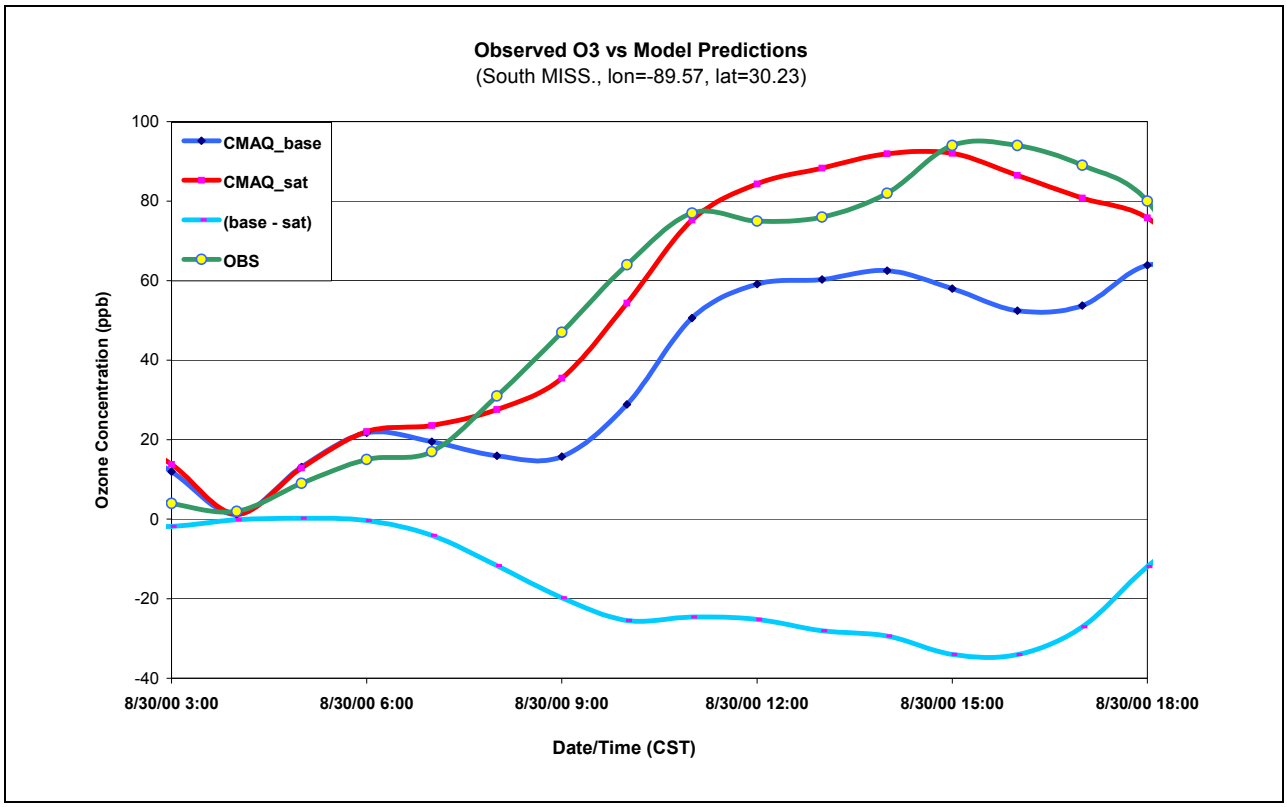

Figure 11. Time series of ozone predictions versus observations (OBS) for a location in South Mississippi on August 30, 2000. CMAQ_base is the control simulation and CMAQ_sat is the satellite assimilation simulation. The light blue line shows the difference between the two model simulations. Control simulation under-predicted ozone by about 35 ppb.

3. IMPROVEMENT IN LAND SURFACE MODELING USING SATELLITE DATA

While BOEMRE is concerned with the near shore and offshore environment, characteristics of the land surface are important to the development of the coastal environment. Development of the thermal structure over land impacts sea breeze and land breeze structure and the transport and dispersion of near shore air pollution sources. The following chapter is based on Mackaro (2008), and Mackaro et al. (2008), and it describes the problem encountered when the technique of McNider et al. 1994 (MCN94) was implemented in the Fifth-Generation Penn State/NCAR Mesoscale Model (MM5) [Grell et al., 1994; NCAR, 2003].

As an example 14 May 2001, a sea breeze circulation (SBC) developed along the coast of the northern Gulf of Mexico (Figure 12). The event, described in detail in Mackaro (2003), was simulated using the PSU/NCAR MM5 v3.A. The primary purpose of this study was to evaluate the possible benefits of land surface data assimilation to simulations of sea breeze circulations. The McN94 method was applied for which Land Surface Temperature (LST) tendencies retrieved from the Geostationary Operational Environmental Satellite (GOES) were dynamically assimilated into the surface energy budget of MM5. Three additional experiments were accomplished with varying land surface schemes to examine the sensitivity of the SBC to differential land surface forcings. The SBC developed in all simulations and was found to be very sensitive to the magnitude of land surface heating resulting from the partitioning of sensible and latent heat flux within the simulated surface energy budget.

The control experiment (CTRL), using a simplified slab Land Surface Model (LSM), simulated a SBC that did not have the inland penetration as observed by radar data (Figure 13). This indicates that the circulation strength was underrepresented. Simulated MM5 air temperatures along the coast were an average of 4K less than observations and there was a gridwide cold bias of 2K (Figure 14). This resulted in a land-sea thermal gradient that was weaker than necessary to initiate the SBC and allow it to fully develop. Examination of the simulated surface energy budget indicated that the majority of solar insolation reaching the surface was partitioned into latent heat flux, limiting the sensible heat flux needed to heat the near surface air sufficiently. One possible explanation for this discrepancy is that the specification of moisture availability values that were too large.

The MCN94 technique was specifically designed to correct such discrepancies in surface moisture specification. This is accomplished by adjusting the surface moisture in the land surface so that ground temperatures agree with the observed satellite tendencies. An overview of the technique is provided in a later section. In essence when surface tendencies are less than observed by satellite then surface moisture is decreased allowing ground temperatures to heat up faster. This appears to be the case here.

The MCN94 assimilation run (ASSIM) was capable of simulating a SBC which penetrated further inland than that simulated by CTRL and which was more consistent with observations (Figure 15). Closer inspection indicated the land surface forcing was responsible for heating the ground sufficiently so that the air temperature rise along the coast closely

matched the observations. The SBC fully developed in response. The assimilation technique reduced the moisture availability within the model and produced LST tendencies $3K/h$ to $4K/h$ larger than observed in CTRL.

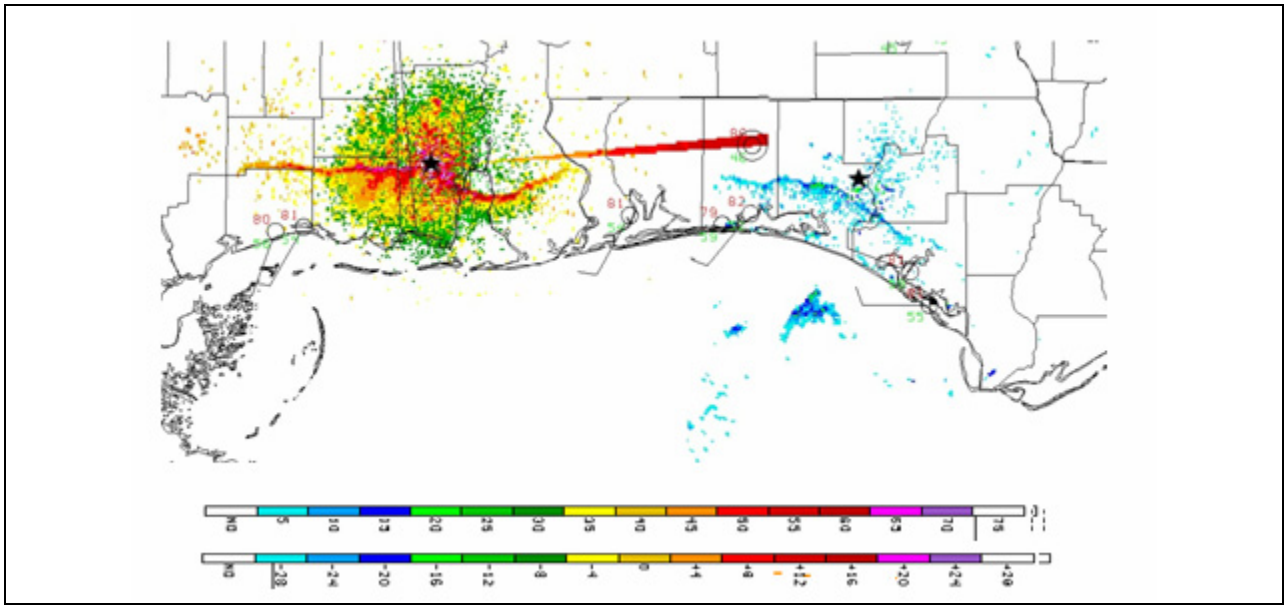

Figure 12. Base reflectivities (dBz) at 0.5 degree tilt angle from the Mobile, AL (MOB; left) and Eglin Air Force Base (EVX; right) WSR-88D radars overlaid on standard National Weather Service ASOS plots. Observations valid 22 UTC 14 May 2001. The color difference is a result of MOB radar in clear air mode, and EVX in precipitation mode. MOB color bar is on the left, EVX is on the right.

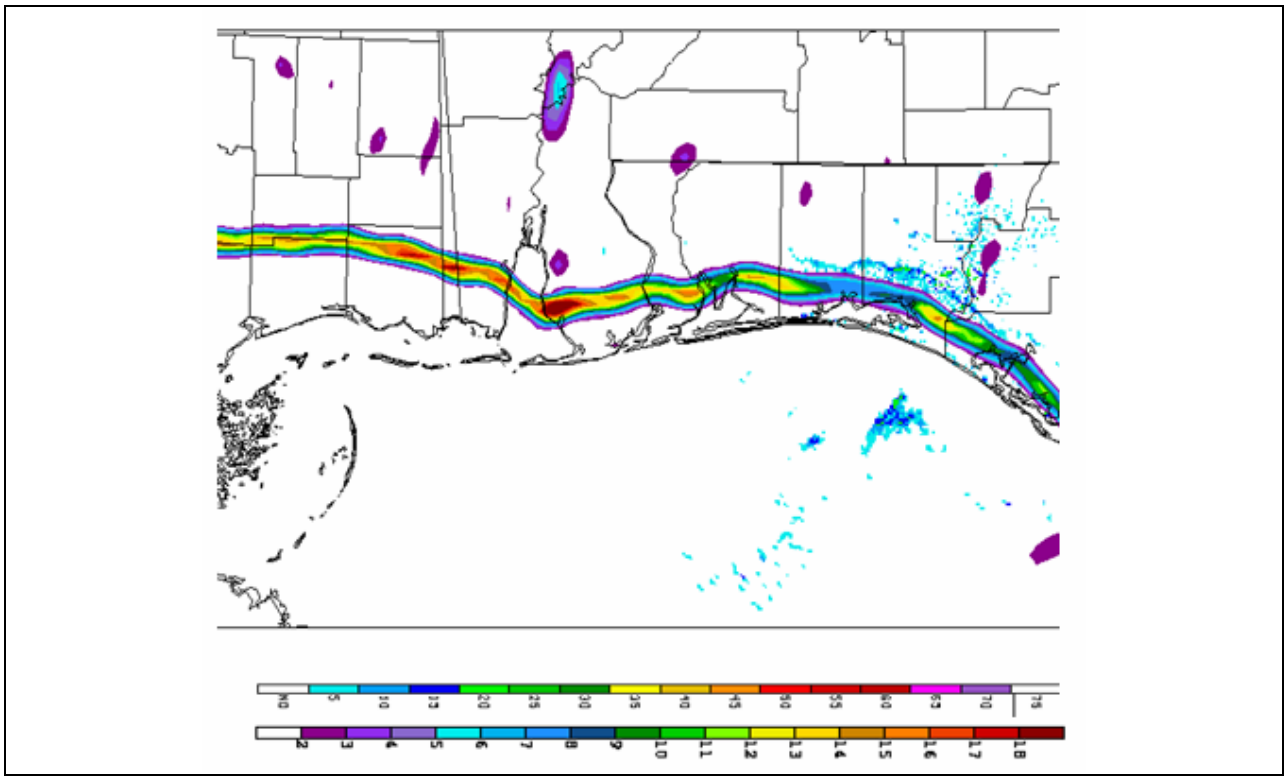

Figure 13. Base reflectivity (dBz) from EVX WSR-88D overlaid on CTRL simulated 1000 mb vertical velocity (cm s^{-1}) valid 22 UTC 14 May 2001.

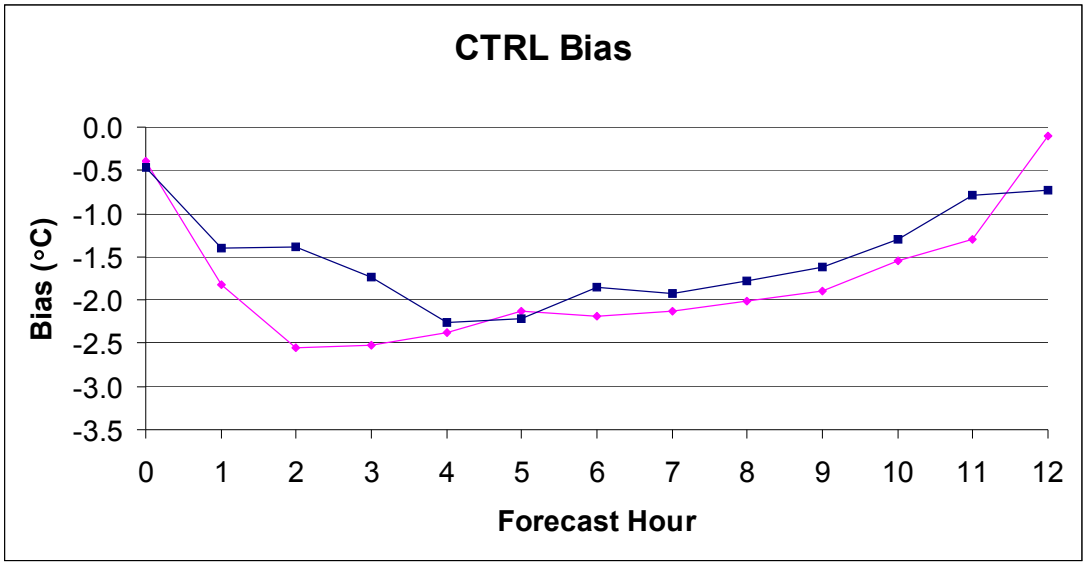

Figure 14. Time series of CTRL simulation 2 m temperature (pink) and dew point (blue) bias valid 12 UTC 14 May 2001 to 00 UTC 15 May 2001.

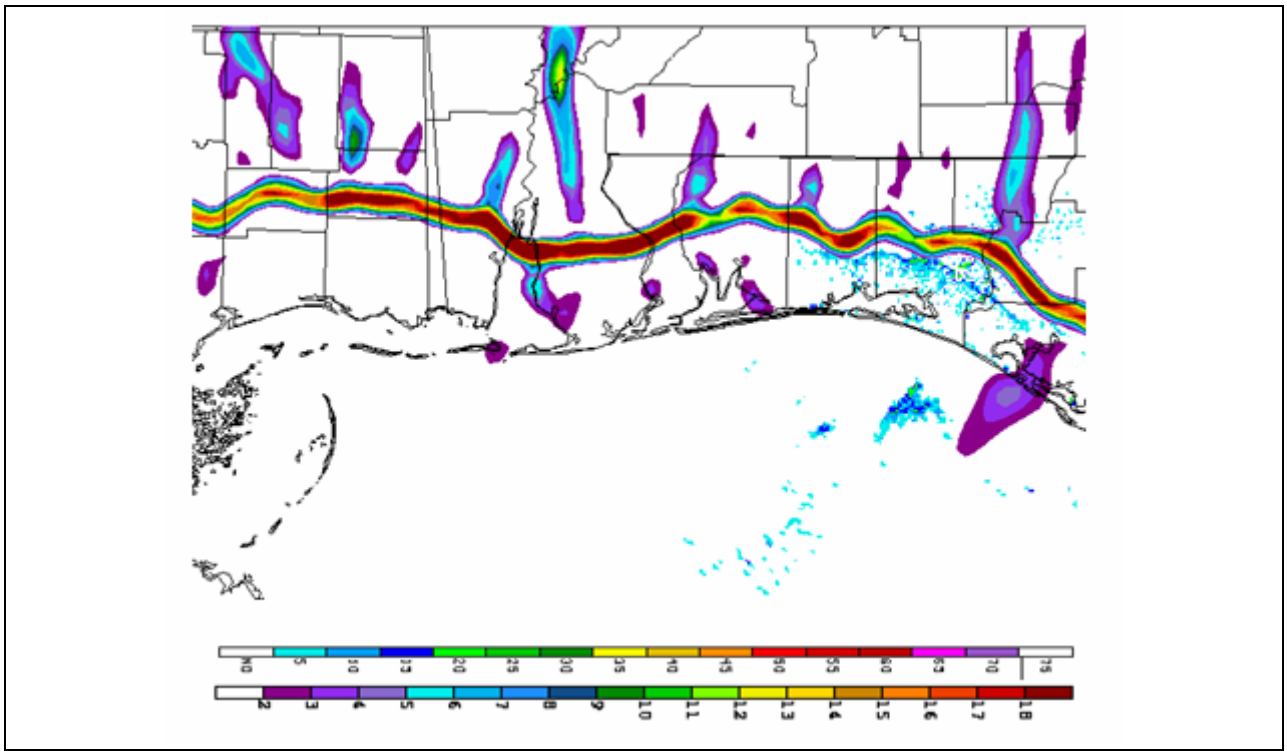

Figure 15. Base reflectivity (dBz) from EVX WSR-88D overlaid on ASSIM simulated 1000mb vertical velocity (cm s^{-1}) valid 22 Z 14 May 2001.

An experiment utilizing the Oregon State University (OSU) soil parameterization scheme was run for comparison with the ASSIM. Note that OSU LSM later developed into the National Oceanic and Atmospheric Administration (NOAA) NOAH LSM. The name NOAH represents the recognition of collaborators for this community model, N for National Centers for Environmental Prediction (NCEP), O for Oregon State University (Dept of Atmospheric Sciences), A for Air Force, and H for National Weather Service's Hydrologic Research Laboratory; http://www.emc.ncep.noaa.gov/mmb/gcp/noahlsm/Noah_LSM_USERGUIDE_2.7.1.htm. The model, using the OSU LSM simulated a SBC similar in magnitude to the CTRL over the Florida panhandle and to ASSIM over the Mississippi coast. This finding was traced to the specification of the volumetric soil moisture content in the upper soil layer of the OSU scheme initialized from the NCEP Eta-based 4-D Data Assimilation System (EDAS) analyses (Eta is one of NCEP's mesoscale numerical weather prediction models and the name "Eta" derives from the model's vertical coordinate known as the "eta" or "step-mountain" coordinate). The soil moisture was 50% less along the Mississippi coast than further east along the Florida panhandle. The result was sensible heat fluxes that sufficiently heated the ground allowing the SBC to fully develop. It was determined that over the entire grid, ASSIM improved the temperature bias while degrading the dew point bias (Figure 16). OSU did just the opposite, degrading the temperature bias while improving the dew point bias. It was also found that ASSIM produced land surface temperatures that were much closer in magnitude to the satellite observations than the CTRL or OSU simulations (Figure 17).

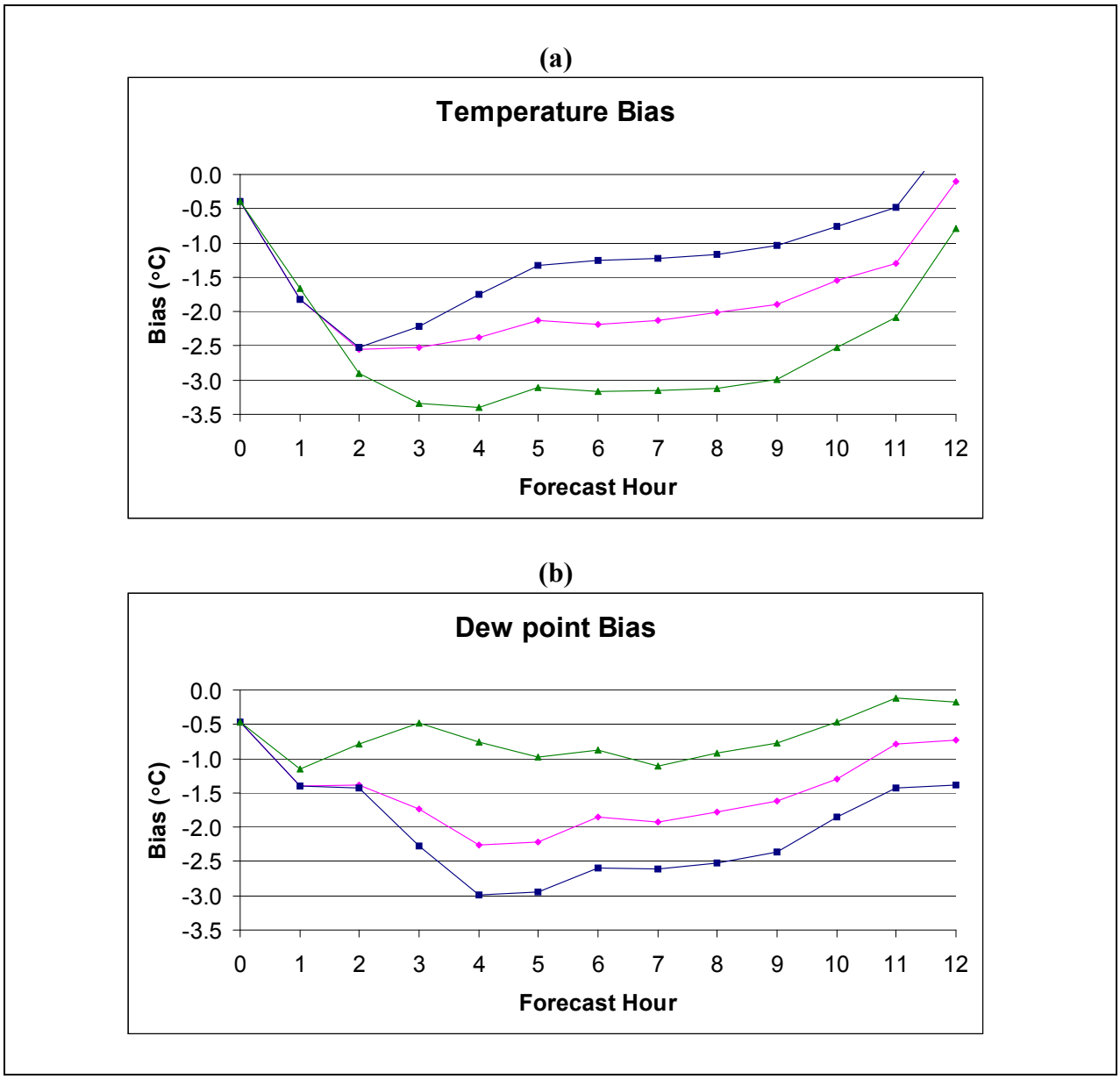

Figure 16. Time series of CTRL (pink), ASSIM (blue) and OSU (green) bias for (a) air temperature (°C) and (b) dew point (°C) valid 12 UTC 14 May 2001 to 00 UTC 15 May 2001.

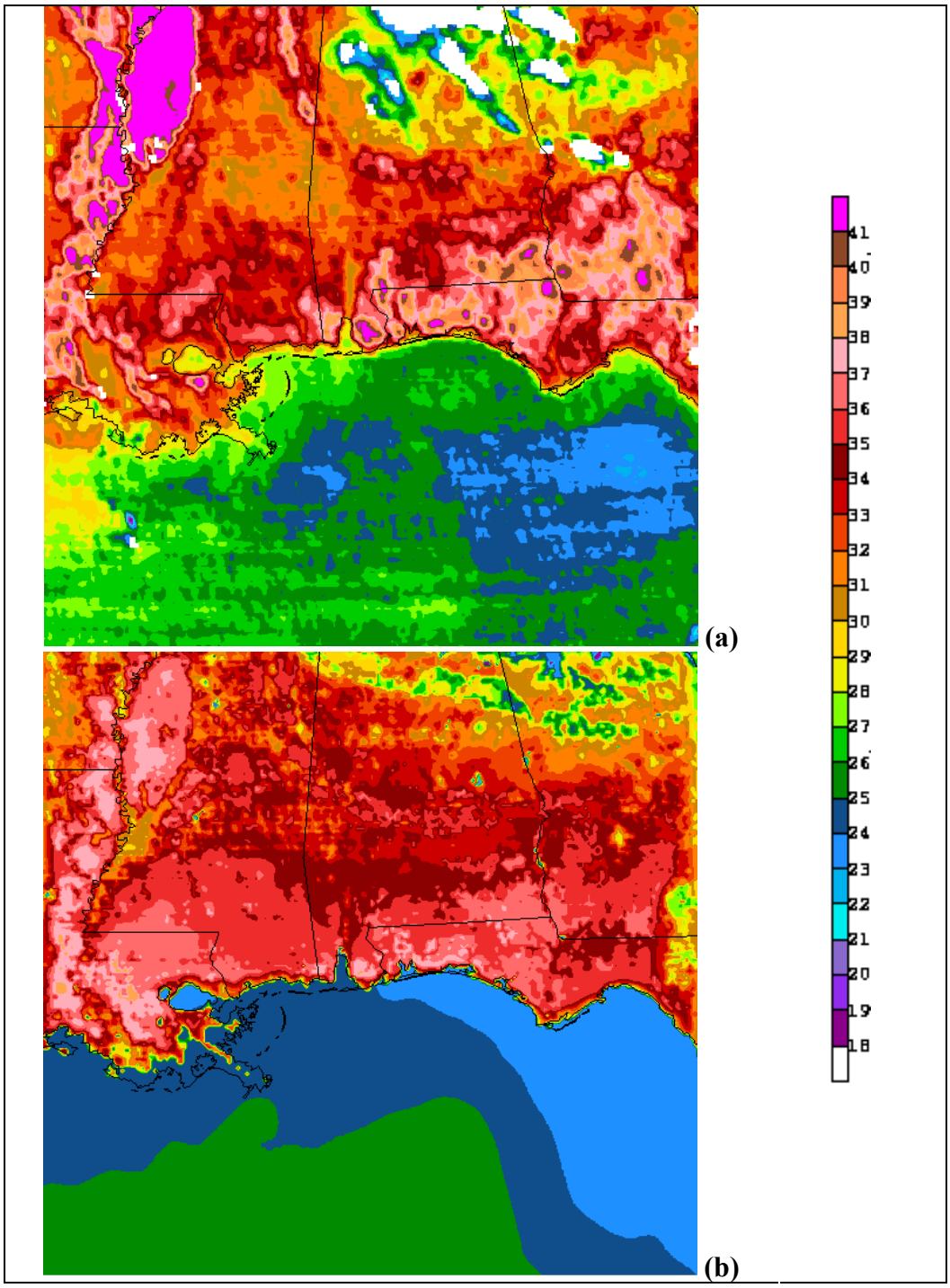

Figure 17. LST (°C) valid 20 UTC 14 May 2001 as retrieved from (a) GOES and (b) ASSIM.

The results of this research indicate that the assimilation of GOES derived LST tendencies have the potential to improve simulations of the SBC. This research demonstrated the ability of the McN94 technique to improve the land surface forcing within the MM5 without the use of advanced soil parameterization techniques.

Upon further review, it was determined that while the ASSIM improved the model results, the success of the simulation is limited by the drastic increase in sensible heat flux needed to arrive at the improved solution (Figure 18, Figure 19). This problem results from over-drying of the land surface within the model as moisture availability values were decreased to 0.05 (Figure 20). This value is actually a hard coded minimum that was implemented within the MM5 so that the latent heat flux would never go to zero. The intense drying found here caused some concern in regards to the way the technique had been implemented within the framework of the model since the original simulation performed in McN94 did not exhibit this problem.

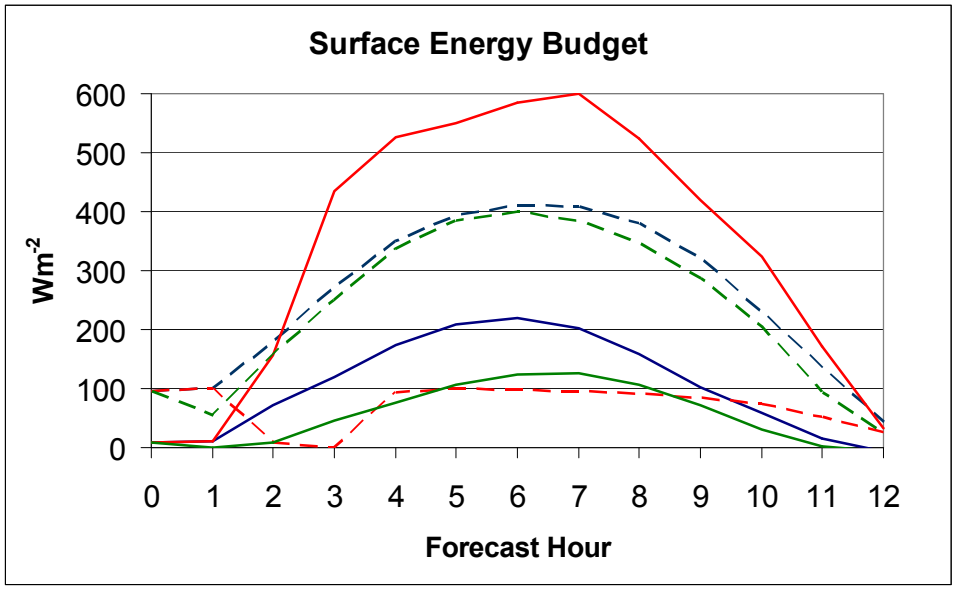

Figure 18. Time series of simulated sensible (solid) and latent (dashed) heat fluxes at VPS from CTRL (blue), ASSIM (red), and OSU (green) valid 12 UTC 14 May 2001 to 00 UTC 15 May 2001.

The intense drying observed in the SBC case was also found in a separate study. MM5 simulations with the same model options as the SBC case of 14 May 2001 were performed for 30 August 2000. The simulations took place during the time period of the 2000 Texas Air Quality (TexAQS 2000) Study using the same model set up as was used for the 14 May 2001 case. These simulations were not part of the actual field experiment and were only performed to examine if the drying observed for the 14 May 2001 case could be reproduced for a different region.

It was found that the McN94 method caused the MM5 to dry out the surface to the hard coded minimum value of moisture availability (0.05). Figure 21 shows the moisture availability for a control run, for which most of the region has a moisture availability of 0.30, and an

assimilation run, for which the moisture availability has been reduced to 0.05 for much of the domain.

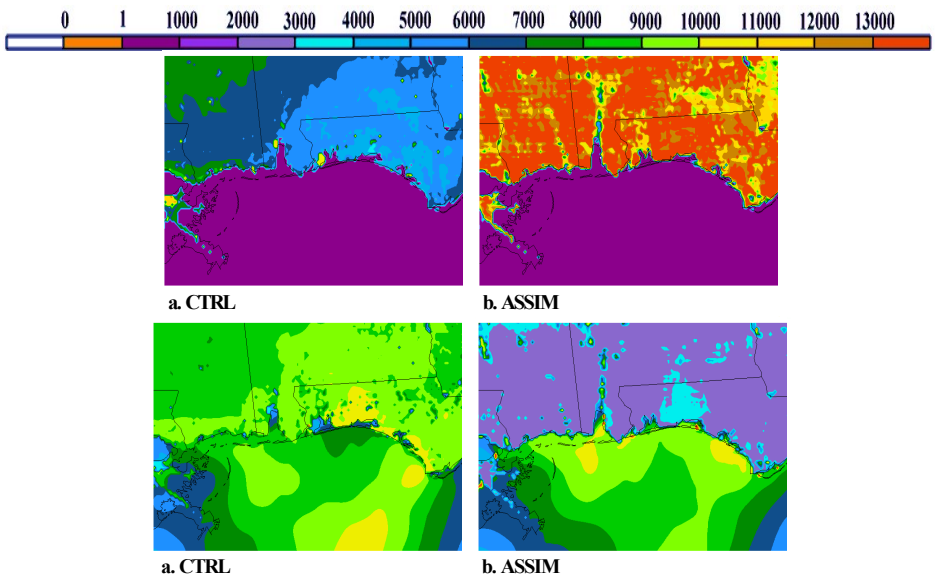

Figure 19. 12-hour accumulated sensible and latent heat flux (KJ).

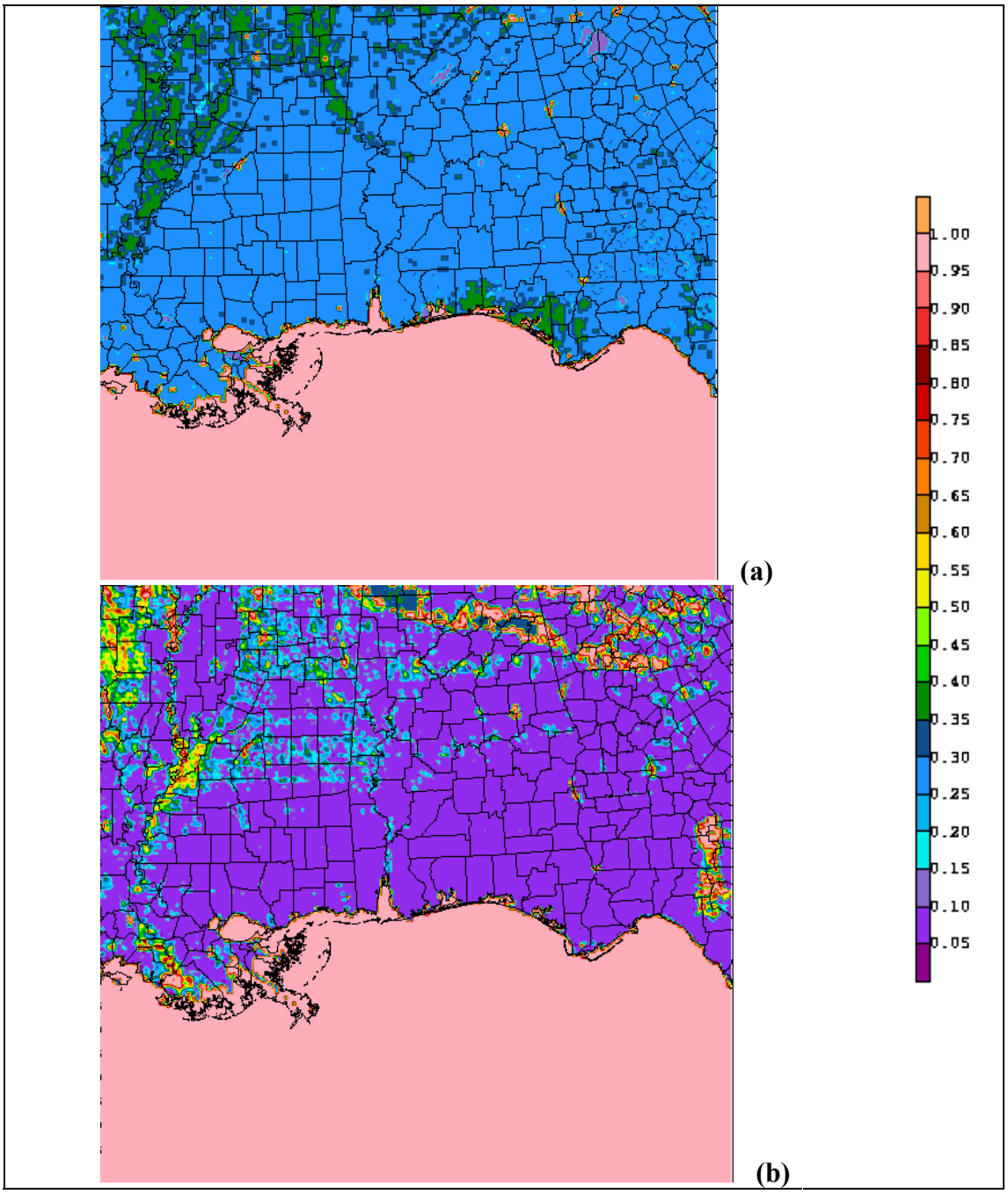

Figure 20. Moisture availability over simulation region valid 15 UTC 14 May 2001 in (a) CTRL and (b) ASSIM.

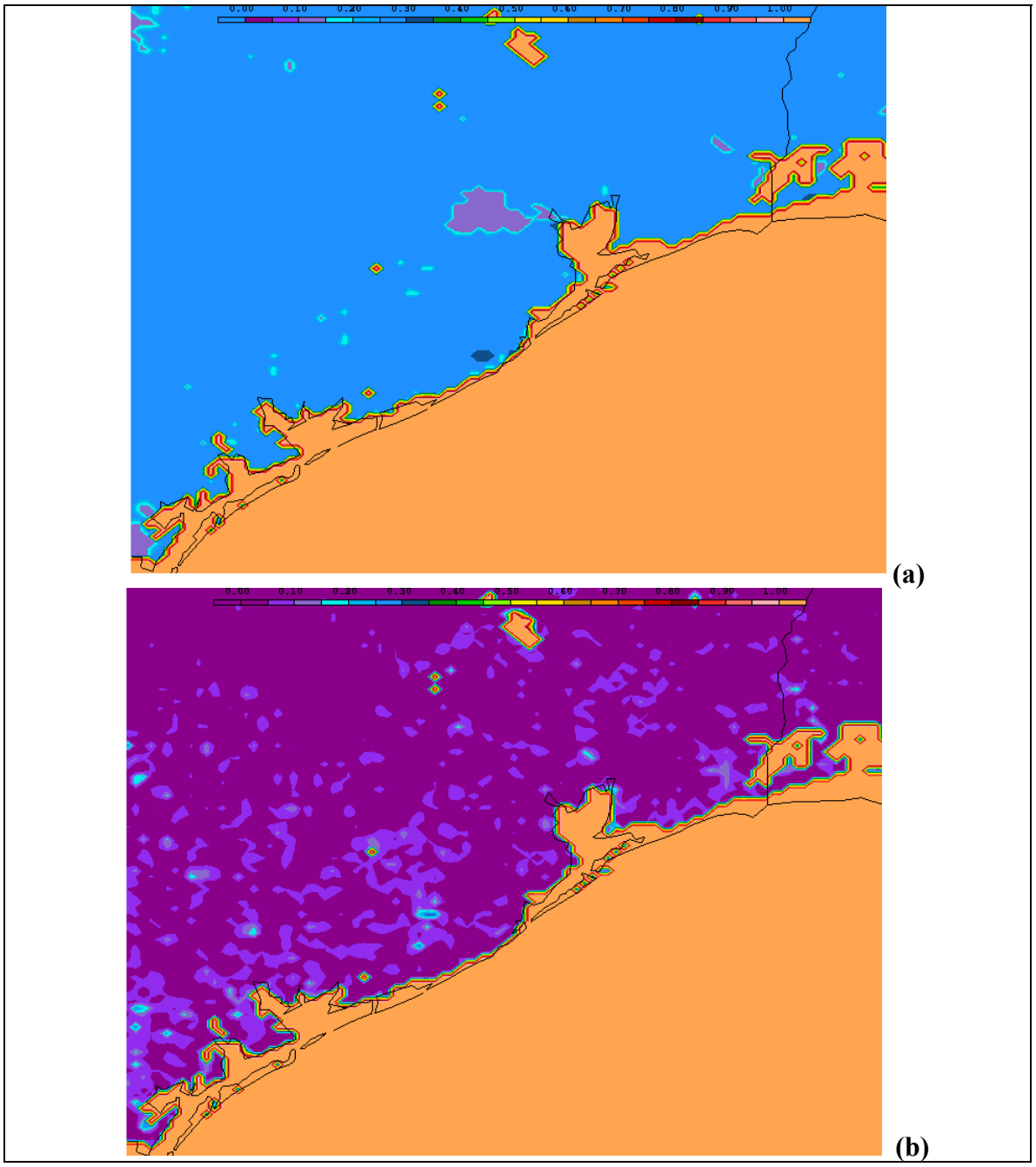

Figure 21. Moisture availability over simulation region valid 15 UTC 30 August 2000 in (a) CTRL and (b) ASSIM.

The goal of the McN94 assimilation technique was to provide more realistic land surface forcing by adjusting the moisture availability within the latent heat flux term of the surface energy budget. Thus, the technique should theoretically improve the moisture specification not degrade it. In fact the original testing of the model in McN94 showed this to be the case. Under the initial phase of this BOEMRE activity, a concerted effort was made to determine what aspect or assumptions in the McN94 technique might be leading to this discrepancy. It has been determined that a discrepancy exists when implementing the McN94 technique within the framework of the MM5. The root of this problem lies within a physical inconsistency in the formulation of surface temperature for which the ground temperature is used for all processes that require a near surface or surface temperature. The importance of the consistent use of aerodynamic temperature is well studied within the boundary layer community but has not always been adhered to in the mesoscale model community as evidenced by developments within MM5. The inconsistency typically only surfaces when an investigator attempts to use measurements of skin temperature or recover that temperature from a diagnostic surface energy budget (Sun and Mahrt 1995; Beljaars and Holtslag 1991).

An investigation took place to make a first attempt to recover a model skin temperature within the MM5 framework for direct comparison with the information provided by the satellite retrievals. The hope is that by recovering a skin temperature from the model, we could apply the McN94 technique and improve model simulated heating rates along with consistent surface fluxes. The results from this feasibility study follow.

4. MODEL GROUND TEMPERATURE TENDENCY COMPARED WITH SATELLITE OBSERVATION

The first step in this study was to compare the ground temperature tendency with the satellite skin temperature tendencies to ensure that they are in fact largely different. A case day was selected and two simulations were performed using the MM5. The simulation was centered over Houston, TX, initialized 00UTC 30 August 2000 and integrated forward in time for 24 h. This case day was chosen in support of research being performed for the Texas air quality study of 2000. Four kilometer horizontal grid spacing was used and applied with the Blackadar PBL parameterization and the Dudhia 5-layer soil model (Dudhia, 1996). The simulation was performed with (ASSIM) and without (CTRL) the McN94 assimilation technique activated between 13 and 15 UTC. Since the moisture availability is most uncertain during the mid morning hours, the adjustment takes place during this time period. The hours from 1245 UTC to 1545 UTC will be examined here.

Comparing the tendencies for 4 h beginning 1245 UTC and ending 1545 UTC from the satellite (Figure 22) and CTRL (Figure 23), it is evident that the surface, as observed by the satellite, is heating much faster than that simulated in CTRL. The satellite retrievals indicate skin temperature tendencies on the order of $3.0x10^{-3} K/s$ while CTRL is simulating tendencies no larger than $1.0x10^{-3} K/s$. ASSIM produced temperature tendencies that were closer to the satellite observed tendencies (not shown), however, as previously found, the improvements were at the expense of moisture and unreasonably large sensible heat fluxes. This finding reaffirms that comparisons of satellite skin temperature tendencies and MM5 ground temperature tendencies are in fact inconsistent.

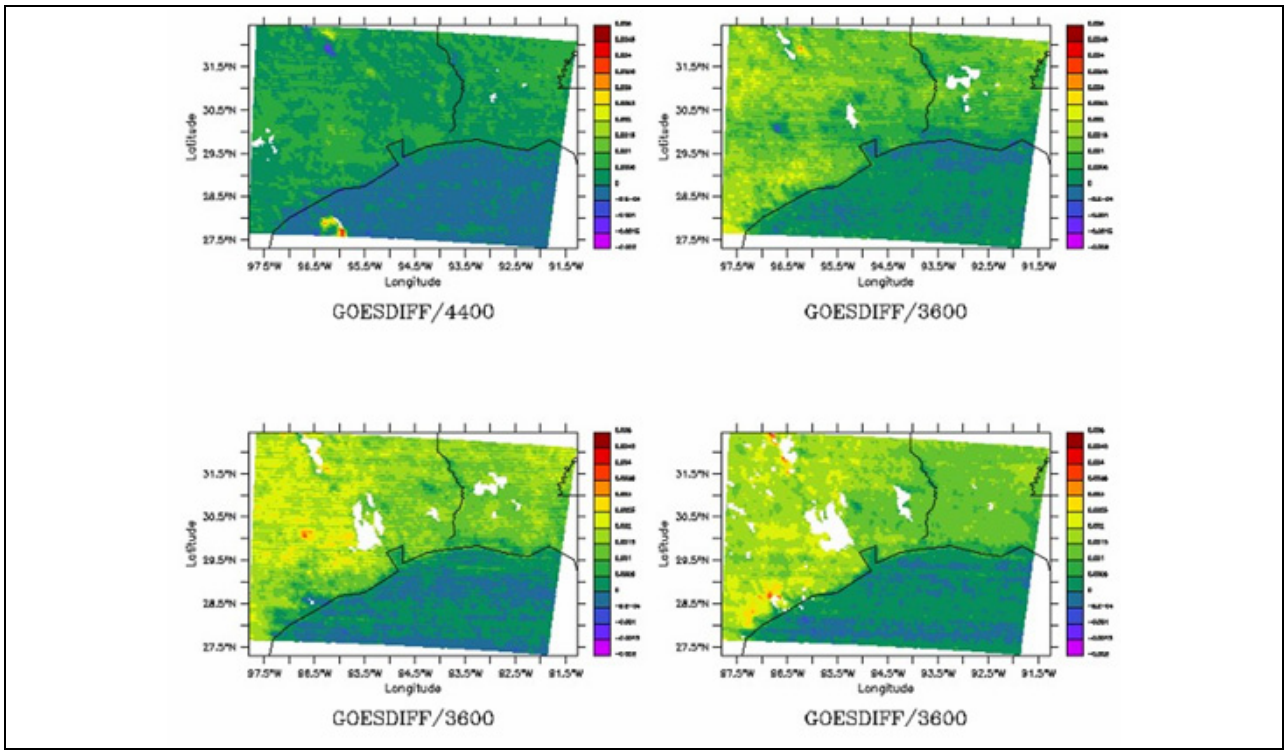

Figure 22. Skin temperature tendencies (K/s) valid 1245 UTC to 1545 UTC 30 August 2000 retrieved from GOES satellite.

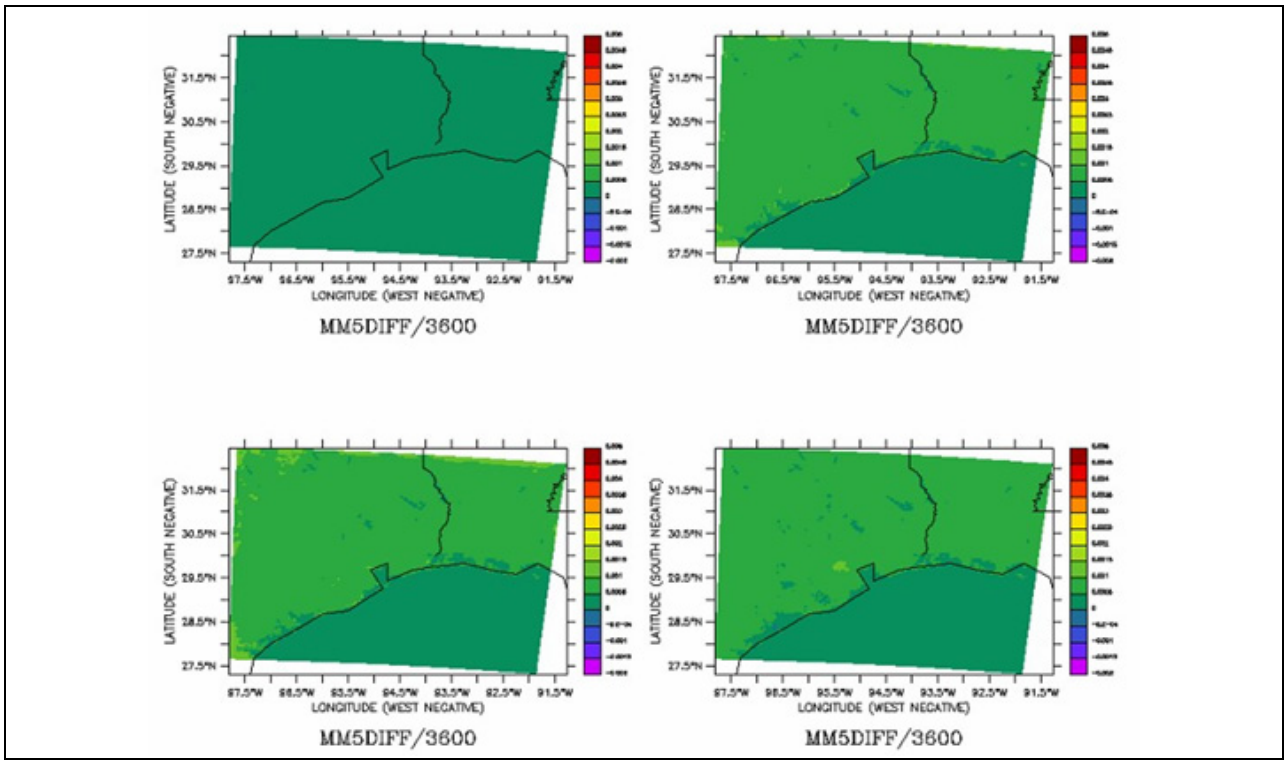

Figure 23. Skin temperature tendencies (K/s) valid 1245 UTC to 1545 UTC 30 August 2000 retrieved from CTRL with no assimilation.

5. RECOVERING SKIN TEMPERATURE WITHIN MM5

The goal of this feasibility study was to recover a model skin temperature for use in the McN94 technique. We will employ the use of an existing relationship first suggested by Zilitinkevich (1970). We begin with the theoretical background of this first attempt.

Zilitinkevich (1970) suggested relating the aerodynamic temperature to the surface skin temperature value using an expression in the form

$$\theta_{Zo} = \theta_G + 0.0962(\theta_* / k)(u_* z_o / \upsilon)^{0.45} \quad , \qquad (13)$$

in which υ is the kinematic viscosity of air, and k is the Von Karman's constant, θ_{Zo} is the aerodynamic potential temperature, and θ_G is the surface skin temperature and not ground temperature (even though the subscript G is present). This equation, the Zilitinkevich adjustment, adjusts the surface skin temperature using the existing similarity functions. The sign of the adjustment is dictated by the sign of θ_*. For a typical unstable condition, where the surface is warmer than the overlying atmosphere θ_* will be negative and the aerodynamic temperature will be cooler than the surface temperature.

Given the fact that we have all of the information needed from the Zilitinkevich adjustment with the exception of the surface skin and aerodynamic temperature, we make the assumption that the ground temperature is representative of the aerodynamic temperature. This assumption, while not physically consistent, is closer in validity then assuming the ground temperature is the same as the skin temperature and will be used in this feasibility study. The Zilitinkevich adjustment is then inverted and applied as,

$$\theta_{RAD} = \theta_{Zo} - 0.0962(\theta_* / k)(u_* z_o / \upsilon)^{0.45} \quad . \qquad (14)$$

The recovered model skin temperature was then used in place of the ground temperature when sent into the McN94 assimilation code. The temperature tendency calculated will then be a skin temperature tendency.

Examining the temperature tendency of the recovered model skin temperature from CTRL (Figure 24) indicated a tendency field that was warming faster than the ground temperature (Figure 23). The temperature tendencies are further improved when the McN94 technique is applied as temperature tendencies valid 1245 UTC and 1545 UTC closely resemble those from the satellite (Figure 25). We now have temperature tendencies that are now more closely linked to the satellite.

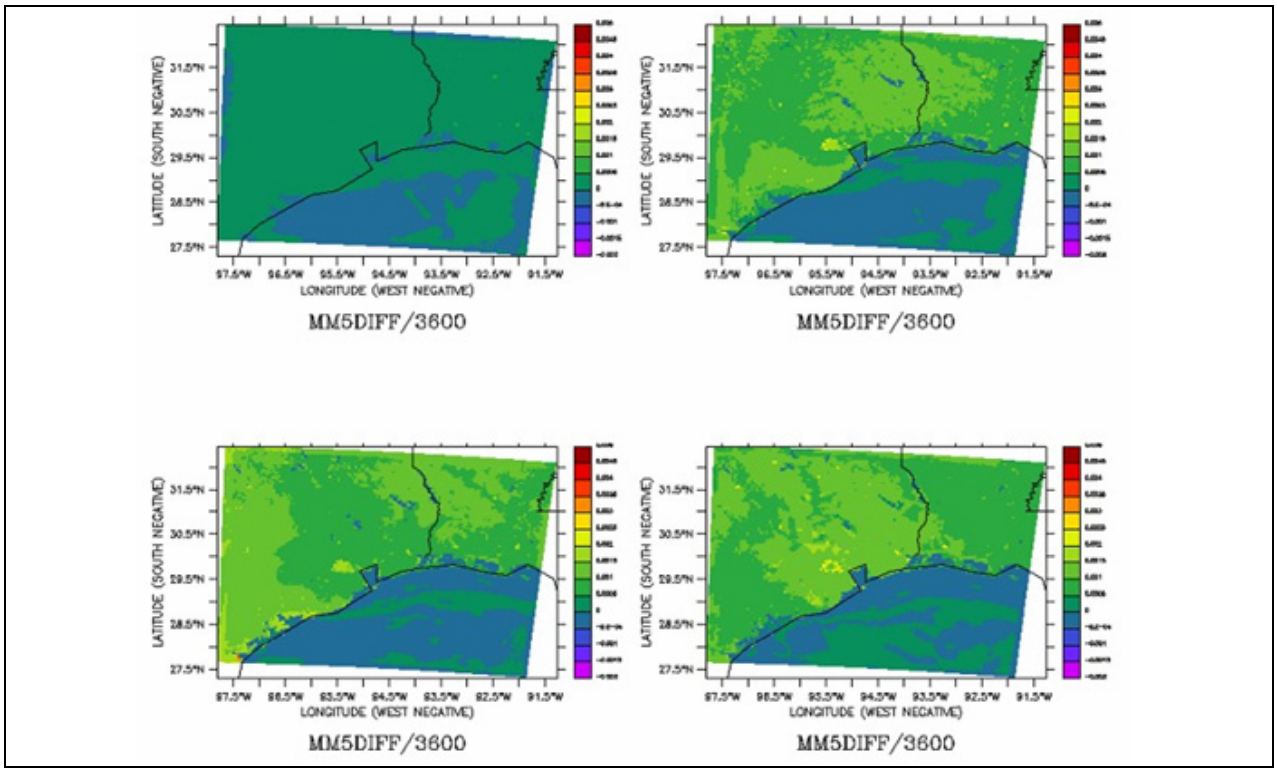

Figure 24. Skin temperature tendencies (K/s) valid 1245 UTC to 1545 UTC 30 August 2000 as simulated by CTRL.

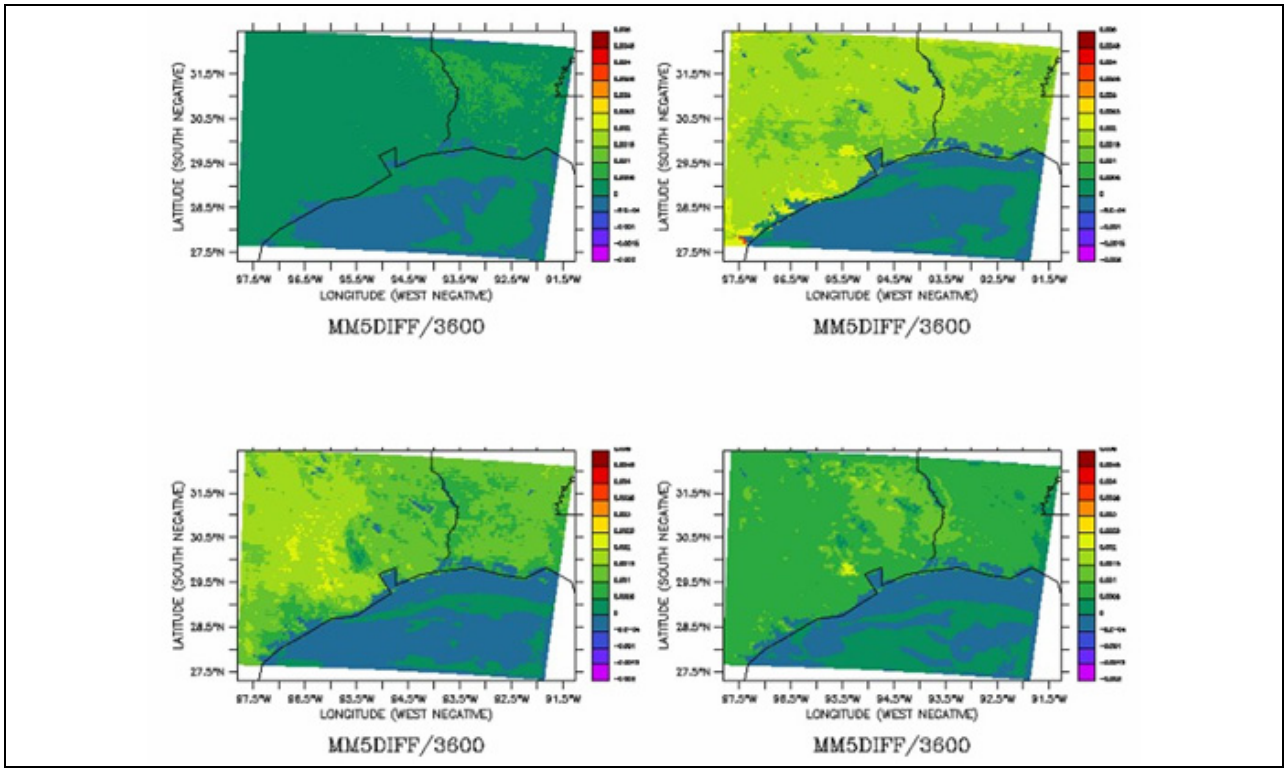

Figure 25. Skin temperature tendencies (K/s) valid 1245 UTC to 1545 UTC 30 August 2000 as simulated by CTRL but for ASSIM.

Comparing the model skin temperature field recovered by ASSIM (Figure 25) to that observed by the satellite (Figure 22) clearly indicates an improved field of surface temperatures over that of CTRL (Figure 24). While it is evident that we have recovered a model skin temperature that closely matches the satellite, it is of equal importance that we recover surface fluxes that are realistic. This is examined below.

The results of this study indicate the use of model skin temperature in the McN94 technique does provide favorable results. This method was described as a first attempt because the model skin temperature was only being used in the McN94 technique, and not in other parts of the model framework. This feasibility study has indicated that the over-drying found in previous studies was a result of the inconsistency in the temperature tendency comparisons. As such, a skin temperature must be made available within the model for the McN94 technique to be implemented in a physically consistent manner. This will be accomplished by use of a three temperature system for which model skin temperature, ground temperature, and aerodynamic temperature are calculated at each time step and used in a physically consistent manner. The system developed in this document is done so within a one-dimensional model to allow for full control over the model physics. That model and the three-temperature system are described in the next section.

6. DEVELOPMENT OF A CONSISTENT THREE TEMPERATURE SYSTEM FOR ASSIMILATING SATELLITE SKIN TEMPERATURES

Over the last few decades, investigators have embraced more physically complete land surface models and land surface satellite assimilation techniques as viable methods to better represent how a model surface reacts to changes in incoming or outgoing energy. Originally this representation was made through parameter specification that was based on climatological means containing no information about short term variations. As mesoscale models have moved to higher resolutions, it became clear that improving land surface representation was needed. Employing more physically complete land surface models by including vegetative layers and/or multiple soil layers, while more sophisticated, require detailed land use characteristics and initial conditions for parameters such as stomatal resistance or vegetative layer conductance for which measurements are not routinely conducted. It is for this reason that the recovery of surface parameters through the use of satellite data has been performed (Wetzel et al., 1984; Wetzel and Woodward, 1987; Carlson et al., 1981, Carlson, 1986; McNider et al., 1994; Anderson et al. 1997). One such technique, MCN94, has been directly employed within several mesoscale model frameworks to recover surface moisture availability with improvements in mesoscale forecasts. Its framework spurred other investigations to recover other parameters e.g. stomatal resistance (Jones et al. 1998a) and grid scale heat capacity (McNider et al. 2005).

Skin temperatures that reflect the radiating temperature of a surface observed by infrared radiometers are one of the most widely available products from polar orbiting and geostationary satellites and the most commonly used satellite data in land surface assimilation. Within a pixel of a satellite footprint, the skin temperature is the radiating temperature of everything within that particular field of view (trees, buildings, roads, etc.). While this intrinsic spatial averaging smears out detail in the surface, it is exactly the type of averaging that models need and as such may be better than land surface classification schemes which require weighting or averaging to be consistent with the model grid. As surface skin temperatures have become more widely used in land surface assimilation, boundary layer investigators began to explore the issue of inconsistencies in the use of skin temperatures in similarity flux forms and issues with using radiometric satellite data in land surface models (Zilitinkevich 1970; Lhomme et al. 1988; Kustas et al. 1989; Sugita and Brutsaert 1990; Brutsaert, 1982).

Beljaars and Holtslag (1991) and Sun and Mahrt (1995) recognized that the original similarity forms for surface layer fluxes could not use these skin temperatures directly. Rather than a skin value, the similarity forms required an aerodynamic temperature. The aerodynamic temperature is not directly measured but rather inferred through an extrapolation of a similarity prediction of the temperature profile to the roughness height. Choudhury et al. (1986) and Beljaars and Holtslag (1991) showed that the temperature difference between the surface skin temperature and the temperature at the roughness height can range from 2 K to 6 K in stable conditions to -2 to -6 K in unstable conditions. Thus, extrapolations of the Monin-Obukhov temperature profiles (Monin and Obukhov, 1954) to the surface boundary rather than the roughness height can lead to errors in the estimation of the lower boundary temperature used in the surface flux calculations (Beljaars and Holtslag 1991). This indicates that using skin

temperature data directly must be done so in a manner which is physically consistent with the bulk aerodynamic formulation of similarity functions.

It is important of attention to pay attention to details such as consistent use of skin and aerodynamic temperature and iteration when incorporating satellite assimilation techniques into mesoscale models, whether for forecasting or air quality simulations. Simply using existing model frameworks that do not always have the consistency in skin temperatures and aerodynamic temperatures can lead to significant problems as satellite data is introduced. This is illustrated through issues encountered in applying the MCN94 satellite assimilation technique within MM5. While this is only one model, other models share similar approaches in their surface formulations, so these techniques may be instructive to the general modeling community. This discussion will also clarify applications of the MCN94 satellite assimilation technique and follow-on use in light of these aforementioned papers on skin temperatures and aerodynamic temperatures. Also included here is the importance in understanding the adjustments that take place when making changes in parameters in the surface energy balance and the use of appropriate computational approaches. The surface energy budget equation is a highly non-linear that though often viewed as a balanced state is changing quickly with time during the day. Changes to any term in the equation means that other terms will change so that a balanced state can be maintained. Thus, one cannot simply change one term and assume that other terms stay the same in an attempt to move from one energy state to another.

6.1. Skin Temperature Assimilation

One of the first methods proposed for using satellite skin temperatures to recover surface variables was that of Carlson (1986) who proposed the use of twice daily data from polar orbiting satellites to recover surface moisture availability and thermal inertia. Wetzel et al. (1984) also hypothesized that skin temperature tendencies from satellite might be able to be used to recover surface moisture availability. As new sensors have been put into space, Carlson and others made continuing progress in coupling surface skin temperatures and other surface properties to refine the recovery of surface moisture availability. However, these studies were diagnostic and did not take the step of using the results in a mesoscale model. One of the first attempts to use satellite data directly in the surface energy budget of a mesoscale model was McN94 followed by the extension of Jones et al. (1998a).

In the Jones 1998b approach, Geostationary Operational Environmental Satellite (GOES)-derived skin temperature tendencies were assimilated into the surface energy budget equation of a mesoscale model so that the simulated rate of temperature change closely agreed with the satellite observations. At approximately the same time Norman et al. (1995) were also beginning to assimilate similar skin temperature tendencies in an offline boundary layer model. The adjustments made using the MCN94 technique are performed within the framework of a simple slab model. A simple slab model assumes all of the vegetative and soil properties that dictate land surface forcings can be described with a limited set of parameters. Note that in the context of the scheme in which satellite data is used, to determine moisture availability and surface resistance, the slab is a composite of vegetation and soil. Thus, even though soils are

used to specify initial conditions, it is more than a bare soil slab. It includes both soil evaporation and plant transpiration.

As discussed in McN94 and Norman et al. (1995), assimilating skin temperature tendencies rather than absolute temperatures is advantageous in that errors in the assumed emissivity of the surface, instrument errors from sensor degradation, as well as drift are largely negated. In the MCN94 assimilation method, a prognostic form of the surface energy budget is defined for both the satellite and model;

$$c_b\left(\frac{dT_G}{dt}\right)_m = \left(R_N + H + G\right)_m + E_m \qquad (8)$$

$$c_b\left(\frac{dT_G}{dt}\right)_S = \left(R_N + H + G\right)_S + E_S \qquad (9)$$

where R_N is the net radiation, including net shortwave, net longwave, and surface radiance, H, E, and G are, in order, the sensible, latent, and soil heat flux and the subscript $(\ )_m$ and $(\ )_S$ are used to infer the model and satellite derived variables respectively. Here a critical assumption is invoked for the mid morning hours, when surface heating is most rapid, the largest uncertainty is due to the moisture availability (embedded within the latent heat energy term) and all the other terms can be considered to have the same magnitude. Taking the difference allows us to obtain an equation relating the satellite and model latent heating terms to the difference in the surface temperature heat rates;

$$E_S = C_b\left[\left(\frac{dT_G}{dt}\right)_S - \left(\frac{dT_G}{dt}\right)_m\right] + E_m \qquad (10)$$

This formulation stems from the use of the prognostic surface energy budget equation for a ground temperature. An inconsistency arises here in that the ground temperature is that for a surface with a finite depth and heat capacity. Fundamentally this is not the same as the radiating skin observed by the satellite. The temperature tendency retrieved from the satellite is that of the skin temperature, and not the ground temperature.

The ground temperature evolution as dictated by the prognostic equation of (8) and (9) allows storage dependency on soil or canopy characteristics through the bulk heat capacity (c_b), but does not produce a skin temperature or an aerodynamic temperature. However, this temperature often works well in similarity flux formulations since it doesn't have the dynamic range of a skin temperature yet can reasonably replace the aerodynamic temperature needed in the prognostic equation. In fact, this is the form employed in the slab formulation of MM5 in that the ground temperature is used as the aerodynamic temperature in flux calculations and in determination of the surface longwave outward radiation (Figure 26). The use of such formulations in MM5 and other models has produced realistic fluxes in real world applications. However, when true skin temperatures are needed for satellite assimilation techniques or in comparison with tower radiometer skin temperatures, the need for consistency is evident.

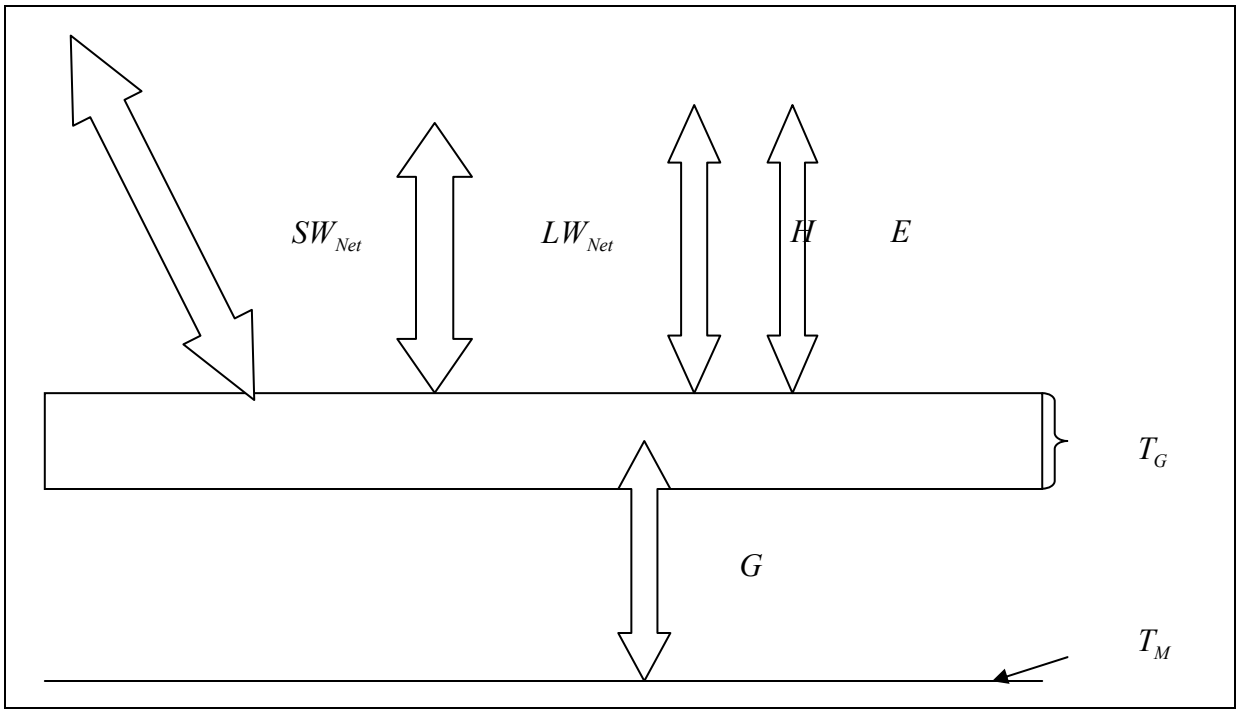

Figure 26. Schematic of the use of ground temperature within the surface to boundary layer interface of the MM5 using a composite slab land surface model.

The original implementation of McN94 serendipitously avoided part of this inconsistency in that in the mesoscale model in which they applied the moisture recovery, a true skin temperature was calculated from a surface energy balance model. The model energy balance skin temperature was calculated by finding the root of a balanced energy budget for an infinitely thing surface. However, the inconsistency was promulgated in that the skin temperatures were used in equation (8). Later applications of the McN94 technique, when used within MM5, indicated problems with mixing the satellite skin temperatures and the slab temperatures. During the morning hours, skin temperature tendencies from the satellite was often much larger than the ground temperature tendencies resulting in erroneously large adjustments. Results from case studies which indicated that using model slab temperatures mixed with satellite skin temperatures, while often improving model performance, usually produced an over drying of the surface (e.g., Mackaro 2003).

In order to correct the problems with mixing skin, aerodynamic and ground temperatures a new slab formulation for use within the MM5 or other mesoscale model was formulated. This is described in the following sections. The need for this formulation is in light of skin temperature research that has made the community aware of issues with its use since the development of the MCN94 technique.

6.2. Three-Temperature System

A one dimensional boundary layer model (hereafter referred to as 1DBLM) was developed for this study. It uses a simple slab model, that is a surface energy budget assuming that the all vegetative and soil properties can be described using a set of surface parameters. The slab takes on a specific land surface type based on the specification of characteristics including albedo, soil heat capacity, moisture availability, roughness length, thermal conductivity, emissivity, soil depth, and soil density. The surface to boundary layer interface in consistency with the traditional bulk aerodynamic formulation of similarity fluxes in which each boundary has its own explicit value of temperature (Figure 27).

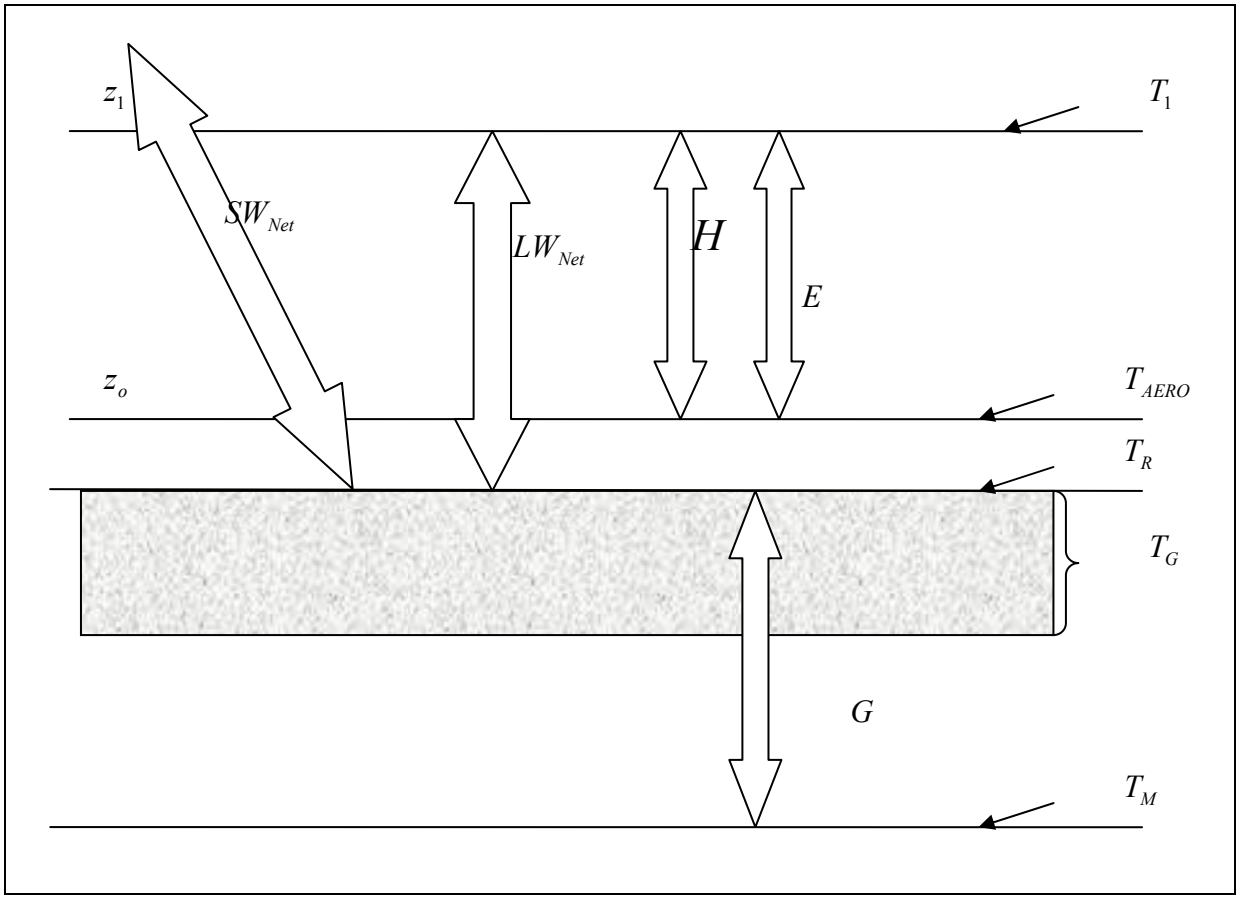

Figure 27. Schematic of a land surface to boundary layer interface that follows the traditional bulk aerodynamic formulation of surface layer fluxes.

The surface energy budget is based on the diagnostic energy balance formulation,

$$R_S + R_{LW}{}^{\downarrow} - \varepsilon\sigma T_R{}^4 - \rho c_p u_* \theta_* - \rho L_V M u_* q_* - \rho_s c_s k_s \left(T_R - T_G\right)\Delta h_{eff}{}^{-1} = 0 \qquad (12)$$

where the first two terms represent the net shortwave and incoming longwave radiation, the outgoing longwave radiation is given as a function of the modeled skin temperature to the fourth

power, T_R^4, M is the moisture availability which describes the total amount of water available for evaporation from 0 to 100%, ρ is the air density, and $u_*\theta_*$ and u_*q_* are the similarity relationship formulations representing the fluxes of heat and moisture. The soil density, ρ_s, specific heat capacity, c_s, thermal diffusivity, k_s, and effective slab depth, Δh^{-1}, combine to describe the soils heat storage capability, while the sign and magnitude of the difference between model skin temperature, T_R, and the ground temperature, T_G, dictate the direction and magnitude of the heat flux from the radiating surface to the slab (Figure 27).

We convert to a prognostic surface energy balance for the temperature of the slab in the form of equation (8). The formulation of the resistance term comes from the simple slab model formulation of Blackadar (1979), where C_b is the thermal heat capacity of the slab per unit area and is related to the thermal inertia of the slab.

To obtain an aerodynamic temperature from information available in 1DBLM, we employ a method suggested by Zilitinkevich (1970) and Deardorff (1972) to relate the temperature at z_o to the model skin temperature;

$$T_{Aero} = T_{Zo} = T_R + 0.0962(\theta_* / k)(u_* z_o / v)^{0.45} \quad (13)$$

where v is the kinematic viscosity of air.

The process of solving for the model skin, ground, and aerodynamic temperature involves the use of the iterative process shown in Figure 28. T_R is first retrieved by use of a root finding technique. The aerodynamic temperature is then recovered by use of Equation (13) and is then used to update fluxes for each iteration. The final step of the process involves calculating the ground temperature as it is time dependent.

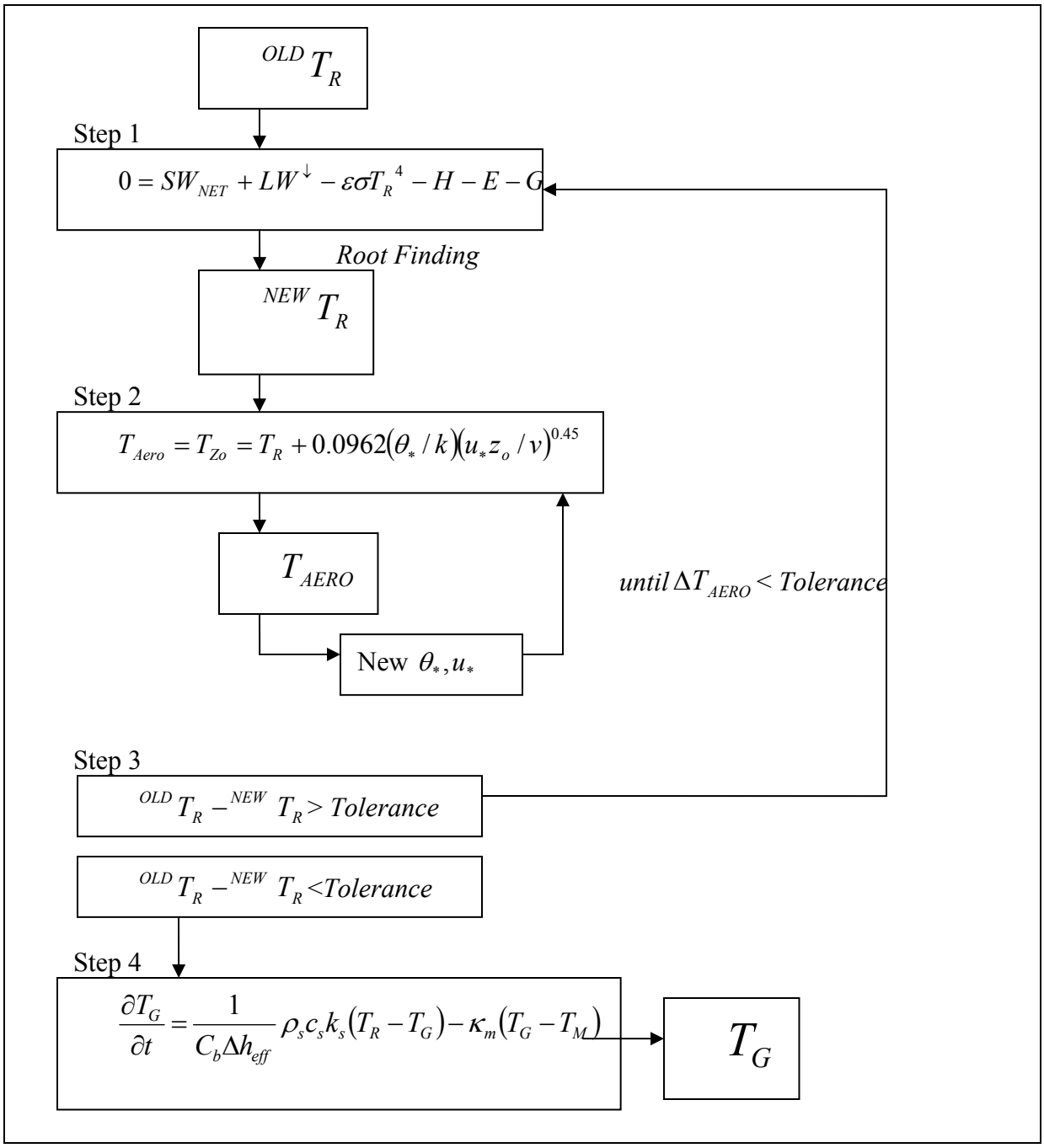

Figure 28. Schematic flow chart of the iteration used to solve the three temperature system used in 1DBLM.

With a physically consistent method of determining aerodynamic, model skin, and ground temperature in place, we now want to invoke the use of the McN94 assimilation technique. In order to do so, we must allow for the fact that the only information from the satellite is the satellite skin temperature not the ground temperature. Using the time rate of change of the satellite skin temperature, we can arrive at the tendency used by the McN94 technique, $\frac{dT_R}{dt}$. The technique was developed from a prognostic form of the surface energy

budget and simply replacing $\frac{dT_G}{dt}$ with $\frac{dT_R}{dt}$ is not valid. A relationship between $\frac{dT_G}{dt}$ and $\frac{dT_R}{dt}$ is thus necessary. Since we are using a closed system of equations for our three temperatures, a relationship then exists between T_G and T_R. We relate the tendency of the ground temperature and skin temperature by α given as,

$$\frac{dT_G}{dt} = \alpha \frac{dT_R}{dt} \tag{14}$$

Since both $\frac{dT_G}{dt}$ and $\frac{dT_R}{dt}$ are available from 1DBLM, we assume that the ratio of the two is the same for both the satellite and model, and solve for the relationship factor, α as

$$\alpha(t) = \frac{dT_G}{dt} / \frac{dT_R}{dt} \tag{15}$$

The behavior of α was found to be smooth and non-linear during the mid morning period for most types of land surfaces. While it is recognized that there may be a more elegant method of relating the radiative and ground temperature, the relationship used above is easily determined and is internally consistent at least within the framework of 1DBLM.

The next step is to replace $\frac{dT_G}{dt}$ with $\alpha(t)\frac{dT_R}{dt}$ in equation (10) to arrive at a form which is physically consistent;

$$E_S = c_b \left[\left(\alpha(t) \frac{dT_R}{dt} \right)_S - \frac{dT_G}{dt}_m \right] + E_m \tag{16}$$

From this we can continue as described in Lapenta (1999) with the model latent heat flux defined as,

$$E_m = \frac{M \rho \kappa u_* \left(q_{VS}(T_{Z_o}) - q_{AIR} \right)}{\ln\left[\frac{z}{z_o} \right] - \psi_H} \tag{17}$$

By replacing E_m with the latent heat flux recovered for the satellite, E_S, we can invert the equation and arrive at an adjusted moisture availability, M_S;

$$M_S = E_S \frac{\ln\left[\frac{z}{z_o} \right] - \psi_H}{\rho \kappa u_* \left(q_{SAT}(T_G) - q_{AIR} \right)}. \tag{18}$$

The adjusted moisture availability then replaces that specified as the initial condition. The adjustment typically takes place on the hour of each subsequent hour within the assimilation period during the mid morning hours. It is the previous hour's temperature tendency used in the adjustment so that no a-priori information is necessary.

6.3. 1DBLM Test Cases

A series of simulations were performed to evaluate 1DBLM's physically consistent framework and its ability to simulate the surface to boundary layer interactions. Of specific interest is the ability of the model to reproduce values of observed skin temperature, air temperature, and surface fluxes of heat and moisture. The impact of the McN94 technique on these modeled variables is also of interest. In order to validate the 1DBLM simulations, surface based observations were obtained from Oklahoma Mesonet (Brock et al.,1995) sites that are part of the Oklahoma Atmospheric Surface Layer Instrumentation System (OASIS; Brotzge and Duchon, 2000) and from the U.S. Department of Energy's Atmospheric Radiation Measurement (ARM) Cloud and Radiation Testbed (CART) Southern Great Plains Central facility (SGP-CF) site. From each site, skin temperature and net radiation from an Infrared thermometer (IRT; Fiebrich et al., 2003) and net radiation, air temperature, wind speed, sensible and latent heat flux from tower mounted instruments were collected. Ground heat flux from ground instruments was also collected.

Results for 4 July 2003 from the Norman, OK (NRMN), and Foraker, OK (FORA) OASIS sites and the ARM-CART SGP-CF site for 28 July 2005 are described here. Clear sky conditions persisted during the morning hours across the state of OK on both days while clouds developed over many of the sites during the afternoon of 4 July 2003, and remained clear on 28 July 2005.

Two sets of simulations were performed utilizing 1DBLM, a control simulation in which MM5 surface properties were used, and an assimilation run in which moisture availability was recovered by utilizing the observations from MESONET sites. For initializing 1DBLM, initial profiles of potential temperature, u- and v-component wind, and specific humidity for 06UTC were obtained from an MM5 4km horizontal resolution forecast. Initial conditions for the MM5 were specified at 00UTC for each day from the NCEP Eta Data Assimilation System 40-km analyses. For MM5 simulations the Blackadar boundary layer scheme and a 5-layer soil model were employed. The closest grid point to the mesonet station was used to initialize 1DBLM. The land use category specified within the MM5 was used to determine the initial land surface specifications for 1DBLM, namely moisture availability, thermal inertia, and roughness length. Table 1 provides values of pertinent parameters for each site. The observed net shortwave radiation, as calculated from the explicit tower measurements of the net radiation components, was used as input to 1DBLM to ensure consistency in the amount of solar radiation input to the system. This also allows us to represent the decrease in incoming radiation resulting from the presence of clouds.

Table 1

Pertinent Initial Model Parameters for the OK and SGP Model Simulations.

Site	Lat	Lon	χ	c_s	ρ_s	λ	MA	z_o	ε	T_M	u_g	v_g
NRMN	35.24	97.46	0.04	1256	1850	1.23	0.30	0.15	1.00	298	-7.24	4.40
FORA	36.84	96.43	0.04	1256	1850	1.23	0.30	0.15	1.00	295.7	-2.69	2.97
SGPCF	36.62	97.50	0.04	1256	1850	1.23	0.30	0.15	1.00	295.0	-2.10	-2.31

A Control (CTRL) simulation was performed at each location for which the 1DBLM model is allowed to run using only the observed net shortwave radiation and the given initial parameters. An assimilation simulation (ASSIM) was then performed for which the McN94 moisture availability adjustment is invoked over a three hour period from 1300UTC to 1500UTC. For the assimilation simulation over each site, the surface skin temperatures from the corresponding IRT were used.

Figure 29 shows the CTRL and ASSIM-case model predictions for surface skin temperature, 2-meter temperature, sensible and latent heat flux, and wind speed as compared with observations from the NRMN site. The net radiation from both the IRT and tower are also plotted along with the model predicted value to show the relationship between the tower measurements and the model. The CTRL, using the physically consistent 3-temperature method produced a time series of model skin and 2-m temperature which matches the observations reasonably well. Thus, since the difference between the model skin temperature and the observed skin temperature is negligible, the adjustment made by our technique is also negligible and in the figure the plots for both CNTRL and ASSIM-case are on top of each other.

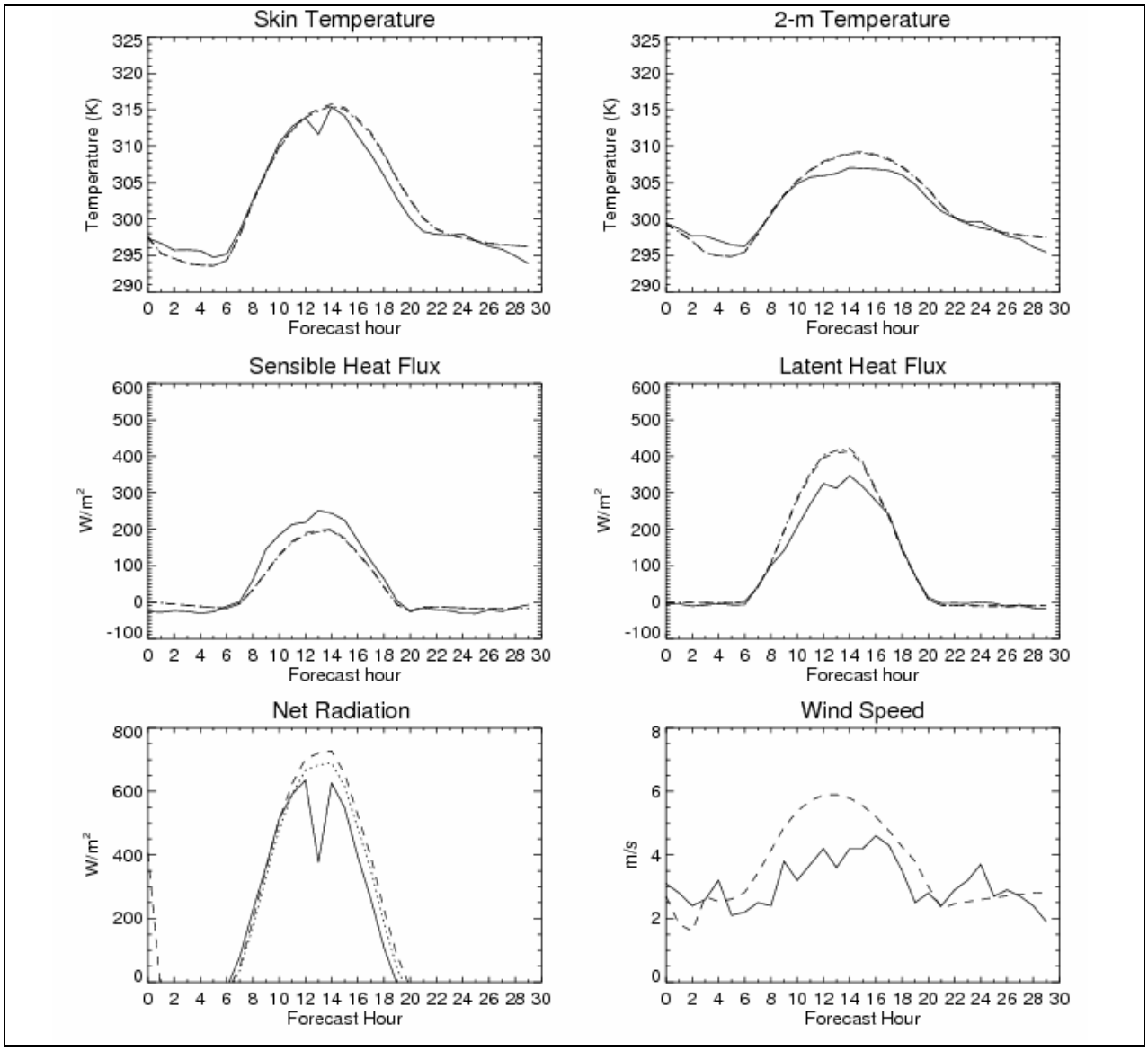

Figure 29. Observed (solid), CTRL simulated (dashed), and ASSIM simulated (dash-dot) variables valid 06 UTC 4 July 2003 to 12 UTC 5 July 2003 for NRMN. Net radiation as measured by the IRT (solid) and tower instruments (dotted line) are given.

The two instruments at the NRMN site (IRT and the sensors on the tower) show some discrepancies with respect to measured net radiation. This is attributed to a combination of differences in the field of view and emissivity of the measurements (Basara, 2007, personal communication) and to differences in incident solar insolation. Since we have been using the tower measurements of insolation in this study, these discrepancies also manifest themselves in the skin temperature plot. The overestimation of winds near the surface, as predicted by the model, is responsible for warmer 2-meter temperatures during the day since the surface shear stress leads to a more well mixed environment. The surface sensible and latent heat fluxes were well represented by the model (both simulations), deviating from the observations on the order or

30 to 50 W/m^2. Perhaps lowering wind speed would have lead to a larger temperature gradient (between skin and the atmosphere) and consequently a larger sensible heat flux, and accordingly a lower latent heat flux. The relative success of the model for NRMN site means that the climatological values for the surface parameters including roughness length, moisture availability, and thermal inertia are representative. Since the observed rise of skin temperature during the assimilation period was well represented by the CTRL run, there was little adjustment made within ASSIM, as indicated by little visible difference between the CTRL and ASSIM time series (Figure 29). The results for NRMN site shows that 1DBLM provided a reasonable representation of the surface to Boundary layer interactions and boundary layer evolution. It also indicated the limitation of the assimilation technique as it was unable to correct errors in partitioning of fluxes and the Bowen ratio (the ratio of sensible heat flux to latent heat flux) when these errors are due to factors (e.g., wind speed) other than surface moisture.

Figure 30 shows the same parameters as Figure 18 except for the FORA site. The FORA site exhibited a surface that was fairly moist, resulting from convective precipitation on the previous days. As a result the CTRL simulation, using the MM5 specified land use parameters, simulated a skin temperature which was much warmer than observed during the daytime, and a 2-meter temperature curve which was slightly warmer than observed. The CTRL simulated a maximum skin temperature 6 degrees K warmer than the observation. In response, the CTRL simulated sensible heat flux was overpredicted, and the latent heat flux underpredicted. When the McN94 technique was applied, the moisture availability increased to 0.48 and a 5 degree K improvement (reduction) in the maximum model skin temperature. This resulted in a reduction of sensible heat flux and an increase in latent heat flux, nearly matching the observations. The success of the assimilation technique for FORA confirms the validity of the assumptions made. The model predicted wind speeds show a much better agreement with the observations; therefore most of the error in the Bowen ratio must be due to the specification of the model surface moisture.

Figure 31 shows the same information as the previous figures but for the SGP-CF site. The CTRL simulated a skin temperature which reached a daytime maximum 6 degrees K cooler than observed. This is in part attributed to an over-representation of the initial moisture availability in the model as compared to the extremely dry surface at the site (indicated by the measured fractional water index surrounding the SGP CF site for 29 July 2005). Consequently, the sensible heat flux was underpredicted by about 50%, and the latent heat flux overpredicted by about twice the observation. When the McN94 technique was applied, the moisture availability was reduced, resulting in a 2.5 degree K improvement to the maximum daytime model skin temperature which was still below the observations. While both sensible and latent heat fluxes were improved, both the sensible and latent heat fluxes were nudged towards the observations.

The assimilation technique as implemented here did not retrieve the exact observed skin temperature or even the rate of temperature change, but does nudge the results in the correct direction. In addition, both the predicted sensible and latent heat fluxes partitioning were nudged in the correct direction. It has never been a requirement that the McN94 technique provide exact results, as one of the major assumptions made in the technique is that all other model parameters are represented well, leaving the largest uncertainty within the moisture availability. The results

indicated here are similar to those found with McN94, however the results were accomplished using a physically consistent method, unlike the previous implementation.

After the relative success of the 4 July 2003 cases, the inability of 1DBLM, with the moisture availability adjustment active, to replicate the large heating rates through the entire heating period of 29 July 2005 lead to an investigation that examined how the surface energy balance was reacting to the changes in surface moisture availability. This is described in the following section.

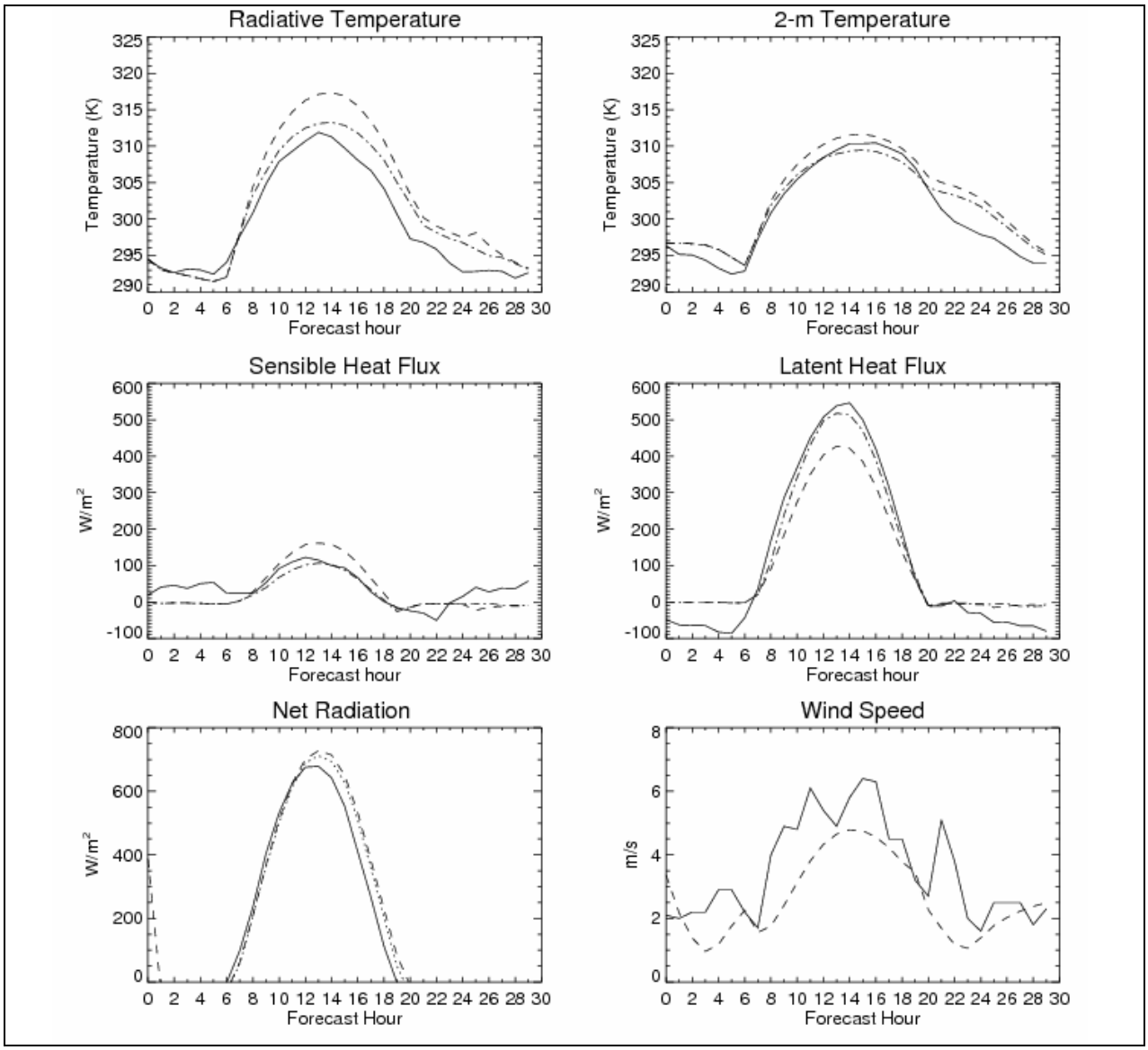

Figure 30. Observed (solid), CTRL simulated (dashed), and ASSIM simulated (dash-dot) variables valid 06 UTC 4 July 2003 to 12 UTC 5 July 2003 for FORA. Net radiation as measured by the IRT (solid) and tower instruments (dotted line) are given.

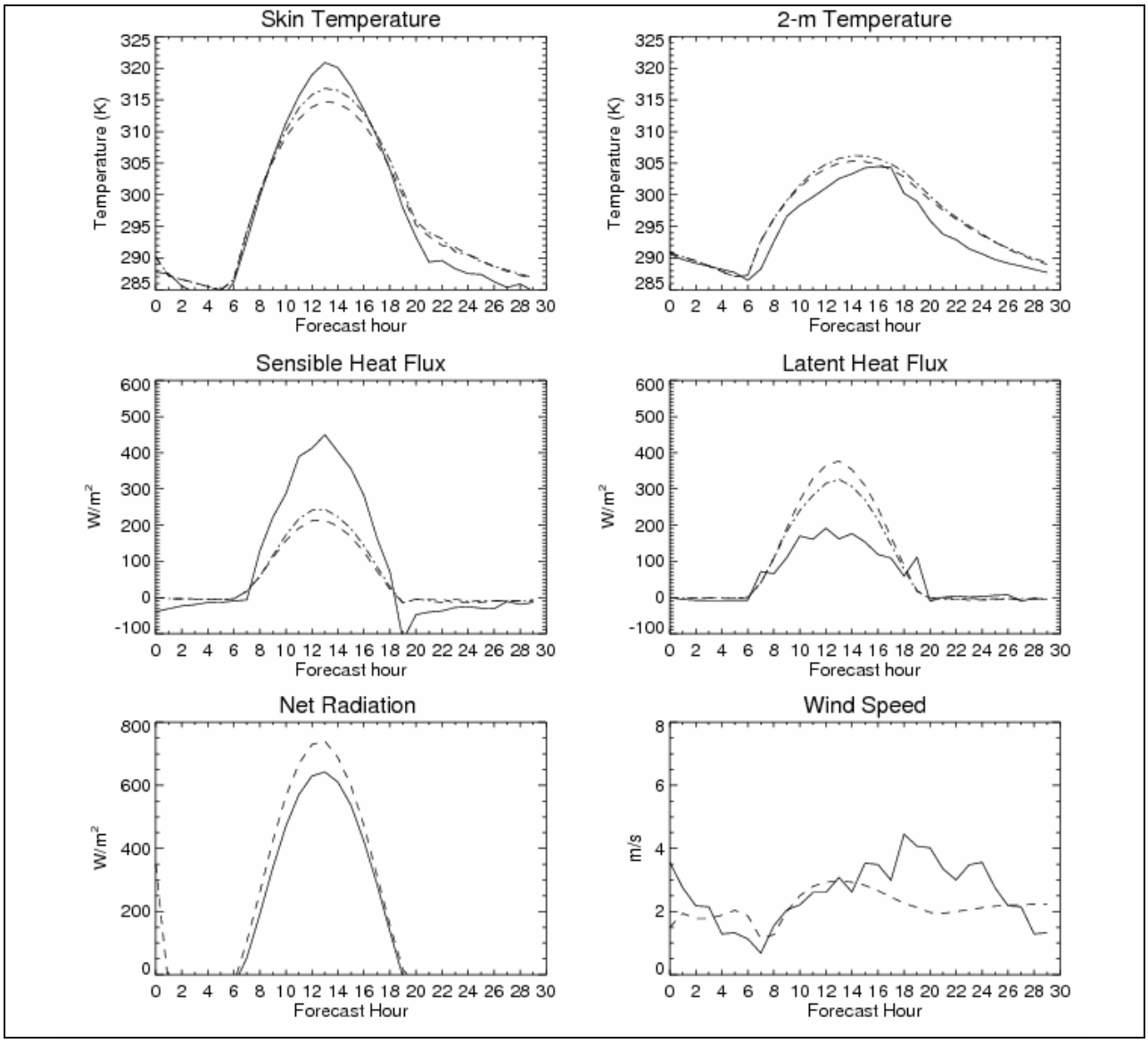

Figure 31. Observed (solid), CTRL simulated (dashed), and ASSIM simulated (dash-dot) variables valid 06 UTC 29 July 2005 to 12 UTC 5 July 2003 for SGP-CF. Net radiation as measure by the IRT (solid) and tower instruments (dotted line) are given.

6.4. Energy Balance Considerations

The simulations at different sites, as described in the previous section, show that the use of observational data can lead to better simulations of an earth-atmosphere system. The observations are not used directly, but rather indirectly to provide some difference measure. Simply replacing parameters within a model system with observations, while conceptually seems the easiest thing to do, can be problematic since actual values of those parameters are typically a product of a different equilibrium state. A direct replacement can shock a system such that it

may lead to numerical instability and ultimately a model crash. For this reason investigators began by attempting to nudge a model state towards observations.

Early problems with attempts to insert surface skin temperatures directly into the surface energy budget were recognized by Stauffer et al. (1991). They encountered difficulties in that the terms in the energy budget no longer supported the temperatures being inserted. Thus the system became unbalanced leading to numerical instability and erroneous results. MCN94, building on the experience of Stauffer et al. (1991), recognized that direct insertion of skin temperature would not work. Rather MCN94, following Wetzel and Woodward (1987) and Carlson et al. (1981), took the approach that fundamental parameters within the surface energy budget such as surface moisture availability or heat capacity must be changed to support the desired temperature result. In this regard they analytically inverted a surface energy model to solve for the moisture availability that would produce the desired temperature change in the morning hours. McNider et al. (2005) (hereafter MCN05) employed a similar technique to solve for the slab heat capacity that would give the desired temperature response in the early evening. Other investigators such as Jones et al. (1998a) have used this analytical inversion to solve for other parameters in more complex surface models to solve for stomatal resistance. However, in all of these analytical inversions the assumption is that other terms remain the same as when the desired parameter is recovered. In reality, once one parameter is changed other terms in the budget equation also change. Thus, attention is required in solution techniques and iteration strategies so that the desired recovery is made.

An examination of the observed, control model, and assimilation simulated heating rate for the SGP-CF case uncovered interesting findings. Figure 32 gives a graphic representation of these heating rates along with the subsequent impact on the skin temperature. The high frequency changes of the surface energy balance can be seen in the time series of temperature tendencies. As expected, the model simulated heating rate was less than the observations. When the moisture availability adjustment takes place, the result was a jump in the surface temperature tendencies and an increase in skin temperature. However; the model very quickly returns to a heating rate close to its previous one. Even with the initial jump in tendency, it can be seen that the average hourly tendency would be below the observation. In order to test the impact of increasing the assimilation frequency, a test case was conducted where the moisture availability was adjusted every 2 minutes. Figure 33 provides the same information as Figure 32 but for this higher frequency assimilation test run. The result is an hourly average tendency that is more closely matched to the observations. A portion of the hourly tendency is much less than previously found, resulting from the fact that the observed tendency was calculated from hourly observations and not the two minute interval. While the time series of tendencies appears to be quite chaotic, the result on the surface skin temperature and fluxes was much improved over the hourly adjustment. This can be seen in Figure 34, which indicates skin temperatures that nearly match the observations. The surface fluxes were further nudged towards observation and could be further improved if more attention was given in correcting the boundary layer processes responsible for the near surface temperature representation and winds.

The results, as depicted in Figure 32-Figure **34**, provide an example of how sensitive the surface energy balance is to changes in any of its components. In order to capture the changes in an

energetically consistent manner, the use of very small time steps was employed. The use of more sophisticated solvers may allow for larger time steps and improve numerical stability.

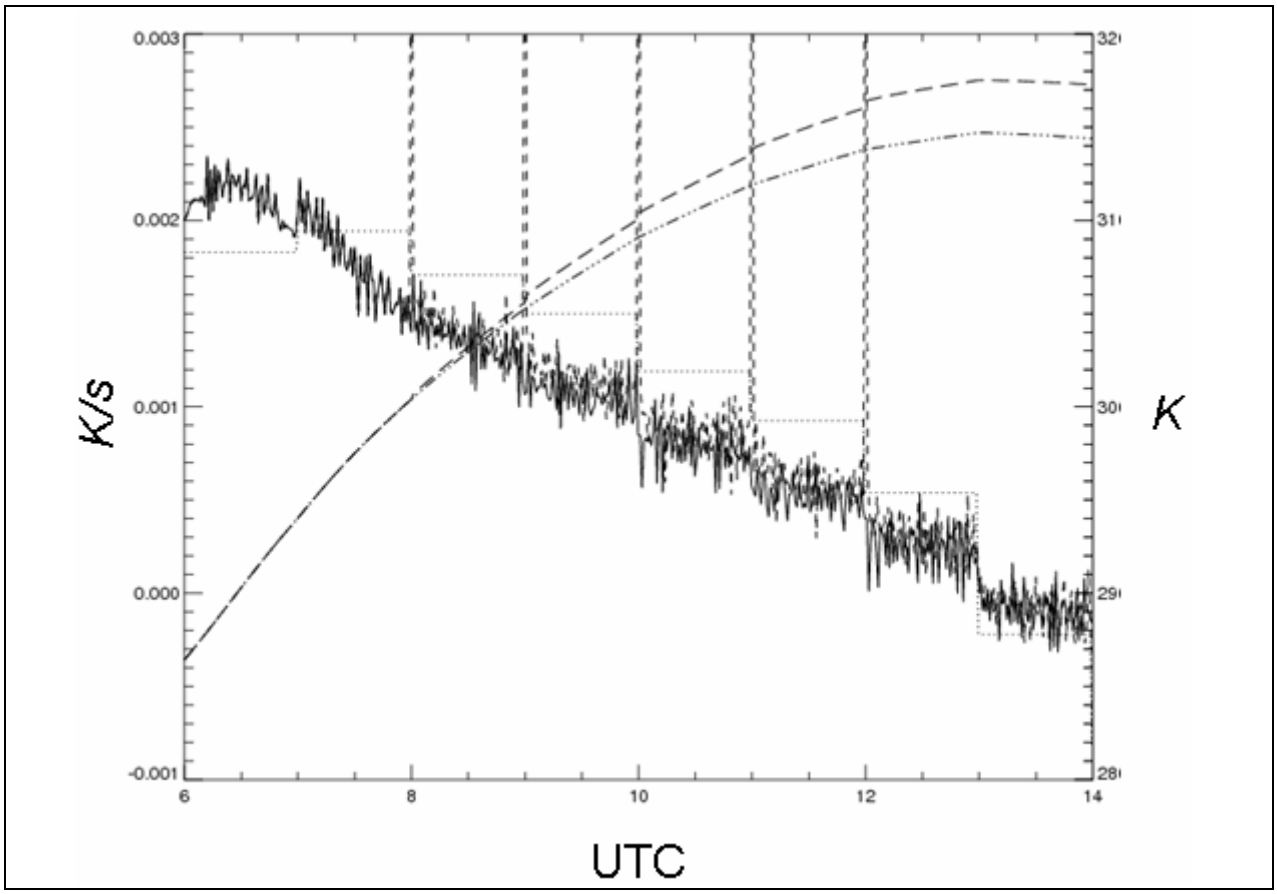

Figure 32. Time series of skin temperature tendency from CTRL (solid), ASSIM (small dash), and observations (dotted) along with time series of skin temperature from CTRL (dash-dot) and ASSIM (large dash). The assimilation is implemented every 60 minutes.

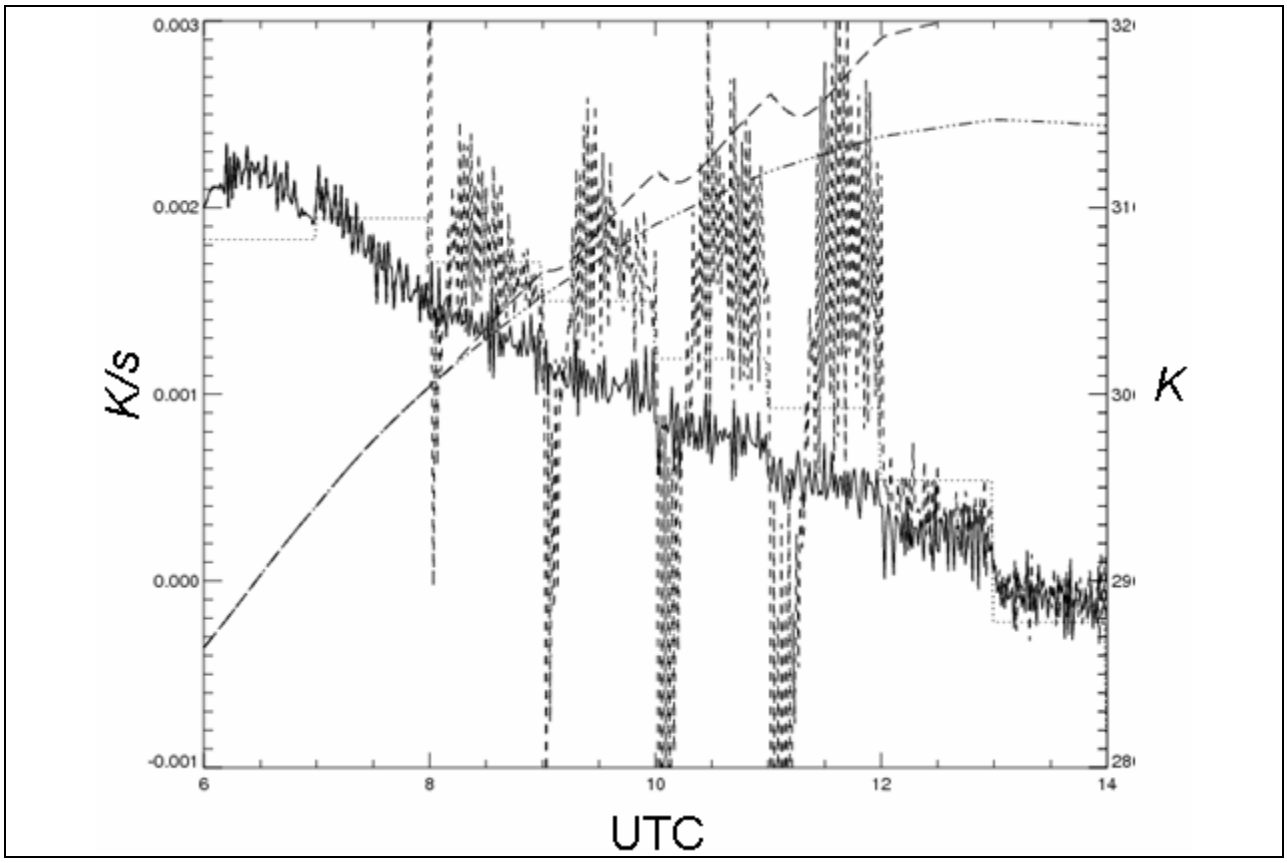

Figure 33. Time series of skin temperature tendency from CTRL (solid), ASSIM (small dash), and observations (dotted) along with time series of skin temperature from CTRL (dash-dot) and ASSIM (large dash). The assimilation is implemented every 2 minutes.

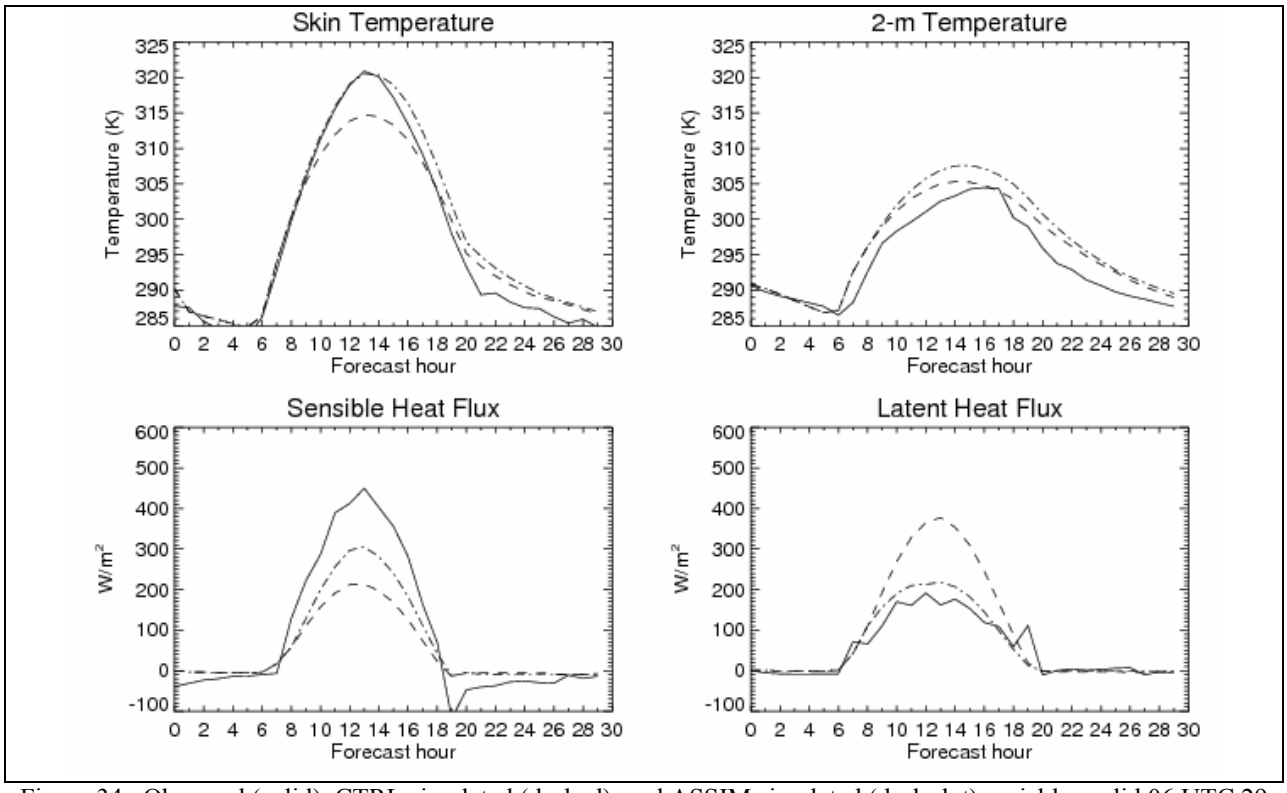

Figure 34. Observed (solid), CTRL simulated (dashed), and ASSIM simulated (dash-dot) variables valid 06 UTC 29 July 2005 to 12 UTC 5 July 2003 for SGP-CF applying the MCN94 assimilation technique every 2 minutes.

6.5. Summary

This discussion has outlined the importance of consistent use of skin and aerodynamic temperature representation and iteration processes when incorporating surface information from satellite data into mesoscale models. The three-temperature system used here can be directly implemented within currently forecasting systems in which the boundary layer parameterization can interact with a slab land surface model. While this is a limited set of model configurations the implications of inconsistent temperature use is likely applicable to all situations where surface information from satellites is used.

The MCN94 satellite assimilation technique was applied in this study. In light of research that took place since its development, some of the problems faced when incorporating this technique within the MM5 were alleviated. This was accomplished by using the aforementioned three-temperature system so that satellite observations could be directly compared with the physically consistent model simulated counterpart. The results of the tests presented here look promising, and provide results similar to those originally produced in MCN94 but within a physically consistent system.

The impact of making adjustments to parameters within a surface energy balance on that balance was discussed. Results from test cases indicated how sensitive the system is to these changes. Future work might examine the impacts of using more elegant and numerically stable solvers in this system, as well as reevaluating how operator splitting is done within models.

7. SUMMARY AND CONCLUSIONS

In this study, satellite-retrieved cloud transmissivity, cloud top height, and observed cloud fraction were used to correct photolysis rates for cloud cover in CMAQ. The results from CMAQ simulations using this method were compared with simulations that used standard MM5-derived cloud fields as input. The simulations were performed with 4-km and 12-km grid cell sizes over Texas, extending east to Mississippi, for the period of August 24 to August 31, 2000.

The results reveal that lack of observed clouds in the model can drastically alter the predicted atmospheric chemical composition within the boundary layer and exaggerate or under-predict ozone concentrations. Cloud impact is acute and more pronounced over the emission source regions and can lead to large errors in the model predictions of ozone and its by-products. Clouds also increased the lifetime of ozone precursors leading to their transport out of the source regions and causing ozone production farther downwind. Longer lifetime for NO_x and its transport out of the source regions and over regions high in biogenic hydrocarbon emissions (in the eastern part of the domain) led to increased ozone production that was missing in the control simulation. Over Houston-Galveston Bay area, the presence of clouds altered the chemical composition of the atmosphere and reduced the net surface removal of reactive nitrogen compounds.

It should be noted that there are many sources of errors in these simulations (e.g., emissions, lateral boundary conditions for a relatively small domain) and the technique presented here only corrects one of the errors. It should also be noted that the modeling domain was extremely dry during the period of this study. Therefore, the impact of inclusion of observed clouds on photochemistry during other periods with more cloud formation could be even more dramatic than presented in this study. This is evident when the statistical analyses of the results are compared to the large error reduction at the individual sites impacted by clouds. The statistics for the entire domain generally show a moderate improvement. Such large errors can lead to major problems in the use of photochemical models for case studies as well as in air quality forecasting. In case studies, simply an inconsistency between the observed cloud field and that of the model can result in erroneous concentrations that cannot be explained by the in-situ measurements. Air quality forecast models often use the model results from the previous forecast (or some adjusted form of it) to initialize the model for the new forecast. Therefore, the errors arising from an inconsistency in the cloud fields can propagate into the future forecasts. Therefore, the use of observed clouds in the preparation of initial concentrations for air quality forecasting is beneficial.

This study showed that at some locations the errors in ozone concentration arising from inaccurate cloud cover specification reached as high as 60 ppb which was mostly corrected by the use of our technique. Such errors are significant and can have considerable impact on air quality modeling efforts. However, other sources of error in the model due to inadequate cloud specification are as important and need to be addressed. The assimilation technique presented here only corrected the photolysis rates and did not account for the inconsistencies in dynamics and aqueous-phase chemistry. The discrepancy in dynamics affects the vertical mixing, which

can lead to over-/under-prediction of pollutants. Such discrepancies also affect the chemistry as the heterogeneous processes in the model will be affected by an inconsistent photolysis rate.

These problems require further research for improving the existing photolytic rate calculations in the current air quality models. Even though in this study the technique was implemented within CMAQ, any model that uses model-generated clouds suffers from the same problems and may benefit equally from using satellite-derived clouds. The method presented here addresses a problem in the chemical transport model while the source of this problem is the inadequate cloud prediction in the model. One approach to resolve this issue would be the assimilation of observed clouds in a dynamically consistent manner in the model.

With respect to the land surface modeling using satellite data, the results of this study have indicated that the highly uncertain specification of surface moisture availability can be improved using satellite data. However, it was also shown that the application of assimilation techniques, such as the MCN94 technique, must be carefully done within a model framework. The original tests of MCN94 showed that it could effectively alter surface moisture. This was done in a model system which explicitly calculated explicitly a surface radiating skin temperature and an aerodynamic temperature. In the transfer of this technique to MM5, it was found that the radiating skin temperature was in fact not a skin temperature and that MM5 used the ground temperature rather than a aerodynamic temperature to calculate surface fluxes, leading to an overadjustment of surface moisture. The study also pointed out inconsistencies in the technique of MCN94 in that in its formulation of using satellite temperature tendencies it also mixed radiating and aerodynamic temperatures.

Also shown is that with careful attention to surface details, satellite data can be effectively assimilated to recover surface moisture and potentially surface heat capacity. However, tests showed that even with these improvements the final skin temperatures, though improved, still did not fully follow the satellite data. Additional work is needed regarding the theory of how to adjust parameters within the complex nonlinear dynamical system at the surface/air interface. Part of the problem is that atmospheric scientists have not been as careful as mathematicians in applying operator splitting. For example, most all atmospheric models split operators by separately carrying out calculations of surface temperature and first level air temperature. At the next time step there is interaction but this step-wize approach might lead to oscillations as previously shown. A better technique may be to solve for the surface and near surface air temperature together, especially if assimilation is going to take place, which disrupts the system balance.

8. REFERENCES

Allen, C.W. 1963. Astrophysical quantities, 2nd ed. London: University of London, Athlone Press. 291 pp.

Allen, D., C. Durrenberger, and TNRCC Technical Analysis Division. 2002. Accelerated science evaluation of ozone formation in the Houston-Galveston Area: Photochemical air quality modeling. Technical Report. Texas Commission on Environmental Management. 47 pp. Internet website: http://www.utexas.edu/research/ceer/texaqsarchive/pdfs/Modeling02_17_02.PDF

Anderson, M.C., J.M. Norman, G.R. Diak, W.P. Kustas, and J.R. Mecikalski. 1997. A two-source time-integrated model for estimating surface fluxes using thermal infrared remote sensing. Remote Sens. Env. 60:195-216.

Arola, A., S. Kalliskota, P.N. den Outer, K. Edvardsen, G. Hansen, T. Koskela, T.J. Martin, J. Matthijsen, R. Meerkoetter, P. Peeters, G. Seckmeyer, P.C. Simon, H. Slaper, P. Taalas, and J. Verdebout. 2002. Assessment of four methods to estimate surface UV radiation using satellite data, by comparison with ground measurements from four stations in Europe. J. Geophys. Res. 107(D16):4310. doi:10.1029/2001JD000462.

Barker, H.W., G.L. Stephens, P.T. Partain, J.W. Bergman, B. Bonnel, K. Campana, E.E. Clothiaux, S. Clough, S. Cusack, J. Delamere, J. Edwards, K.F. Evans, Y. Fouquart, S. Freidenreich, V. Galin, Y. Hou, S. Kato, J. Li, E. Mlawer, J.J. Morcrette, W. O'Hirok, P. Räisänen, V. Ramaswamy, B. Ritter, E. Rozanov, M. Schlesinger, K. Shibata, P. Sporyshev, Z. Sun, M. Wendisch, N. Wood, and F. Yang. 2003. Assessing 1D atmospheric solar radiative transfer models: Interpretation and handling of unresolved clouds. Journal of Climate 16(16):2676–2699.

Beljaars, A.C.M. and A.A.M. Holtslag.1991.Flux parameterization over land surfaces for atmospheric models. Journal of Applied Meteorology 30:327-341.

Biazar, A.P. 1995. The role of natural nitrogen oxides in ozone production in the southeastern environment. Ph.D. Dissertation, Atmospheric Science Department, University of Alabama in Huntsville, AL. 271 pp.

Blackadar, A.K. 1979. High Resolution Models of the Planetary Boundary Layer. Adv. Environ. Sci. Eng. 1:50-85.

Brock, F.V., K.C. Crawford, R.L. Elliott, G.W. Cuperus, S.J. Stadler, H.L. Johnson, and M.D. Eilts. 1995. The Oklahoma mesonet: A technical overview. Journal of Atmospheric and Oceanic Technology 12:5-19.

Brotzge, J.A. and C.E. Duchon. 2000. A field comparison among a domeless net radiometer, two four-component net radiometers, and a domed net radiometer. Journal of Atmospheric and Oceanic Technology 17:1569-1582.

Brutsaert, W. 1982. Evaporation into the atmosphere-theory, history, and applications. Higham, MT, USA: D. Reidel Publishing Company. 299 pp.

Carlson, T.N. 1986. Regional scale estimates of surface moisture availability and thermal inertia using remote thermal measurements. Remote Sens. Rev. 1:197-246.

Carlson, T.N., J.K. Dodd, S.G. Benjamin, and J.N. Cooper. 1981. Satellite estimation of the surface energy balance, moisture availability and thermal inertia. Journal of Applied Meteorology 20:67-87.

Castro, T., L.G. Ruiz-Suarez, J.C. Ruiz-Suarez, M.J. Molina, and M. Montero. 1997. Sensitivity analysis of a UV radiation transfer model and experimental photolysis rates of NO_2 in the atmosphere of Mexico City. Atmospheric Environment 31:609-620.

Chang, J.S., R.A. Brost, I.S.A. Isaksen, S. Madronich, P. Middleton, W.R. Stockwell, and C.J. Walcek. 1987. A three-dimensional Eulerian acid deposition model: Physical concepts and formulation. J. Geophys. Res. 92(D12):14681-14700.

Choudhury, B.J., R.J. Reginato, and S.B. Idso. 1986. An analysis of infrared temperature observation of wheat and calculation of latent heat flux. Agric. For. Meteor. 37:75-88.

Collins, D.R.; H.H. Jonsson, H. Liao, R.C. Flagan, J.H. Seinfeld, K.J. Noone, and S.V. Hering. 2000. Airborne analysis of the Los Angeles aerosol. Atmospheric Environment 34(24): 4155-4173.

Coulson, K.L. 1959. Characteristics of the radiation emerging from the top of a Rayleigh atmosphere, 1 and 2. Planet. Space Sci. 1:256-284.

Deardorff, J.W. 1972. Theoretical expression for the countergradient vertical heat flux. J. Geophys. Res. 77:5900-5904.

Diak, G.R., and C. Gautier. 1983. Improvements to a simple physical model for estimating insolation from GOES data. J. Appl. Meteor. 22:505-508.

Diak, G. and M. Whipple. 1995. Note on estimating surface sensible heat fluxes using surface temperatures measured from geostationary satellite. J. Geophys. Res. 100:25453-25461

Dickerson, R.R., S. Kondragunta, G. Stenchikov, K.L. Civerolo, B.G. Doddridge, and B.N. Holben. 1997. The impact of aerosols on solar ultraviolet radiation and photochemical smog. Science 278:827-830.

Dudhia, J. 1996. A multi-layer soil temperature model for MM5. The Sixth PSU/NCAR Mesoscale Model Users' Workshop, Boulder, Colorado, National Center for Atmospheric Research. Pp. 49-50.

Fiebrich, C.A., J.E. Martinez, J.A. Brotzge, and J.B. Basara. 2003. The Oklahoma Mesonet's skin temperature network. Journal of Atmospheric and Oceanic Technology 20:1496-1504.

Fritz, S., and J.S. Winston. 1962. Synoptic use of radiation measurements from satellite TIROS-II. Mon. Weather Review 90:1-9.

Gautier, C., G. R. Diak, and S. Mass. 1980. A simple physical model for estimating incident solar radiation at the surface from GOES satellite data. J. Appl. Meteor. 19:1005-1012.

Gery, M.W., G.Z. Whitten, J.P. Killus, and M.C. Dodge. 1989. A photochemical kinetics mechanism for urban and regional scale computer modeling. J. Geophys. Res. 94(D10):12,925–12,956.

Grell, G.A. 1993. Prognostic evaluation of assumptions used by cumulus parameterizations. Mon. Wea. Rev. 121:764–787.

Grell, G.A., Y.H. Kuo, and R. Pasch. 1991. Semi-prognostic tests of cumulus parameterization schemes in the middle latitudes. Mon. Wea. Rev. 119:5–31.

Grell, G.A., J. Dudhia, and D.R. Stauffer. 1994. A description of the fifth-generation Penn State/NCAR mesoscale model (MM5). NCAR Technical Note NCAR/TN-398+STR, National Center for Atmospheric Research, Boulder, Colorado. 138 pp.

Haines, S.L., R.J. Suggs, and G.J. Jedlovec. 2004. The GOES product generation system. NASA Technical Memorandum, NASA/Marshall Space Flight Center. Document ID: 20050019524. Report Number: M-1118, NASA TM-2004-213286. (http://hdl.handle.net/2060/20050019524)

Jacobson, M.Z. 1998. Studying the effects of aerosols on vertical photolysis rate coefficient and temperature profiles over an urban airshed. J. Geophys. Res. 103(D9):10593-10604. doi:10.1029/98JD00287.

Jedlovec, G.J., J.A. Lerner, and R.J. Atkinson. 2000. A satellite-derived upper-tropospheric water vapor transport index for climate studies. J. Appl. Meteor. 39:15-41.

Jones, A.S., I.C. Guch, and T.H. Vonder Haar. 1998a. Data assimilation of satellite-derived heating rates as proxy surface wetness data into a regional atmospheric mesoscale model. Part II: A case study. Monthly Weather Review 126:646-667.

Jones, A.S., I.C. Guch, and T.H. Vonder Haar. 1998b. Data assimilation of satellite-derived heating rates as proxy surface wetness data into a regional atmospheric mesoscale model. Part I: Methodology. Monthly Weather Review 126:634-645.

Kustas, W.P., B.J. Choudhury, M.S. Moran, R.J. Reginato, R.D. Jackson, L.W. Gary, and H.L. Weaver. 1989. Determination of sensible heat flux over sparse canopy using thermal infrared data. Agric. For. Meteor. 44:197-216.

Lacis, A.A. and J.E. Hansen. 1974. A parameterization for absorption of solar radiation in the earth's atmosphere. J. Atmos. Sci. 31:118-133.

Lhomme, J.P., N. Katerji, A. Perrier, and J.M. Bertolini. 1988. Radiative surface temperature and convective flux calculation over crop canopies. Boundary-Layer Meteorology 43:383-392.

Liao, H., Y.L. Yung, and J.H. Seinfeld. 1999. Effects of aerosols on tropospheric photolysis rates in clear and cloudy atmospheres. J. Geophys. Res. 104(D19):23697-23708. doi:10.1029/1999JD900409.

Mackaro, S. 2003. Applications of land surface data assimilation to simulations of sea breeze circulations. M.S. Thesis, Atmospheric Science Department, University of Alabama in Huntsville. 86 pp.

Mackaro, Scott. 2008. The importance of physically consistent temperature representation in land surface satellite assimilation. Ph.D. Dissertation, Atmospheric Science Department, University of Alabama in Huntsville. 157pp.

Mackaro, Scott M., R.T. McNider, and A.P. Biazar. 2008. A physically consistent method for the assimilation of land surface temperature tendencies. Proceedings of American Meteorological Society 88th Annual Meeting, 12th Conference on Integrated Observing and Assimilation Systems-Assimilation of Ocean and Land Surface Observations into Models-I (12IOAS-AOLS), New Orleans, LA, January 20-24.

Madronich, S. 1987. Photodissociation in the atmosphere: 1. actinic flux and the effects of ground reflections and clouds. J. Geophys. Research 92:9740-9752.

McNider, R.T., A.J. Song, D.M. Casey, P.J. Wetzel, W.L. Crosson, and R.M. Rabin. 1994. Toward a dynamic thermodynamic assimilation of satellite surface temperature in numerical atmospheric models. Mon. Wea. Rev. 122:2784-2803.

McNider, R.T., J.A. Song, and S.Q. Kidder. 1995. Assimilation of GOES-derived solar insolation into a mesoscale model for studies of cloud shading effects. Int. J. Remote Sens. 16:2207-2231.

McNider, R.T., W.B. Norris, D.M. Casey, J.E. Pleim, S.J. Roselle, and W.M. Lapenta. 1998. Assimilation of satellite data in regional air quality models. Pp. 25-35, Air Pollution Modeling and Its Application XII, S.E. Gryning and N. Chaumerliac (eds.), NATO/CCMS, Plenum Press, NY.

McNider, R.T., W.M. Lapenta; A.P. Biazar, G.J. Jedlovec, R.J. Suggs, and J. Pleim. 2005. Retrieval of model grid-scale heat capacity using geostationary satellite products. Part I: First case-study application. Journal of Applied Meteorology 44(9):1346-1360. (AN18622838).

Monin, A.S. and A.M. Obukhov. 1954. Basicl of turbulent mixing in the ground layer of the atmosphere. Trans. Geophys. Inst. Akad. Nauk. USSR, 151:163-187.

NCAR. 2003. MM5 Modeling System Version 3, NCAR. Internet website: http://www.mmm.ucar.edu/mm5/doc1.html.

Norman, J.M., W.P Kustas, and K.S. Humes. 1995. A two-source approach for estimating soil and vegetation energy fluxes in observations of directional radiometric surface temperature. Agricultural and Forest Meteorology 77:263−293.

Paltridge, G.W. 1973. Direct measurement of water vapor absorption of solar radiation in the free atmosphere. J. Atmos. Sci. 30:156-160.

Pour-Biazar, A., R.T. McNider, S.J. Roselle, R. Suggs, G. Jedlovec, S. Kim , D.W. Byun, J.C. Lin, T.C. Ho, S. Haines, B. Dornblaser, and R. Cameron. 2007. Correcting photolysis rates on the basis of satellite observed clouds, J. Geophys. Res. 112:D10302. 17 pp. doi:10.1029/2006JD007422.

Ruggaber, A., R. Dlugi, and T. Nakajima. 1994. Modeling radiation quantities and photolysis frequencies in the troposphere. Journal of Atmospheric Chemistry 18 :171–210.

Stauffer, D.R., N.L. Seaman, and F.S. Binkowski. 1991. Use of four-dimensional data assimilation in a limited-area mesoscale model. Part II: Effects of data assimilation within the planetary boundary layer. Monthly Weather Review 119:734-754.

Stephens, G.L. 1978. Radiation profiles in extended water clouds. II: Parameterization Schemes. Journal of the Atmospheric Sciences 35(11):2123–2132.

Sugita, M. and W. Brutsaert. 1990. How similar are temperature and humidity profiles in the unstable boundary layer. Journal of Applied Meteorology 29:489-497.

Sun, J. and L. Mahrt. 1995. Determination of surface fluxes from the surface radiative temperature. Journal of the Atmospheric Sciences 52:1096-1106.

U.S. Enviromental Protection Agency. 1999. Science algorithms of the EPA Models-3 Community Multiscale Air Quality (CMAQ) modeling system. EPA-600/R-99/030.

Wetzel, P.J. and R.H. Woodward. 1987. Soil moisture estimation using GOES-VISSR infrared data: A case study with a simple statistical method. Journal of Applied Meteorology 26:107-117.

Wetzel, P.J., D. Atlas, and R.H. Woodward. 1984. Determining soil moisture from geosynchronous satellite infrared data: A feasibility study. Journal of Applied Meteorology 23:375-391.

Zilitinkevich, S.S. 1970. Dynamics of the atmospheric boundary layer. Leningrad Gidrometeor. 291 pp.